Immune Tolerance Disruption by Human Parvovirus B19 Viral Infection Mechanisms

Sanna Rauhamäki
Master's Thesis
University of Jyväskylä
Biological and Environmental Science
Cell and Molecular Biology
16.12.2013

Preface

This thesis was performed during spring 2011 in Leona Gilbert's group which focuses on microbial research and nano-biosensors. The group is a part of Cell and Molecular Biology in the Department on Biological and Environmental Science in the University of Jyväskylä. The study was part of a project supported by the Academy of Finland Contract Number 122061. The funders had no role in study design, data collection and analysis, decision to publish, or preparation of the thesis.

I would like to thank my supervisor Leona Gilbert for professional guidance and inspirational work environment. Her group welcomed me like a family and everyone in the group patiently helped me even with the simplest problems. I would also like to specifically thank Kanoktip Thammasri and Artemis Filippou for performing part of the confocal microscopy work while I was located elsewhere due to internships. Thanks to this project, I feel at home in Ambiotica, in laminar flow cabinets, in murky confocal microscopy rooms and staring at computer screens. There is no denying that the path from start to finish has been longer than expected and needlessly winding. Nevertheless, despite of all turns I have taken, I can finally count myself into the special group that has taken up the challenge of *Pro Gradu* and come out on top.

Finally, I would like to thank my family for a childhood that enabled me to grow a vast interest for natural phenomena already early on. Picking blueberries, skiing through winters and being allowed to play in forests, in addition to witnessing fishing and hunting from close range have been irreplaceable experiences in this sense. Special thanks belong also to Erkki Hautala for peer support and for being there through this journey.

In Jyväskylä, 16th of December 2013

Sanna Rauhamäki

University of Jyväskylä **Abstract of Master´s Thesis**

Faculty of Mathematics and Science

Author: Sanna Rauhamäki
Title of thesis: Immune Tolerance Disruption by Human Parvovirus B19 Viral Infection Mechanisms
Suomenkielinen otsikko: Häiriö immunitoleranssissa parvovirus B19:n infektiomekanismien takia
Date: 16.12.2013 **Pages:** 64 + 16

Department: Department of Biological and Environmental Science
Chair: Cell and Molecular Biology
Supervisor: Dr. Leona Gilbert, Ph.D.

Abstract:

There are several factors, of which viral infections are increasingly regarded as the greatest environmental cause of autoimmunity, influencing the development of an autoimmune disease. For example human parvovirus B19 (B19V) has been previously connected to systemic lupus erythematosus and rheumatic arthritis. It has also been shown that nonstructural protein 1 (NS1) of B19V induces apoptosis in cells not normally permissive for B19V infections. In addition, it has been recently demonstrated that apoptotic bodies resulting from apoptosis can present antigens to antigen presenting cells (APCs) such as macrophages or dendritic cells. The aim of this study is to detect self antigens related to B19V infections and study the immune response caused by NS1. For that, the NS1 has been fused with enhanced green fluorescent protein (EGFP) and incorporated into baculovirus vector under cytomegalovirus immediate early promoter. These recombinant baculovirus particles were amplified in Sf9 insect cell line. The resulting virus was then used to transduce HepG2 human hepatocytic cells. The transduction efficiency of the virus was measured with flow cytometry, employing the presence of the EGFP as a sign of transduction. Based on the transduction efficiency, a volume providing 70 % transduction efficiency of the virus stock was used to produce apoptotic bodies. These apoptotic bodies were first purified by filtering and then pelleted by ultracentrifugation. Collected apoptotic bodies were immunolabeled using nuclear antigens apolipoprotein H (ApoH), histone 4 (H4), histone 2B (H2B), lysosomal-associated membrane protein 2 (Lamp2), Ku80 and Smith. The selected nuclear antigens as well as NS1 were detected from the apoptotic bodies, except for H2B. The presence of nuclear antigens in the apoptotic bodies is a potential method for immune tolerance disruption which was then addressed by utilizing APCs. The APCs of choice were acute monocytic leukemia derived human monocytes (THP-1) due to their close resemblance to peripheral blood mononuclear cells. THP-1 cells were differentiated using phorbol-12-myristate-13-acetate (PMA). The cells were incubated in medium containing PMA for three days and then five more days in fresh medium to ensure proper differentiation. Differentiated THP-1 cells (dTHP-1) were next fed with purified apoptotic bodies. Internalization of B19V NS1 induced apoptotic bodies was observed using confocal microscopy. Since the APCs were capable of internalizing apoptotic bodies, the following cytokine profile was tentatively studied. The examination of possible immunological effects derived to a conclusion that only the presence of interferon γ inducible protein 10 (IP-10) separated the EGFP or EGFP-NS1 fusion protein containing samples from the control conditions. Although the underlying mechanisms leading into immune tolerance disruption by B19V infection mechanisms warrants further investigation, the data here supports the hypothesis that B19V NS1 induced apoptotic bodies from nonpermissive cells contain self-antigens which could be introduced to the immune system though APCs.

Keywords: Human parvovirus B19, immune tolerance, apoptotic bodies, nuclear antigens, self-antigens

Jyväskylän yliopisto
Matemaattis-luonnontieteellinen tiedekunta

Pro Gradu-tutkielman tiivistelmä

Tekijä: Sanna Rauhamäki
Tutkielman nimi: Häiriö immunitoleranssissa parvovirus B19:n infektiomekanismien takia
English title: Immune Tolerance Disruption by Human Parvovirus B19 Viral Infection Mechanisms
Päivämäärä: 16.12.2013 **Sivumäärä:** 64 + 16

Laitos: Bio- ja ympäristötieteiden laitos
Oppiaine: Solu- ja molekyylibiologia
Tutkielman ohjaaja: Leona Gilbert, FT

Tiivistelmä:

Virusinfektioita pidetään kasvavissa määrin suurimpana ympäristöperäisenä syynä, joka vaikuttaa autoimmuunisairauksien kehitykseen ja autoimmuniteetin muodostukseen. Esimerkiksi parvovirus B19 (B19V) on yhdistetty punahukkaan sekä nivelreumaan. On todettu, että B19V:n ei-rakenteellinen proteiini 1 (NS1) aiheuttaa apoptoosia soluissa, jotka eivät tavallisesti ole B19V infektion kohteena. Lisäksi hiljattain on osoitettu, että apoptoosin seurauksena muodostuvat apoptoottiset kappaleet kykenevät esittelemään antigeenejä niitä esittelemään erikoistuneille soluille, kuten makrofageille tai dendriittisoluille. Tämän tutkimuksen tarkoituksena on löytää B19V infektioon liittyviä autoantigeenejä sekä tarkastella NS1:n aiheuttamaa immuunivastetta. Tätä varten NS1 on yhdistetty vihreään fluoresoivaan proteiiniin (EGFP) ja kloonattu bakulovirusvektoriin sytomegaloviruksen välittömän aikaisen promoottorin alle. Tämän jälkeen näitä yhdistelmä-bakuloviruksia lisättiin Sf9-hyönteissolulinjan avulla. Tällä tavoin tuotettua virusta käytettiin ihmisen maksasta peräisin olevien HepG2-solujen transduktiossa. Kyseisen transduktion tehokkuus mitattiin virtaussytometrillä, hyödyntäen EGFP-signaalia merkkinä onnistuneesta transduktiosta. Transduktion tehokkuuden perusteella määritettiin viruskannasta sellainen tilavuus, mikä tuottaa 70 prosentin transduktion. Tätä tilavuutta käytettiin apoptoottisten kappaleiden tuotannossa. Apoptoottiset kappaleet puhdistettiin ensin suodattamalla ja koottiin sitten pelleteiksi ultrasentrifugilla. Kootuista apoptoottisista kappaleista immunoleimattiin tumaperäiset antigeenit apolipoproteiini H (ApoH), histoni 4 (H4), histoni 2B (H2B), lysosomiin liittyvä kalvoproteiini 2 (Lamp2), Ku80 ja Smith. Kaikki tumaperäiset antigeenit, poissulkien H2B, löydettiin apoptoottisista kappaleista yhdessä NS1 kanssa. Tumaperäisten antigeenien löytyminen apoptoottisista kappaleista saattaa aiheuttaa häiriön immunitoleranssissa, mitä tutkittiin seuraavaksi hyödyntäen antigeenejä esitteleviä soluja. Tähän tarkoitukseen valittiin akuutista monosyyttisesta leukemiasta peräisin olevat ihmisen monosyytit (THP-1), jotka erilaistettiin forboli-12-myristaatti-13-asetaatilla (PMA). Soluja viljeltiin PMA:a sisältävällä kasvatusalustalla ensin kolme päivää ja viljelyä jatkettiin vielä erilaistumisen varmistamiseksi puhtaalla alustalla viiden päivän ajan. Seuraavaksi THP-1 soluja stimuloitiin apoptoottisilla kappaleilla ja niiden päätyminen solujen sisään varmistettiin konfokaalimikroskopialla. Koska erilaistetut THP-1 solut pystyivät ottamaan apoptoottisia kappaleita sisäänsä, tästä johtuvaa sytokiiniprofiilia tarkasteltiin vielä alustavasti tarkoitukseen sopivan kaupallisen tuotteen avulla. Mahdollisia immunologisia vaikutuksia tarkasteltaessa tultiin lopputulokseen, jossa ainoastaan yhden proteiinin, γ-interferonin indusoima proteiini 10:n (IP-10), läsnäolo erotti EGFP- ja EGFP-NS1-fuusioproteiinien avulla tuotetut näytteet kontrollinäytteistä. Vaikka B19V:n infektiomekanismien aiheuttamat häiriöt immunitoleranssiin vaativatkin vielä lisätutkimuksia, tässä tutkimuksessa saadut tulokset tukevat alkuperäistä hypoteesia. B19V NS1:n avulla tuotetut apoptoottiset kappaleet, jotka ovat peräisin soluissa, joita B19V ei tavallisesti infektoi, sisältävät autoantigeenejä ja nämä autoantigeenit voidaan esitellä immuunijärjestelmälle antigeenejä esittelevien solujen kautta.

Avainsanat: Parvovirus B19, immunitoleranssi, apoptoottiset kappaleet, tumaperäiset antigeenit, autoantigeenit

Table of Contents

Abbreviations

*Ac*CMV-EGFP	*Autographa californica* viral vector created with a modified pFastBac1 vector having enhanced green fluorescent protein under cytomegalovirus immediate-early promoter
*Ac*CMV-EGFP-NS1	*Autographa californica* viral vector created with a modified pFastBac1 vector having enhanced green fluorescent protein and human parvovirus B19 nonstructural protein 1 under cytomegalovirus immediate-early promoter
APC	Antigen presenting cell
ApoH	Apolipoprotein H (previously known as β_2-glycoprotein I)
B19V	Human parvovirus B19
CD40 ligand	Cluster of differentiation 40 ligand
CMV	Cytomegalovirus
C5a	Protein fragment released from complement component C5
DIC	Differential interference contrast
dTHP-1	PMA-stimulated THP-1 cell
EGFP	Enhanced green fluorescent protein
GM-CSF	Granulocyte macrophage colony-stimulating factor
GROα	Growth regulated oncogene α
HepG2	Human hepatocytes
H2B	Histone 2B
H4	Histone 4

IFN-γ	Interferon γ
IL	Interleukin
IP-10	IFN- γ inducible protein 10
I-TAC	Chemokine C-X-C motif ligand 11
I-309	Chemokine C-C motif ligand 1
Lamp2	Lysosomal-associated membrane protein 2
MIF	Macrophage migration inhibitory factor
MIP	Macrophage inflammatory protein
NS1	Nonstructural protein 1
PBS	Phosphate buffered saline
PMA	Phorbol-12-myristate-13-acetate
RA	Rheumatoid arthritis
RANTES	Regulated on activation, normal T-cell expressed and secreted
RCF	Relative centrifugal force
SDF-1	Stromal cell derived factor 1
SerpinE1	Serine protease inhibitor E1
Sf9	*Spodoptera frugiperda* derived cells
sICAM-1	Soluble intercellular adhesion molecule 1
SLE	Systemic lupus erythematosus
sTREM-1	Soluble triggering receptor expressed on myeloid cells 1
THP-1	Acute monocytic leukemia derived human monocytes
TNF-α	Tumor necrosis factor α

1. Introduction

Human parvovirus B19 (B19V) was first observed in human sera by Yvonne Cossart in 1975 (Cossart et al., 1975). It belongs to the genus of *Erythrovirus*, in the subfamily of *Parvovirinae* of the *Parvoviridae* family. However, B19V is yet to be assigned to an order (King et al., 2012). Typically for *Erythrovirus* genus, B19V replicates in and destroys erythroid progenitors. The approximately 5 600 nucleotides long genome of B19V consists of linear single-stranded DNA and the complementary strands may be located in separate virions (Clewley, 1984). B19V forms icosahedral, non-enveloped capsids of 25 nm in diameter from two proteins. The minor capsid protein of 84 kD is called viral protein (VP) 1 and the 58 kD major capsid protein is VP2. VP2 makes up more than 90 % of the capsid and it is generated from the same sequence with VP1 using alternative splicing. In comparison to VP2, VP1 has additional 227 amino acid domain in the amino terminus. Closer to the 5'-end from the sequence encoding the capsid proteins, B19V genome encodes 77 kD nonstructural protein 1 (NS1) (Shade et al., 1986; Ozawa et al., 1987; Agbandje et al., 1994). Moreover, Shade et al. (1986) recognized open reading frames which might code smaller proteins (Shade et al., 1986), while Ozawa et al. (1987) characterized small RNA species without known protein products. Despite of these initial findings implying other genome products about 25 years ago, functions for a 7.5 kD protein are yet to be reported but a 11 kD protein has recently been linked to stronger apoptosis induction in erythroid progenitor cells in comparison to NS1 (Chen et al., 2010).

The lethality of NS1 in transfected cells was originally suggested by Ozawa et al. (1988). By failing to establish stable transformation of cervical cancer derived HeLa cells when the constructed plasmids contained functional B19V genome regions encoding NS1, toxicity of NS1 to nonpermissive cells was indicated. Although it was not possible to distinguish whether the transformation failure was due to NS1 blocking cell proliferation or causing cell death rather than NS1 affecting the stability of transfected DNA, NS1 cytotoxicity was hypothesized to account for certain clinical manifestations seen during B19V infection (Ozawa et al., 1988). Later on NS1 has been shown to posses multiple functions which also

contribute to the cytotoxicity. For instance, NS1 is capable of transactivating the B19V p6 promoter and thus controls the transcription of the B19V genome (Doerig et al., 1990). Consequently, mutations to so called NS1 nucleoside triphosphate binding domain in plasmids carrying the NS1 gene reduce cytotoxicity in transfected cells (Momoeda et al., 1994). The control over the activity of B19V p6 promoter may take place either through direct binding to DNA or through transcription factors specificity protein 1 and 3 (Raab et al., 2002). Moreover, NS1 is capable of altering the gene expression in host cells which might be part of the B19V pathogenesis (Moffatt et al., 1996; Kivovich et al., 2010; Nykky et al., 2010; Poole et al., 2011; Kivovich et al., 2012; Thammasri et al., 2013).

Human parvovirus B19 is a common virus. About half the population carries specific anti-B19V antibodies by the age of 15 and although the infection continues at a lower rate through adulthood, most of the elderly population is B19V seropositive (Kerr et al., 1999). The virus spreads usually via respiratory tract (Anderson et al., 1985) but transmissions through blood products (Williams et al., 1990) and from infected mother to the fetus (Clewley et al., 1987) can occur. The infection is often asymptomatic (Woolf et al., 1989). Nonetheless, the most common clinical manifestation is erythema infectiosum, a childhood illness characterized by exanthematous rash of the face, torso and limbs (Anderson et al., 1985). In about half of the adult manifestations, B19V infection may lead into arthropathy, including arthralgia and inflammatory arthritis (White et al., 1985), mimicking rheumatoid arthritis (RA). However, arthropathy associated with B19V usually resolves without joint destruction (Woolf et al., 1991). Since B19V targets erythroid progenitors, it may aggravate transient aplastic crisis with severe anemia in patients with underlying erythropoiesis disorders (Anderson et al., 1985). Due to transplacental transmission, the fetuses of B19V infected mothers are at risk of spontaneous abortion or hydrops fetalis. The most critical time for infection seems to be the period before 16th week of gestation (Yaegashi et al., 1999), yet B19V is not significant cause of birth defects (Barton et al., 1997). All the more at risk of B19V infection are the hosts with acquired immune deficiency syndrome, patients receiving treatments that compromise the immune system or otherwise immunocompromised individuals. Because in these cases antibodies against B19V cannot be produced, red-cell aplasia and resulting severe anemia are likely

consequences. In addition, B19V is emerging as a contributing factor in autoimmune diseases (for review on B19V pathology, see (Corcoran and Doyle, 2004; Young and Brown, 2004)).

Similarity between B19V infection and certain autoimmune disease manifestations has led to speculations of B19V being causative agent in autoimmune conditions like systemic lupus erythematosus (SLE) and RA. Coincidental presence of autoantibodies and anti-B19V antibodies in patient sera observed after B19V infection seems to support this theory as well (Kerr and Boyd, 1996). Cope et al. (1992) were the first to report B19V infection coinciding with the onset of SLE in their case study of a 59 year old female patient (Cope et al., 1992). In a separate case, acute B19V infection was considered to cause a flare of existing SLE (Hemauer et al., 1999). Since SLE is characterized by the presence of both IgG and IgM autoantibodies against one or more nuclear components, the occurrence of anti-neutrophil cytoplasmic antibodies and anti-cardiolipin antibodies in patient sera together with B19V DNA has drawn added attention to this connection (Chou et al., 2000). In comparison to other autoimmune conditions, B19V DNA has only been found in SLE or in autoimmune inner ear disease patients and in the case of SLE, more frequently when anti-B19V IgG and IgM are not detected (Hsu and Tsay, 2001) (for review, see (Pavlovic et al., 2010)). B19V DNA has also been found in the synovial tissue of RA patients but infrequently in those with other arthralgic issues (Takahashi et al., 1998). RA is an autoimmune disease causing chronic inflammatory synovitis and augmented cell-mediated immune response in the joints, including cytokines responsible for the inflammation process. Rheumatoid factor (RF), a series of antibodies used to diagnose RA, has also been linked to B19V infection. Other autoimmune diseases connected with B19V include additional connective tissue diseases and systemic vasculitides (for review, see (Meyer, 2003)).

The formation of autoreactive cells during lymphocyte development is kept under control by apoptosis which is a method of programmed cell death devoid of destructive inflammation. Relapse in detection and removal of these cells can result in autoimmune

disease. For that reason, apoptosis has been for awhile now considered as a possible causative factor for example in SLE and RA (for review, see (Thompson, 1995; Opferman and Korsmeyer, 2003)). Apoptosis is also in significant role in B19V infection. That is to say, apoptosis has been reported to occur as a result of B19V infection. More specifically, apoptosis occurs in the presence of NS1 not only in permissive erythroid lineage cells (Moffatt et al., 1998) but also in nonpermissive fibroblast-like COS-7 cells (Hsu et al., 2004) and in liver-derived human hepatocytes (HepG2) cells (Poole et al., 2006).

Another reason for considering apoptosis as an inducer of autoimmune diseases is the presence of nucleosomes on the surface of apoptotic cells. Radic et al. (2004) demonstrated that nuclear fragments emerge as blebs on the surface of apoptotic cells and those fragments can be recognized by autoantibodies to the nucleosome core particle or to DNA and histones to be exact (Radic et al., 2004). However, they are not the first ones to suggest a connection between apoptosis and autoimmune diseases. In 1994, Casciola-Rosen et al. (1994) provided evidence of the presence of autoantigens targeted in SLE in various structures observed during the course of apoptosis. More specifically, they recognized two populations of blebs at the surface of apoptotic keranocytes, of which the smaller blebs contained fragmented endoplasmic reticulum, ribosomes and ribonucleoprotein Ro. The larger blebs included nucleosomal DNA, ribonucleoprotein La in addition to Ro as well as small nuclear ribonucleoproteins (Casciola-Rosen et al., 1994). Later on, the ribonucleoprotein Ro was found to collocate with viral antigens into the smaller blebs when apoptosis was induced by Sindbis virus infection (Rosen et al., 1995). Given that systemic exposure to apoptotic cells (Mevorach et al., 1998) and coimmunization with a complex containing both viral and self-antigens (Dong et al., 1994) has been shown to break tolerance to self in a murine model, virus induced apoptosis could provide a mechanism at least for certain autoimmune diseases.

Autoimmune reactions cannot occur unless self-antigens are made available to the immune system. Macrophages are known for their phagocytic capabilities and for the ability to clear apoptotic cells. While macrophages in this way maintain the general cellular

homeostasis, they also actively suppress inflammation (for review on phagocytosis of apoptotic material, see (Savill and Fadok, 2000; Fadok and Chimini, 2001)). It has been shown that the peripheral blood mononuclear cells activated by bacterial lipopolysaccharides produce more of the anti-inflammatory cytokine interleukin (IL) 10 than the pro-inflammatory cytokines tumor necrosis factor α (TNF-α), IL-1β and IL-12 in the presence of apoptotic peripheral blood lymphocytes (Voll et al., 1997). In a study by Fadok et al. (1998) the causal relationship between the phagocytosis of apoptotic cells by peripheral blood mononuclear cells and related cytokines was researched further. It was noticed that the phagocytosis actively inhibited the production of pro-inflammatory cytokines IL-1β, IL-8, granulocyte macrophage colony-stimulating factor (GM-CSF) and TNF-α, but also IL-10 and eicosanoids leucotriene C_4 and thromboxane B2. On the other hand, increase was seen in the production of TGF-β1, prostaglandin E2 and platelet activating factor. These soluble anti-inflammatory mediators were additionally observed to inhibit the pro-inflammatory cytokine production. However, if the apoptotic cells were opsonized with IgG to induce uptake by fragment crystallizable receptors for IgG, increased production of all measured cytokines was observed except for TGF-β1 (Fadok et al., 1998). The internalization mechanism for apoptotic cell has also been shown to be separate from the way macrophages internalize necrotic cells (Krysko et al., 2006). Thus, efficient clearance of apoptotic material is utterly important for maintaining homeostasis and disruptions along the way can have significant biological consequences such as inflammation and autoimmune diseases.

Due to the fact that macrophages are vital components of host defense, their activation must remain tightly controlled. Indeed, classically activated macrophages which arise as a reaction to interferon γ (IFN- γ) production are key mediators in immunopathology of several autoimmune diseases (for review on macrophage activation, see (Mosser and Edwards, 2008)). Synovial tissue macrophages in RA have been shown to produce IL-8, growth regulated oncogene (GRO) α and IFN- γ inducible protein 10 (IP-10) chemokines from the CXC group, macrophage inflammatory protein (MIP) 1α and regulated on activation, normal T-cell expressed and secreted (RANTES) from the CC chemokine group but also IL-1, IL-6, IL-12, TNF-α, macrophage migration inhibitory factor (MIF)

and granulocyte macrophage colony-stimulating factor (GM-CSF) from the cytokine and growth factor groups. These secretory products may have pro-inflammatory, chemoattractant, angiogenic and antiangiogenic effects in RA (for full review on macrophages and their products in RA, see (Szekanecz and Koch, 2007)). Some of the cytokines connected to RA have also been observed in patients during B19V infection. GM-CSF, IL-6, TNF-α, IL-8 and in addition IL-1β, have shown elevated levels during the first weeks of acute B19V infection. In persistently infected patients however, no evident imbalance was seen in their cytokine pattern, apart from elevated IFN- γ levels (Isa et al., 2007). The cytokine pattern in SLE patients as a response to apoptotic cells has been studied as well. When peripheral blood mononuclear cells isolated from SLE patients were exposed to apoptotic cells, TNF-α response was enhanced in contrast to expectations. Typically, the uptake of apoptotic cells by macrophages is associated with increase in TGF-β secretion and diminished production of TNF-α (Sule et al., 2011). In addition, the IL-12 levels in SLE patients are significantly higher compared to normal subjects and the high IL-12 levels have also been connected to increase in interferon γ (IFN-γ) levels (Tokano et al., 1999).

Despite of the comprehensive research done in the field of viral infections and autoimmune diseases, one thing remains clear. The definitive link connecting the dots is yet to be found. Although the answer may lay behind a combination of multiple explanations, this thesis is aimed at investigating one possible reason for how B19V infection might break tolerance to self. Since the B19V NS1 can cause apoptosis in nonpermissive cells, it is hypothesized here that there are self-antigens present in apoptotic bodies which can be introduced to cells responsible for host defense.

2. Aim of the Study

Prior to this study, it had been established that B19V NS1 induces apoptosis in nonpermissive HepG2 cells by damaging DNA and triggering S phase arrest (Kivovich et al., 2012). Since both B19V NS1 (Moffatt et al., 1998; Hsu et al., 2004; Poole et al., 2006) and autoimmune diseases (for review, see (Thompson, 1995; Opferman and Korsmeyer, 2003)) have been connected to apoptosis, this thesis focuses on a mechanism which might cause disruption of tolerance to self as a result of B19V infection. Thus, the first aim of the study was to purify apoptotic bodies created due to B19V NS1 expression in nonpermissive cell line and show the presence of potent self-antigens in those apoptotic bodies. The second aim was then to stimulate differentiated macrophages with these purified apoptotic bodies and to observe the consequence of the phagocytosis.

The two main goals of this study were:

1) To characterize the purified apoptotic bodies produced by expressing B19V NS1 in nonpermissive cells.
2) To show that the purified apoptotic bodies are engulfed by phagocytes of the immune system.

In addition, initial step were taken towards investigating the immune response following engulfment of apoptotic bodies.

3. Materials and Methods

3.1. Cell Culture

Sf9 cells (ATCC-CRL-1711, American Type Culture Collection [ATCC], Manassas, VA, USA), derived from *Spodoptera frugiperda*, were cultured in BioWhittaker® Insect-XPRESS™ Media System (Lonza Walkersville Inc., Walkersville, MD, USA), using shaker flasks and 120 rpm rotation, at 27 ºC. Human hepatocytes, HepG2 cells (ATCC-HB-8056, ATCC, Manassas, VA, USA) were cultured in Minimum Essential Medium (Gibco®, Invitrogen, Carlsbad, CA, USA) supplemented with 10 % heat inactivated fetal bovine serum (Gibco®, Invitrogen, Carlsbad, CA, USA), 100 U or 100 µg/ml penicillin-streptomysin (Gibco®, Invitrogen, Carlsbad, CA, USA) and 2 mM L-glutamine (Gibco®, Invitrogen, Carlsbad, CA, USA). Acute monocytic leukemia derived human monocytes, THP-1 cells (ATCC-TIB-202, ATCC, Manassas, VA, USA) were cultured in RPMI-1640 Medium Hybri-Max™, modified with L-glutamine, 4500 mg/l glucose and 15 mM HEPES (Sigma, Sigma-Aldrich Inc., St. Louise, MO, USA), supplemented with 10 % fetal bovine serum (Gibco®, Invitrogen, Carlsbad, CA, USA), 1 % penicillin-streptomysin (Gibco®, Invitrogen, Carlsbad, CA, USA) and 0.05 mM β-mercaptoethanol. Both HepG2 and THP-1 cells were cultured at 37 ºC, 5 % CO_2, in tissue culture flasks.

3.2. Virus Production

Human parvovirus B19 (B19V) nonstructural protein 1 (NS1) had been previously cloned together with enhanced green fluorescent protein (EGFP) under cytomegalovirus (CMV) immediate-early promoter in a modified pFastBac1 vector (Kivovich et al., 2010). The modified pFastBac1 vector was then used to generate recombinant baculovirus in *Autographa californica* viral vector, forming a structure from now on referred to as *Ac*CMV-EGFP-NS1. Recombinant baculovirus stocks had been prepared using the Bac-to-

Bac® Baculovirus Expression system as previously described by Kivovich et al. (2010). The same way created recombinant baculovirus with only EGFP (*Ac*CMV-EGFP) was generated as a control (Kivovich et al., 2010). *Autographa californica* viral vector (Invitrogen, Carlsbad, CA, USA) stock lacking recombination was used as wild type (WT) control in determining the transduction efficiency (Figure 1) of the amplified baculovirus stocks. Viral stocks were amplified utilizing 50 ml of Sf9 cell culture at a concentration of $2 \cdot 10^6$ cells/ml. The cell culture was infected with 0.5-1.0 ml of second generation viral stock and the infection was followed in 24 h intervals by counting the cells. The viruses were collected when the cell count was 2-3 $\cdot$ 10^6 cells/ml, but no later than 72 h post infection. The cells were spun down for 3 min at 500 relative centrifugal force (RCF). The clarified supernatant was filtered through 0.20 µm low protein binding Filtropur Syringe Filter (Sarstedt, Sarstedt AG & Co., Nümbrecht, DE) and 2.5 % fetal bovine serum (Gibco®, Invitrogen, Carlsbad, CA, USA) concentration was added. The virus stocks were stored at 4 ºC, protected from light.

3.3. Transduction Efficiency of the Baculovirus Stock in HepG2 Cells

HepG2 cells were seeded in above described medium and grown over night. The resulting $1 \cdot 10^6$ cells were washed with warm and sterile 1 x phosphate buffered saline (PBS, 137 mM NaCl, 2 mM KH_2PO_4, 8 mM $Na_2HPO_4 \cdot 2H_2O$ and 3 mM KCL in H_2O) before transducing them with two concentrations (indicated with 200 and 400 in figure 1) of WT, *Ac*CMV-EGFP or *Ac*CMV-EGFP-NS1 baculovirus stocks concluding to multiplicity of infection of ~10. 1 x PBS was used to increase the volume in order to cover the surface area. The treated cells were protected from light and kept in room temperature for 4 h, on a swing. After the incubation period, the baculovirus solution was removed, the cells were washed once with 1 x PBS and returned into growth medium. The cells were incubated at 37 ºC, 5 % CO_2 for 24 h before measuring the transduction efficiency utilizing flow cytometry as described below.

24 h post transduction, the treated cells were washed with 1 x PBS and collected using trypsinization (0.05 % trypsin with EDTA in PBS, Gibco®, Invitrogen, Carlsbad, CA, USA). The trypsin was removed by centrifugation at 500 RCF for 3 min. The cells were washed twice with ice cold 1 x PBS and collected using the same settings. Afterwards the cells were resuspended into 500 µl of 1 x PBS before analyzing the samples. The analysis was done with BD FACSCalibur, collecting 10 000 events using BD Cell Quest Pro Software version 5.2.1. (BD; Becton, Dickinson and Company, Franklin Lakes, NJ, USA). FlowJo Flow Cytometry Analysis Software version 8.4.5. (Tree Star Inc., Ashland, OR, USA) was used for the statistical analysis of the samples. The transduction efficiencies (Figure 1) per both concentrations of analyzed baculovirus stocks are presented as percentages of EGFP signal observed in comparison to total of 10 000 events. Standard deviations (Figure 1) between three separate analyses, one for each produced baculovirus stock, were calculated with Microsoft® Office Excel® 2007 (Microsoft Corporation, Redmont, WA, USA).

3.4. Apoptotic Body Production

Transduction of HepG2 cells was performed as described above. Based on the transduction efficiency analysis of the virus stock, volume providing 70 % transduction efficiency was used to transduce $20 \cdot 10^6$ cells. The volume of the baculovirus solution was increased with 1 x PBS if needed in order to cover the surface area. After the transduction, the cells were incubated in 20 ml of growth medium for 72 h. S4400 Staurosporine from *Streptomyces sp.* (Sigma-Aldrich Inc., St. Louise, MO, USA) treatment was used as a positive control. HepG2 cells seeded simultaneously, using the same seeding density as with the transduced cells, were treated with 1 µM concentration of staurosporine in growth medium 24 h prior to isolation of apoptotic bodies.

The growth medium was collected into sterile Falcon tubes and clarified by centrifugation at 500 RCF for 3 min. The supernatant was filtered through 5.00 µm Millex®-SV Syringe

Driven Filter Unit, PVDF, 25 mm, sterile (Durapore®, Millipore, Billerica, MA, USA) with gravitational force. Apoptotic bodies were then collected with Optima^{TM} L-90K Ultracentrifuge (Beckman Coulter, Brea, CA, USA) at 500 000 RCF for 1 h at 4 º. The supernatant was discarded and the apoptotic bodies purified this way were further treated either for immunolabeling or for feeding experiments.

3.5. Differentiation of THP-1 Cells

$5 \cdot 10^5$ THP-1 cells were seeded in above mentioned medium with additional 200 nM concentration of phorbol-12-myristate-13-acetate (PMA) (Sigma, Sigma-Aldrich Inc., St. Louise, MO, USA) and incubated for 3 days. Differentiation was then further enhanced by replacing the PMA containing medium with fresh RPMI-1640 with the normal supplements and incubating the cells for additional 5 days as described by Daigneault et al. (2010) (Daigneault et al., 2010). All the experiments were done on days 8 to 9 post initiation of differentiation. Differentiation was confirmed with flow cytometry, measuring the size and granularity of the cells with forward and side scatter light and auto-fluorescence on channel FL-1 (Figure 6). BD Biosciences Blue Laser is used on channel FL-1, providing excitation at 488 nm and emission at 530/30 nm (BD; Becton, Dickinson and Company, Franklin Lakes, NJ, USA). PMA-stimulated THP-1 cells (dTHP-1) were compared to untreated THP-1 cells (Daigneault et al., 2010). PMA treated cells were collected by trypsinization. Both cells were washed once with 1 x PBS before the analysis. During the sample preparation, 500 RCF were used to spin the cells down (Eppendorf Centrifuge 5415 D, Eppendorf AG, Hamburg, DE). BD FACSCalibur was used for the flow cytometry, collecting 10 000 events with BD Cell Quest Pro Software version 5.2.1. (BD; Becton, Dickinson and Company, Franklin Lakes, NJ, USA). The statistical analysis was done with FlowJo Flow Cytometry Analysis Software version 8.4.5. (Tree Star Inc., Ashland, OR, USA).

3.6. Stimulating THP-1 Cells

THP-1 cells were stimulated for two purposes. For immunolabeling, apoptotic bodies collected from $20 \cdot 10^6$ Hep2G cells as described above were suspended into 500 µl of Hank's Balanced Salt Solution (Eurobio, Eurobio Laboratories, Courtaboeuf Cedex B, FR), supplemented with 3 mM $CaCl_2$ of which half was used to stimulate $1 \cdot 10^5$ cells. The ratio between stimulated cells and cells used to produce apoptotic bodies was thus 1:100. The apoptotic bodies were added to fresh RPMI-1640 medium, supplemented as described above, and used to cover the cells. The cells were then incubated for 2 h at 37 ºC, 5 % CO_2. After the feeding, the cells were fixed with 4 % paraformaldehyde for 10 min. As a negative control, phagocytosis was inhibited as follows. THP-1 cells were treated for 30 min with $1 \cdot 10^{-5}$ M cytochalasin B (Figure 9) (Axline and Reaven, 1974) from *Helminthosporium dematioideum* (Sigma, Sigma-Aldrich Inc., St. Louise, MO, USA) before the stimulation and the given cytochalasin B concentration was maintained throughout the feeding.

3.7. Cytokine analysis

For analyzing cytokine production, the THP-1 cells were differentiated as described above. The debris, collected during the clarification step of apoptotic body production, was resuspended into 2 ml of RPMI-1640 medium and placed on top of the cells. The cells were incubated for 24 h before collecting the medium. The medium was clarified by centrifuging at 16 100 RCF for 3 min (Eppendorf Centrifuge 5415 D, Eppendorf AG, Hamburg, DE). 1.5 ml sample was taken from the medium and stored at -80 ºC before analysis.

Proteome Profiler™ Array, Human Cytokine Array Panel A (R&D Systems, Inc. Minneapolis, MN, USA) was used to detect cytokines in samples taken from stimulated

THP-1 cells. The protocol for cell culture supernatants was followed according to the commercial kit. SuperSignal® West Dura Extended Duration Substrate (Thermo Scientific, Thermo Fisher Scientific Inc., Rockford, IL, USA) was utilized for chemiluminescence detection. The signal was recorded with ChemiDoc XRS System (Bio-Rad, Bio-Rad Laboratories, Inc., Hercules, CA, USA). The membranes were exposed and the chemiluminescence was recorded every 30 s. The images taken 5 min after exposure (Figures 10A-D and 11A-D) were analyzed with ImageJ version 1.4.3.67 (Schneider et al., 2012), using Dot Blot Analyzer by Gilles Carpentier (Faculte des Sciences et Technologies, Universite Paris 12 Val-de-Marne, FR, http://image.bio.methods.free.fr/dotblot.html) (Figures 10-11). Resulting pixel densities were processed using Microsoft® Office Excel® 2007 (Microsoft Corporation, Redmont, WA, USA).

First, the mean value of the parallel signal spots was calculated and given to each signal location representing a cytokine. The values were then corrected for background signal and the locations not having any signal present were left out. This narrowed the 36 cytokines tested into protein fragment released from complement component C5 (C5a), cluster of differentiation 40 ligand (CD40 ligand), GM-CSF, growth regulated oncogene α (GROα), chemokine C-C motif ligand 1 (I-309), soluble intercellular adhesion molecule 1 (sICAM-1), IFN-γ, IL-1β, IL-1ra, IL-8, IL-10, IL-12 p70, IL-16, IL-17, IL-17E, IL-32α, IP-10, chemokine C-X-C motif ligand 11 (I-TAC), MIF, MIP-1α, MIP-1β, serine protease inhibitor E1 (serpin E1), RANTES, stromal cell derived factor 1 (SDF-1), TNF-α and soluble triggering receptor expressed on myeloid cells 1 (sTREM-1), totaling to 26 cytokines. Later on, the results were normalized using the positive control value of each membrane as a standard. The normalized results of two separate experiments were then combined by calculating mean values and standard deviations for each cytokine and the results were plotted on figures 10 and 11.

3.8. Immunolabeling

Purified apoptotic bodies (Figures 2-5) were blocked for 10 min with 0.15 % glycine (Sigma, Sigma-Aldrich Inc., St. Louise, MO, USA) in PBS and permeabilized for 20 min with 0.1 % Triton X-100 (Fisher, Hampton, NH, USA), 0.01 % NaN_3 and 1 % bovine serum albumin (Sigma, Sigma-Aldrich Inc., St. Louise, MO, USA) in PBS. Primary antibodies (Table 1) were incubated for 1 h and secondary antibodies (Table 1) for 30 min in room temperature. The used antibody products, their dilutions and proper references are collected into table 1. Both labeling steps were followed by permeabilization step with above mentioned solution. In addition, DNA was labeled by incubating the samples for 1 min in 1:1000 Hoechst 33258 (Sigma, Sigma-Aldrich Inc., St. Louise, MO, USA) in H_2O. After each step, the apoptotic bodies were spun down for 10 min at 16 100 RCF (Eppendorf Centrifuge 5415 D, Eppendorf AG, Hamburg, DE). Samples were mounted on glass slides with Mowiol® 4-88 (Calbiochem®, Merck Chemicals Ltd., Nottingham, UK) supplemented with 2.5 % w/v of 1,4-diazabicyclo[2.2.2]octane (DABCO) (Sigma, Sigma-Aldrich Inc., St. Louise, MO, USA). In order to visualize the possible phagocytosis (Figures 7 and 8), the THP-1 or dTHP-1 cells fed with apoptotic bodies were immunolabeled and mounted using the same protocol as above. However, the DNA labeling step with Hoechst 33258 lasted 10 min and dTHP-1 cells did not require centrifuging steps since they are adherent cells. Lysosomal membranes were labeled using lysosomal-associated membrane protein 2 (Lamp2) and Alexa Fluor® 594 (Table 1). For the phagocytic activity analysis (Table 2, Figure 9), part of the samples were labeled using ER-Tracker™ Red (glibenclamide BODIPY® TR) (Molecular Probes Inc., Eugene, OR, USA) with 1:1000 dilution in PBS instead of Lamp2. When Using the ER-Tracker, the permeabilization steps were omitted.

Table 1. Primary and secondary antibodies used for immunolabeling.

Antigen	Isotype	Clonality	Reactivity	Host	Concentration	Working Dilution	Manufacturer / Reference
PRIMARY ANTIBODIES							
Apolipoprotein H (ApoH)	*IgG*	*Polyclonal*	*Human*	*Sheep*	*1 mg/ml*	*1:50*	*Invitrogen, Carlsbad, CA, USA / (Niessen et al., 2000)*
Histone 4 (H4)	*IgG*	*Polyclonal*	*Human/ Mouse/ Rat*	*Rabbit*	*0.5 mg/ml*	*1:25*	*BioVision, Inc., Mountain View, CA, USA*
Ku80	*IgG1*	*Monoclonal*	*Human/ Monkey*	*Mouse*	*0.2 mg/ml*	*1:10*	*Abcam, Cambridge, UK / (Schulz et al., 2007)*
Lysosomal-associated membrane protein 2 (Lamp 2) (H4B4)	*IgG1*	*Not provided*	*Human*	*Mouse*	*1 mg/ml*	*1:50*	*Developmental Studies Hybridoma Bank, University of Iowa, IA, USA / (Kuronita et al., 2002)*
Phospho-histone H2B	*IgG*	*Monoclonal*	*Human*	*Rabbit*	*0.7 mg/ml*	*1:30*	*Upstate Cell Signaling Solutions, Lake Placid, NY, USA / (Neeli et al., 2008)*
Smith	*IgG3*	*Monoclonal*	*Human/ Pig/ Rabbit/ Rat*	*Mouse*	*0.2 mg/ml*	*1:10*	*GeneTex Inc., Irvine, CA, USA / (Lech et al., 2011)*
SECONDARY ANTIBODIES							
Alexa Fluor® 568	*IgG (H+L)*		*Sheep*	*Donkey*	*2 mg/ml*	*1:200*	*Invitrogen, Carlsbad, CA, USA / (Michel et al., 2006)*
Alexa Fluor® 594	*IgG (H+L)*		*Rabbit*	*Goat*	*2 mg/ml*	*1:200*	*Invitrogen, Carlsbad, CA, USA / (Oberti et al., 2010)*
Alexa Fluor® 633	*IgG (H+L)*		*Mouse*	*Goat*	*2 mg/ml*	*1:200*	*Invitrogen, Carlsbad, CA, USA / (Sekerkova et al., 2004)*

3.9. Confocal Imaging

Olympus IX81 microscope with Olympus FluoView 1000 (version 1.76) confocal and ULSAPO oil immersion objective with 60x magnification and 1:35 numerical aperture were used in all of the experiments (Olympus Corporation, Tokyo, JP). Start wavelength for detecting Hoechst 33258 labeled DNA was 425 nm and bright field range 50 nm. For all EGFP labeled objects these values were 500 nm and 30 nm and for Alexa Fluor® 568 as well as for Alexa Fluor® 594 labeled objects 555 nm and 70 nm. Start wavelength for Alexa Fluor® 633 was 650 nm with long-pass filter BA650IF, respectively. The images were processed using with ImageJ version 1.4.3.67 (Schneider et al., 2012). MBF ImageJ collection of plug-ins and macros (McMaster Biophotonics Facility, Hamilton, ON, CA, http://www.macbiophotonics.ca/imagej/) was used for the multichannel merges in figures 3-5 and 7-9. In order to create the orthogonal views on figures 7 and 8 from xyz-stacks, OrthoSaver by Pedro Almada (Instituto Gulbenkian de Ciência, Oieras, PT, http://uic.igc.gulbenkian.pt/macros/OrthoSaver.ijm) was applied. For the phagocytic activity, the Analyze Particles -function of ImageJ was utilized. Particles visible on the channel applied for EGFP were calculated both in and outside of the cells, in two experimental image sets, featuring dTHP-1 cells fed with *Ac*CMV-EGFP or *Ac*CMV-EGFP-NS1 transduced or staurosporine induced apoptotic bodies in xy-dimensions. Approximately 50 cells per treatment, in two sets totaling to about 100 cells, were included into the calculation of the phagocytic activity, depending on how many cells were present on the randomly selected images. Representative images from the experiment can be seen in figure 9. The phagocytic activity (Table 2) was calculated as the following equation (Frisoni et al., 2005) indicates:

$$\frac{Number\ of\ dTHP-1\ Cells\ Engulfing\ Apoptotic\ Bodies}{Total\ Number\ of\ dTHP-1\ Cells} \times 100\ \%$$

Errors presented in table 2 were calculated using the standard deviation equation on Microsoft® Office Excel® 2007 (Microsoft Corporation, Redmont, WA, USA).

4. Results

4.1. Transduction Efficiency of Baculovirus Stock in HepG2 Cells

In order to produce apoptotic bodies effectively and with constant transduction efficiency, the transduction efficiency of the baculovirus stock was measured prior to use (Kivovich et al., 2010). Since HepG2 cells are nonpermissive by default for B19V, high transduction efficiency was required to ensure proper apoptotic body production. The transduction efficiency (Figure 1) was determined using flow cytometry. A percentage of events presenting signal originating from EGFP out of total 10 000 events (Figure 1) were measured from wild type (WT), *Ac*CMV-EGFP and *Ac*CMV-EGFP-NS1 transduced samples, in two baculovirus concentrations, designated as 200 and 400. The WT acted as the negative control. Three separate measurements were performed so as to have baculovirus stocks with known transduction efficiency at hand for the production of apoptotic bodies. The known transduction efficiencies varied to some extent between experiments which can be seen in figure 1 standard deviation. As expected, the higher baculovirus concentration indicated with 400 in *Ac*CMV-EGFP and *Ac*CMV-EGFP-NS1 samples gave higher transduction efficiencies in comparison to the lower concentration indicated with 200. The difference between these concentrations was approximately 10 % which does not clearly relate to the doubling of the concentration. Considerably bigger difference could be expected without having knowledge of high baculovirus concentration being able to exhaust the system by killing vast amount of the cells prior to the experiment. This was taken into account when using the newly measured transduction efficiencies to calculate 70 % constant transduction efficiency for apoptotic body production. Thus, the calculations were always based on the transduction efficiency measured using the lower 200 concentration if the system displayed effects of exhaustion by not exhibiting clearly higher transduction efficiency in the samples designated as 400.

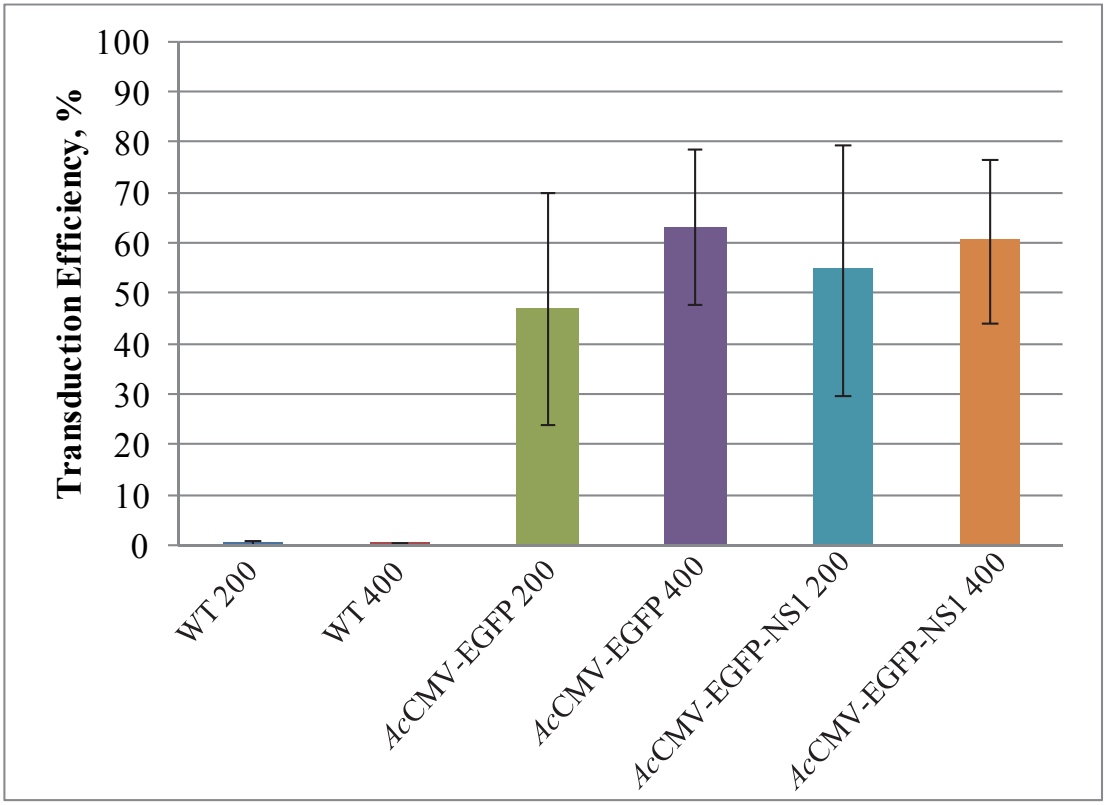

Figure 1. Transduction efficiency of the baculovirus stocks. Transduction efficiency was measured for the *Ac*CMV-EGFP and *Ac*CMV-EGFP-NS1 baculovirus stocks, as the presence of signal originating from EGFP in comparison to WT negative control, using flow cytometry and FL1-H channel (excitation at 488 nm, emission 530 nm). The bars represent the percentage of cells positive for EGFP signal out of the total 10 000 events after transduction with selected baculovirus stock. Three separate analyses were performed and the variation between experiments is indicated as the standard deviation visualized with error bars. Two concentrations per baculovirus stock were used, highlighted here with 200 and 400, 400 representing two times higher concentration in comparison to 200, respectively.

4.2. Nucleosomal and Cytosolic Self-Antigens Are Present in Apoptotic Bodies Induced by B19V NS1 Expression

Formation of apoptotic bodies implies that these entities contain proteins originating from the dying cells. Since NS1 has been previously associated with DNA damage resulting to apoptosis (Kivovich et al., 2010; Poole et al., 2011; Kivovich et al., 2012), this study was executed in order to characterize the purified apoptotic components. Induction period of 72 h was used in order to ensure sufficient initiation of apoptosis (Moffatt et al., 1998) in HepG2 cells with *Ac*CMV-EGFP, *Ac*CMV-EGFP-NS1 and staurosporine. Comparison of the extent of the apoptotic body production in each of the conditions is presented in figure

2. The extent of apoptosis is clearly higher in samples produced using *Ac*CMV-EGFP-NS1 (Figure 2B) as can be stated based on the higher amount of apoptotic bodies present in the differential interference contrast (DIC) image in comparison to *Ac*CMV-EGFP (Figure 2A) induced and staurosporine treated samples (Figure 2C). Additionally, the signal originating from EGFP in figure 2B further highlights the vast amount of apoptotic bodies in *Ac*CMV-EGFP-NS1 compared to *Ac*CMV-EGFP (Figure 2A) induced samples. As EGFP is not present in the staurosporine treated samples (Figure 2C), signal originating from EGFP cannot be detected in these samples. Despite of the apoptotic bodies being filtered through 5.0 µm filter, some of the apoptotic bodies seen in figures 2-5 are remarkably larger. The increase in size is an indication of aggregation due to the centrifugation step which should be addressed by decreasing the RCF.

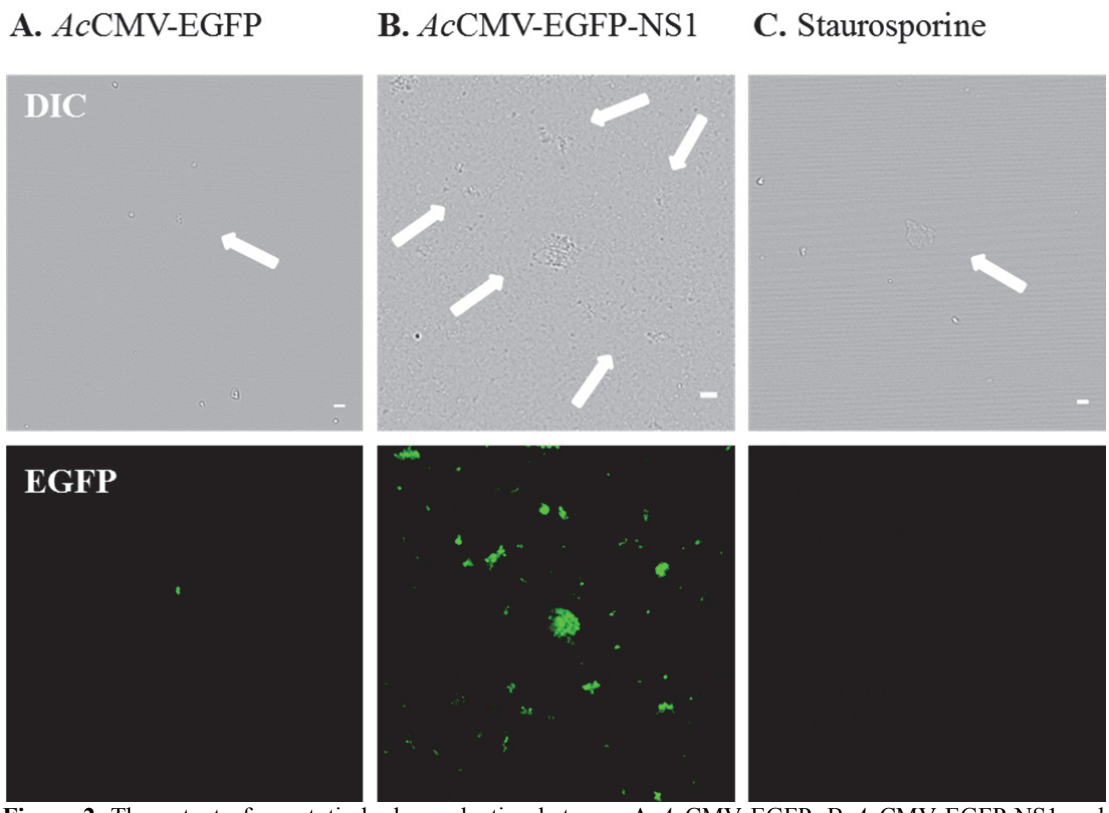

Figure 2. The extent of apoptotic body production between A *Ac*CMV-EGFP, B *Ac*CMV-EGFP-NS1 and staurosporine treated samples. Alexa Fluor® 488 channel was used to visualize the EGFP signal (excitation wavelength 488 nm) with green and DIC microscopy to visualize the morphology of the apoptotic bodies. The extent of apoptosis is the highest in B, *Ac*CMV-EGFP-NS1 induced samples as visualized by the elevated level of apoptotic bodies present in the sample in comparison to A, *Ac*CMV-EGFP induced or C, staurosporine treated samples. Scale bars 10 µm.

Subsequently, the resulting apoptotic bodies were purified and immunolabeled for nuclear self-antigens, H4 and Ku80 (Figure 3) as well as Smith and H2B (Figure 5) and for cytosolic constituents, ApoH and Lamp2 (Figure 4). In addition, DNA (Figures 3-5) was stained from the apoptotic bodies with Hoechst 33258 and then imaged using confocal microscopy. The signal originating from each of the channels used for visualization of the labels was merged together in order to examine the location of the labels in each apoptotic body. By comparing the merge image (Figures 3-5) to the individual labels and to the DIC image of the sample in question, it was confirmed that all observed antigens and EGFP, when applicable, are actually present in the examined apoptotic body. Consequently, each of the observed labels was also confirmed to be truly present by ruling out possible bleed through effect and by performing appropriate isotype controls. As expected, only signals originating from channels dedicated to visualization of DNA and EGFP were observed in the isotype controls in relevant samples (results not presented here). The DIC images (Figures 3-5) were additionally used to demonstrate the granular morphology characteristic for apoptotic bodies.

The representative images from samples produced by *Ac*CMV-EGFP and *Ac*CMV-EGFP-NS1 transduction and by staurosporine treatment indicate that DNA, visualized with blue (Figures 3-5), H4 and Ku80, visualized with yellow and purple (Figure 3) are all present in resulting apoptotic bodies in all tested conditions. Additionally, EGFP and EGFP-NS1, visualized with green can be seen in the produced apoptotic bodies (Figures 3-5, panels A and B). Parallel experiments were conducted both for ApoH and Lamp2 (Figure 4) and for H2B and Smith (Figure 5). Cytosolic constituents, ApoH and Lamp2, visualized with yellow and purple (Figure 4) as well as nuclear antigen Smith, visualized with purple (Figure 5), were found to be present in the apoptotic bodies. However, nuclear antigen H2B was absent in all tested conditions (Figure 5). Thus, these results seem to indicate the presence of specific nucleosomal and cytosolic antigens in the purified apoptotic bodies induced by NS1 expression.

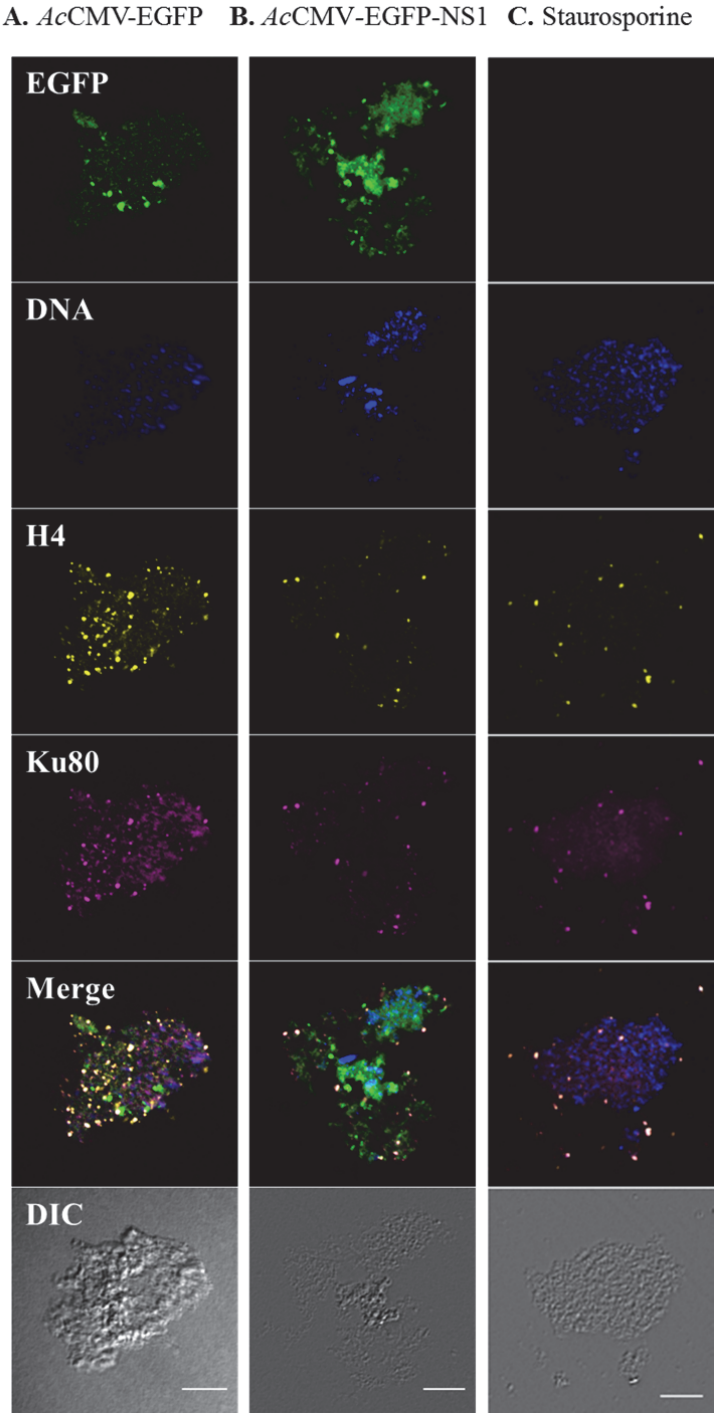

Figure 3. Nuclear antigens DNA, H4 and Ku80 are present in *Ac*CMV-EGFP-NS1 induced apoptotic bodies. Confocal microscope images of apoptotic bodies produced using A, *Ac*CMV-EGFP, B *Ac*CMV-EGFP-NS1 transduced and C, staurosporine treated HepG2 cells. Purified apoptotic bodies were visualized through suitable channels. Applied channels were: DAPI channel, using excitation wavelength 405 nm for DNA, Alexa Fluor® 488 for EGFP (488 nm), Alexa Fluor® 594 for H4 (543 nm) and Alexa Fluor® 633 for Ku80 (633 nm). Channel merge was utilized to visualize the location of the labels and DIC microscopy to visualize the morphology of the apoptotic bodies. Scale bars 10 µm.

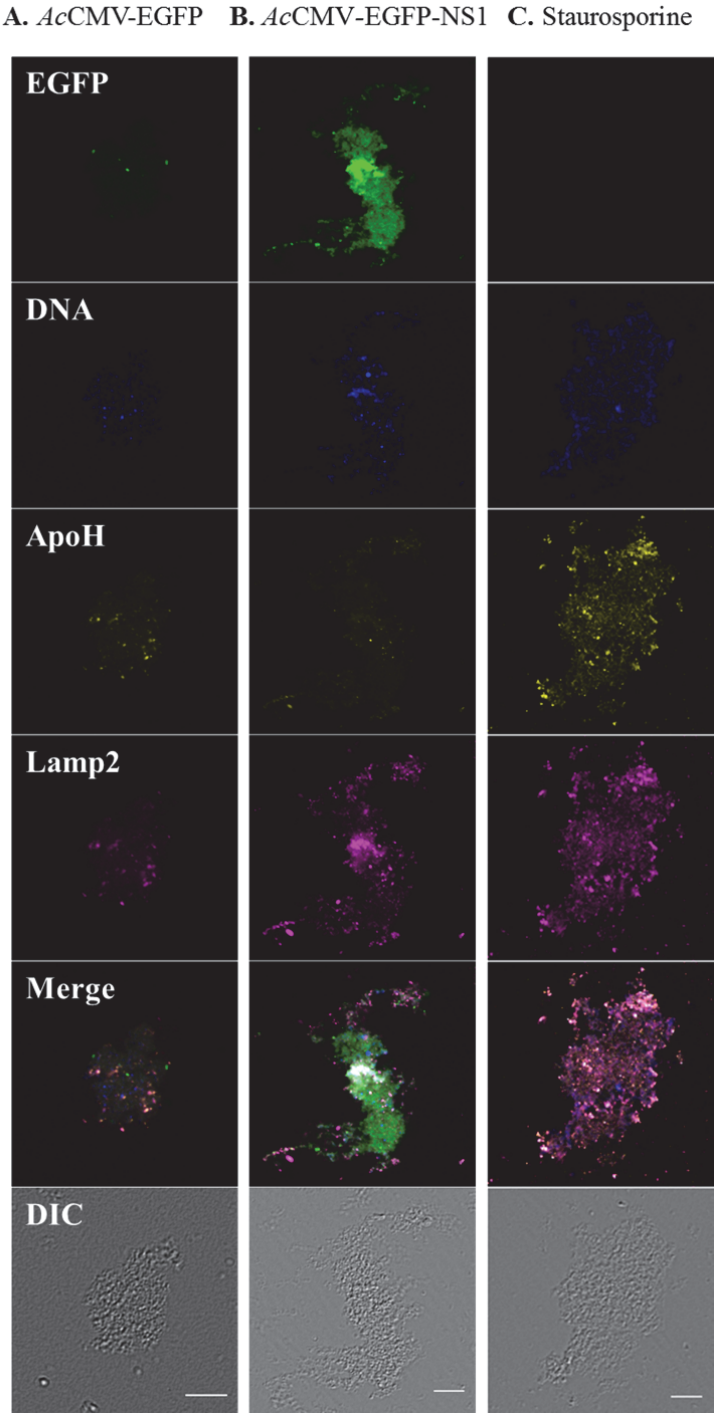

Figure 4. Nuclear antigen DNA and cytosolic antigens ApoH and Lamp2 are present in *Ac*CMV-EGFP-NS1 induced apoptotic bodies. For the images, apoptotic bodies produced using A, *Ac*CMV-EGFP, B *Ac*CMV-EGFP-NS1 transduced and C, staurosporine treated HepG2 cells were visualized using confocal microscopy. Purified apoptotic bodies were imaged through suitable channels which were DAPI channel, using excitation wavelength 405 nm for DNA, Alexa Fluor® 488 for EGFP (488 nm), Alexa Fluor® 568 for ApoH (543 nm) and Alexa Fluor® 633 for Lamp2 (633 nm). Channel merge facilitated the observation of the location of the labels and DIC microscopy facilitated the visualization of the explicit morphology of the apoptotic bodies. Scale bars 10 µm.

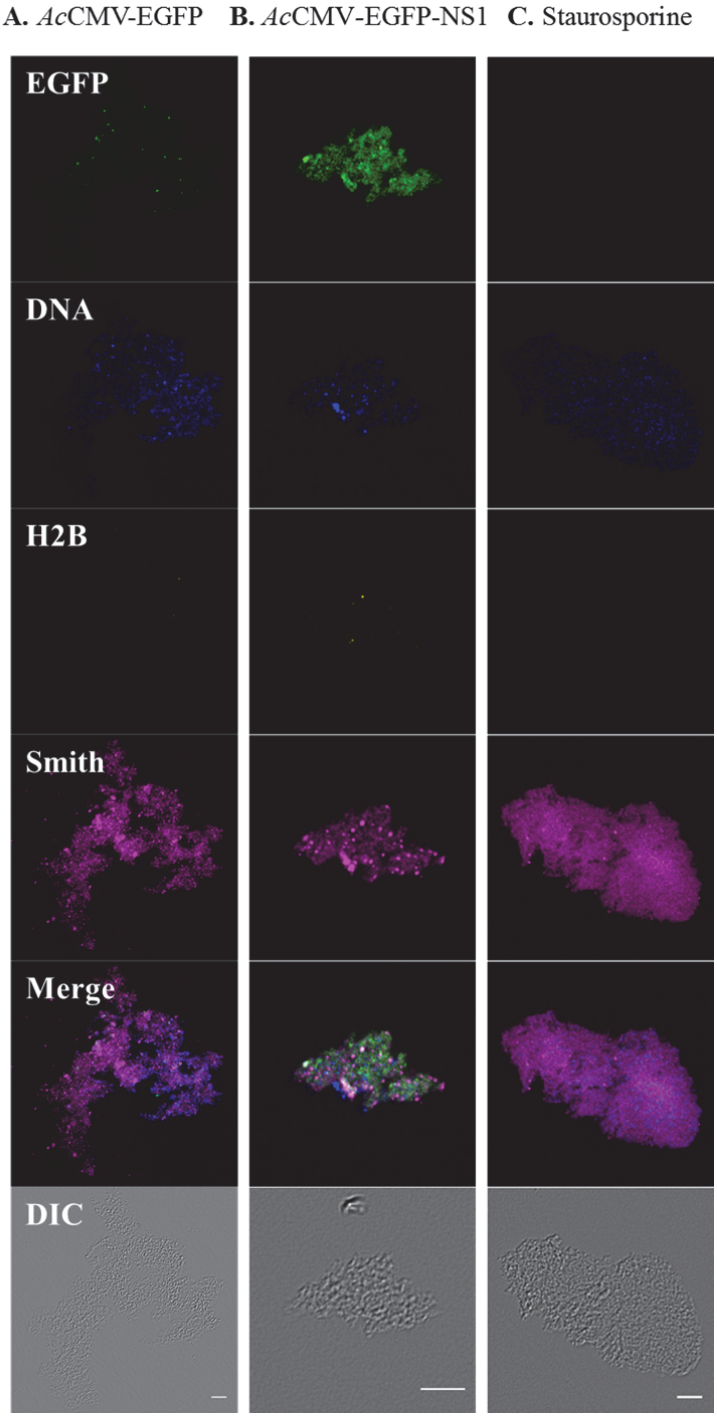

Figure 5. Nuclear antigens DNA and Smith are present but H2B is not, in *Ac*CMV-EGFP-NS1 induced apoptotic bodies. Confocal microscope images of apoptotic bodies were produced using A, *Ac*CMV-EGFP, B *Ac*CMV-EGFP-NS1 transduced and C, staurosporine treated HepG2 cells. Purified apoptotic bodies were visualized through suitable channels considering the labels used: DAPI channel with excitation wavelength 405 nm for DNA, Alexa Fluor® 488 for EGFP (488 nm), Alexa Fluor® 594 for H2B (543 nm) and Alexa Fluor® 633 for Smith (633 nm). The location of the labels was confirmed using channel merge and the granular morphology of the apoptotic bodies was visualized using DIC microscopy. Scale bars 10 µm.

4.3. PMA-Stimulated THP-1 Cells Resemble Monocyte-Derived Macrophages

Daigneault et al. (2010) showed that PMA-stimulated THP-1 cells resemble monocyte-derived macrophages more closely than 1,25-dihydroxyvitamin D3 stimulated cells. It was shown that 5 day resting period in culture medium free of PMA was central for higher cytoplasmic to nuclear ratio, increased mitochondrial and lysosomal numbers. The differentiation-dependent cell surface markers also started to more closely resemble those of monocyte-derived macrophages (Daigneault et al., 2010). Following the protocol by Daigneault et al. (2010), similar results were reached after 3 day PMA-stimulation and 5 day resting period in three independent experiments. Using flow cytometry, comparable forward light scatter (FSC-H) and side light scatter (SSC-H) plots as well as autofluorescence histograms were seen in THP-1 and dTHP-1 cells (Figure 6B and 6C). The increase seen after the differentiation in the FSC-H signal points toward the higher cytoplasmic to nuclear ratio and in SSC-H signal toward increase in granularity as more certain membrane bound organelles are formed. Another distinguishing characteristic in the macrophage differentiation is autofluorescence. Although the autofluorescence is not as high as in the study by Daigneault et al. (2010) in the dTHP-1 cells, there is a clear difference in comparison to THP-1 cells when examining the mean values given in figure 6C. The morphology was additionally analyzed using confocal microscopy. The change in morphology resulting from the increase in cytoplasmic volume in dTHP-1 cells in comparison to THP-1 cells can be seen in the DIC image (Figure 6A). Therefore it can be concluded that PMA-stimulated THP-1 cells differentiate into macrophages.

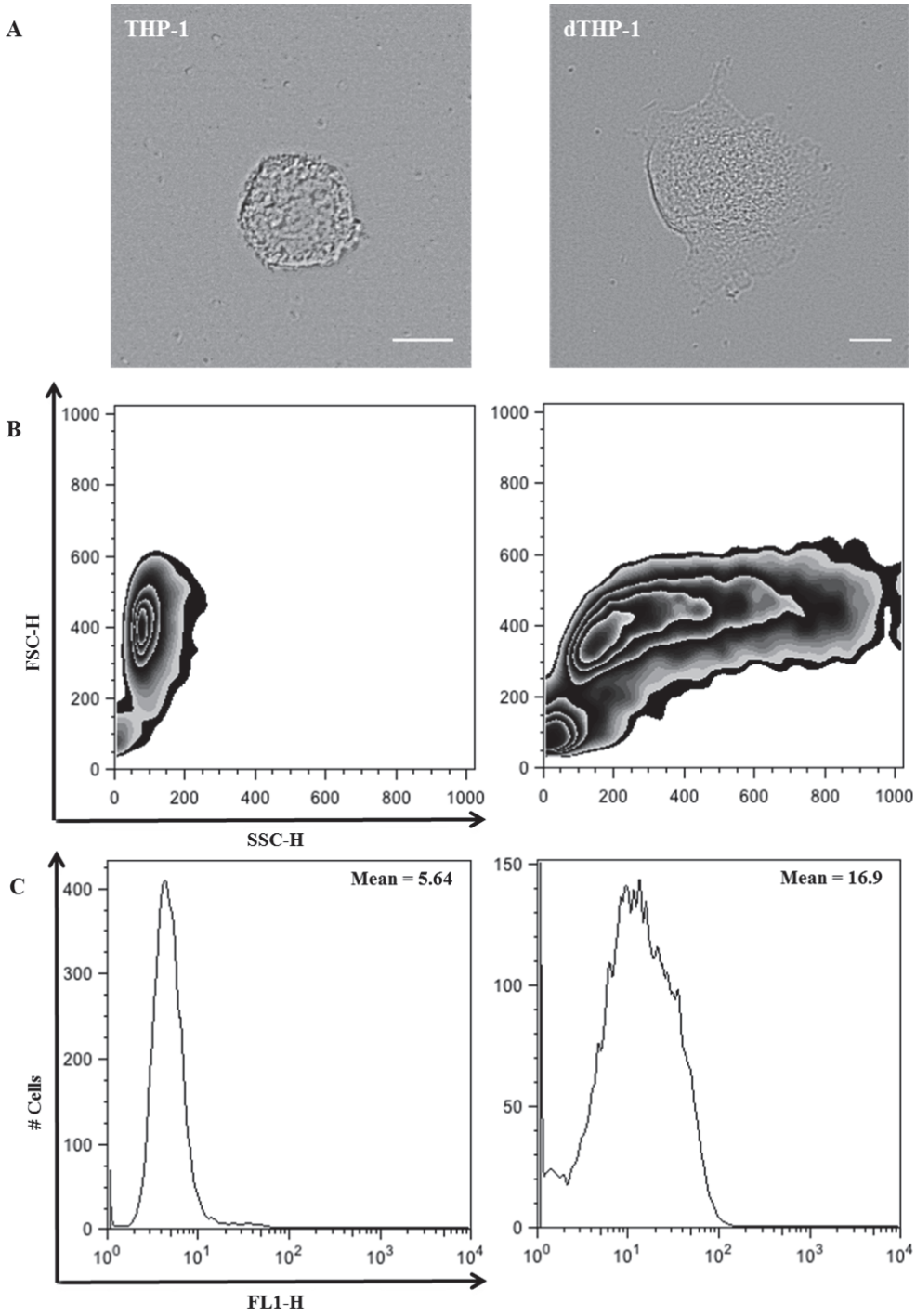

Figure 6. PMA-stimulated THP-1 cells differentiate into macrophages. A, DIC microscopy was used to visualize the difference in morphology between THP-1 and dTHP-1 cells. Scale bars 10 µm. B, increasing FSC-H signal on y-axis indicates enhanced cell size after the PMA-stimulation and the increase in SSC-H signal on x-axis indicates higher granularity in dTHP-1 cells in comparison to THP-1 cells. C, dTHP-1 cells are and THP-1 cells are not autofluorescent when visualized through the FL1-H channel of the used flow cytometer (excitation at 488 nm, emission 530 nm). This conclusion is drawn from the fact that in dTHP-1 sample most of the cells (y-axis) give values higher than 10^1 through the FL1-H channel (x-axis) while most of the THP-1 cells are located below this value.

4.4. Introduction of Apoptotic Bodies to Differentiated Macrophages

In order to investigate if there could be immunological consequences from the purified apoptotic bodies, dTHP-1 cells were treated with *Ac*CMV-EGFP, *Ac*CMV-EGFP-NS1 and staurosporine induced apoptotic bodies. Stimulation was executed for 2 h and afterwards the dTHP-1 cells were washed, fixed and immunolabeled for lysosomes. DNA/nucleus was stained using Hoechst 33258. Normal dTHP-1 cells (Figure 7A) and dTHP-1 cells exposed to apoptotic bodies from *Ac*CMV-EGFP (Figure 7B) and *Ac*CMV-EGFP-NS1 (Figure 7C) transductions can be seen in figure 7. The dTHP-1 cells exposed to apoptotic bodies from staurosporine treatment are in figure 7D. The figures 7A-D are each divided into seven sections of which the main panel includes a merge of the all observed channels on the particular xy-layer of the z-axis selected for optimal representation of the cell as a whole. The white lines cutting through the main panel indicate the locations selected for composing the orthogonal views next to each main panel. The white line from top to bottom is the location for the orthogonal view on the right and the line from left to right is the location for the orthogonal view on the bottom. As all of the xy-layers on z-axis come together in the orthogonal views, this angle aid in judging whether an apoptotic body is inside a cell or not. Under the main panel, all of the channels seen in the main panel are separated into individual panels. That way each of the channels can be evaluated without interference from the other channels as the nucleus is visualized in blue, signal from EGFP or from autofluorescence in green and lysosomes in red. The morphology of the imaged cells can be seen in the remaining DIC panel in order to confirm the examined cell is dTHP-1 (Figure 7).

In figure 7B, signal resulting from *Ac*CMV-EGFP and in figure 7C from *Ac*CMV-EGFP-NS1 transduced apoptotic bodies can be seen inside the dTHP-1 cell. The internalization of apoptotic bodies visible on top of the nucleus in the main panels of both figure 7B and 7C is confirmed in the orthogonal views. The autofluorescence of the dTHP-1 cells is additionally seen through the same channel as the signal from EGFP but signal originating from apoptotic bodies is not present in the images representing staurosporine treated cells

(Figure 7D) nor the cells that were not treated with apoptotic bodies (Figure 7A), respectively.

Similar experiment, leaving out the cells without feeding, was carried out with THP-1 cells. THP-1 cells, as represented in figure 8, exposed to *Ac*CMV-EGFP transduced apoptotic bodies (Figure 8A) does not seem to internalize apoptotic bodies. However, THP-1 cells can internalize *Ac*CMV-EGFP-NS1 transduced apoptotic bodies as shown in figure 8B. There an apoptotic body can be seen on the right side of the nucleus and the internalization is confirmed through the orthogonal views. The THP-1 cells fed with apoptotic bodies from staurosporine treated cells (Figure 8C) provide the null value in this experiment (Figure 8).

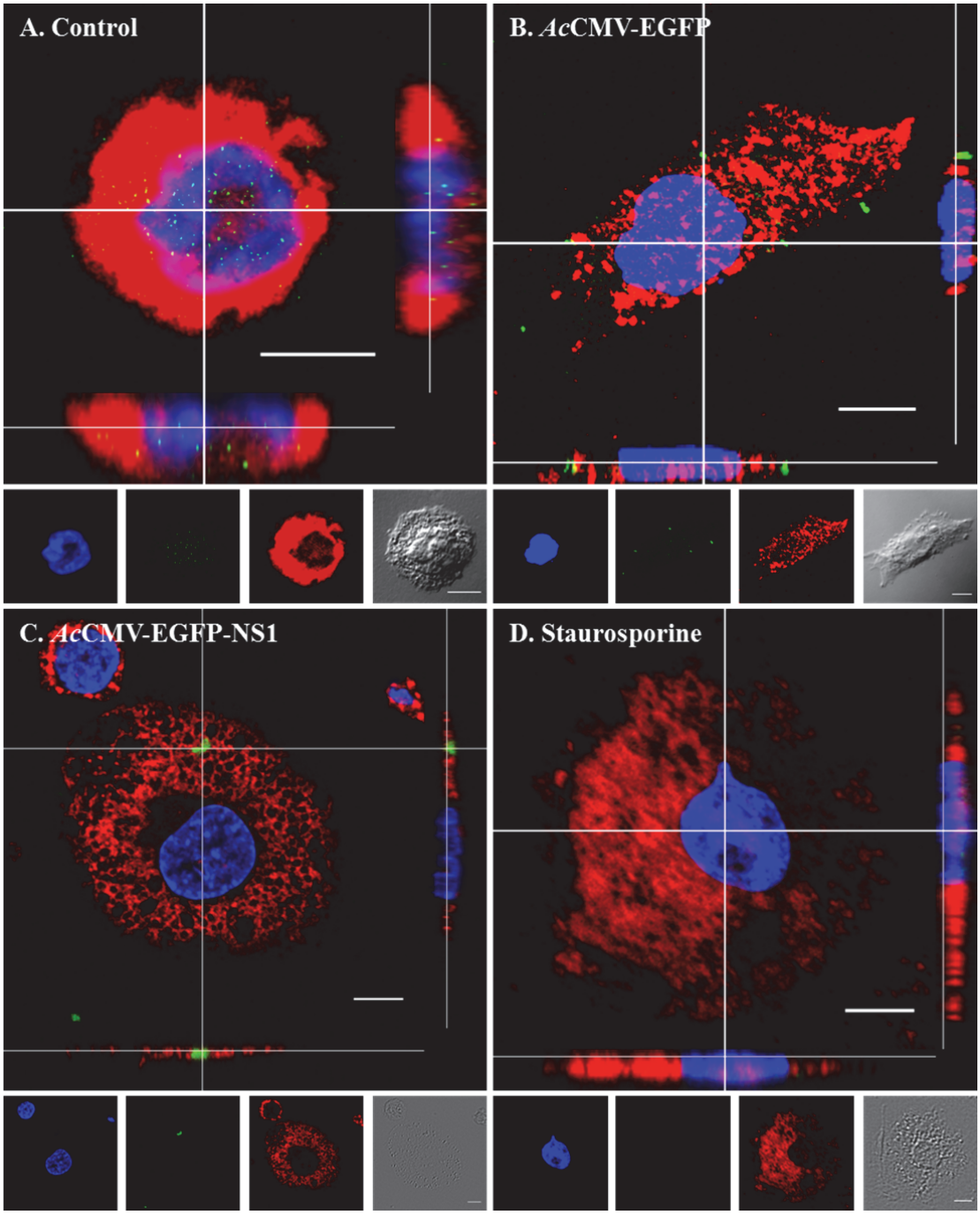

Figure 7. *Ac*CMV-EGFP and *Ac*CMV-EGFP-NS1 transduced apoptotic bodies are engulfed by dTHP-1 cells. xyz-stacks were used to visualize the engulfment. Selected xy-layer can be seen in the main images, as well as in the subscript panels, and xz- and yz-orthogonal views on the right and bottoms sides of the main images. DNA/nucleus was visualized through DAPI channel, using excitation wavelength 405 nm, EGFP and autofluorescence through Alexa Fluor® 488 (488 nm) and lysosomes, by immunolabeling Lamp2, through Alexa Fluor® 633 (633 nm). DIC microscopy was utilized to visualize the dTHP-1 cell morphology. A no apoptotic bodies, B apoptotic bodies from *Ac*CMV-EGFP transduction, C apoptotic bodies from *Ac*CMV-EGFP-NS1transduction and D apoptotic bodies from staurosporine treatment. Scale bar 10 µm.

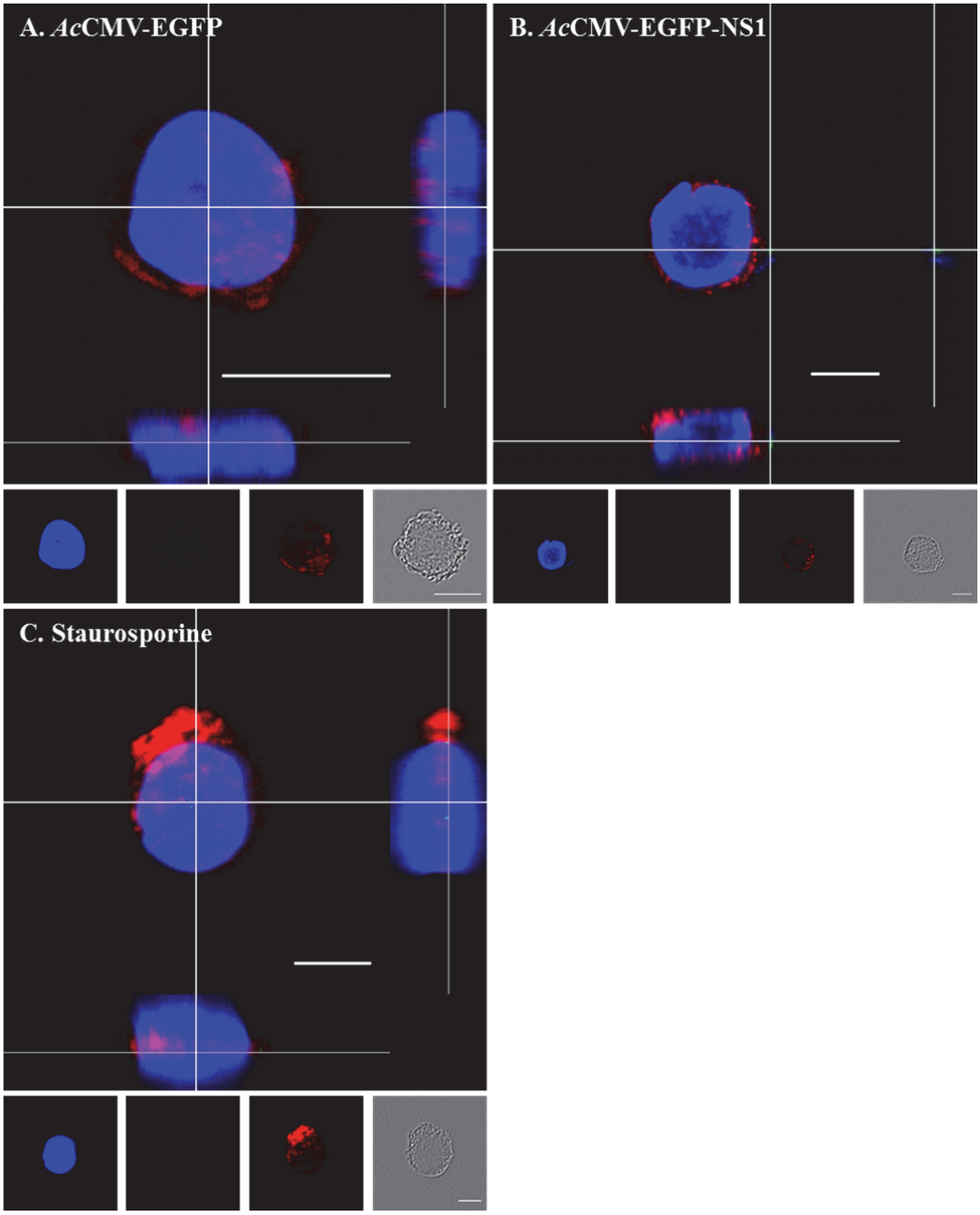

Figure 8. THP-1 cells are capable of engulfing apoptotic bodies but in lesser degree than dTHP-1 cells. xyz-stacks were used to visualize the possible engulfment. Selected xy-layer can be seen in the main images, as well as in the subscript panels, and xz- and yz-orthogonal views on the right and bottoms sides of the main images. DNA/nucleus was visualized through DAPI channel, using excitation wavelength 405 nm, EGFP through Alexa Fluor® 488 (488 nm) and lysosomes, by immunolabeling Lamp2, through Alexa Fluor® 633 (633 nm). DIC microscopy was utilized to visualize the THP-1 cell morphology. A apoptotic bodies from *Ac*CMV-EGFP transduction, B apoptotic bodies from *Ac*CMV-EGFP-NS1transduction, one possibly internalized on the right side of the nucleus and C apoptotic bodies from staurosporine treatment. Scale bar 10 µm.

dTHP-1 cells were additionally exposed to inhibition studies, utilizing phagocytosis inhibitor cytochalasin B. The phagocytic activity of dTHP-1 cells, when exposed to apoptotic bodies with or without cytochalasin B treatment, were examined by calculating apoptotic bodies present in cells from single layer confocal images (Table 2). The number of cells engulfing apoptotic bodies was compared to the total number of macrophages both in normal and cytochalasin B treated samples resulting into the phagocytic activity (Table 2). The inhibition percentage was derived by calculating the decrease in phagocytic activity due to cytochalasin B. Representative images from cytochalasin B treatment in dTHP-1 cells fed with apoptotic bodies from *Ac*CMV-EGFP (Figure 9A) and *Ac*CMV-EGFP-NS1 (Figure 9B) transduced HepG2 cells can be seen in figure 9. There DNA/nucleus is labeled with Hoechst 33258 and visualized with blue and lysosomes with Lamp2, visualized in red. Signal originating from EGFP can be seen as green. These separate channels come together in the merge image (Figure 9) where the location of the apoptotic bodies can be better evaluated. DIC microscopy was used to determine the morphology of the dTHP-1 cells. The phagocytic activity of dTHP-1 cells exposed to *Ac*CMV-EGFP-NS1 transduced apoptotic bodies was the most active at 24.5±4.5 %, in comparison to 19.4±3.2 % in cells exposed to *Ac*CMV-EGFP transduced apoptotic bodies or 21.0 ± 2.8 % in cells treated with staurosporine apoptotic bodies. The phagocytosis seemed to be inhibited the most, 76.2 %, with cytochalasin B in cells treated with apoptotic bodies produced using staurosporine. While the phagocytic activity decreased notably in the dTHP-1 cells fed with *Ac*CMV-EGFP transduced apoptotic bodies, 51.0 %, the decrease was only slight, 6.0 %, in the cells fed with *Ac*CMV-EGFP-NS1 transduced apoptotic bodies (Table 2).

Table 2. The phagocytic activity is highest in dTHP-1 macrophages stimulated with *Ac*CMV-EGFP-NS1 transduced apoptotic bodies. Following formula was used to calculate the phagocytic activity in normal and cytochalasin B treated samples: (number of macrophages containing engulfed apoptotic bodies / total number of counted macrophages) x 100 %. The decrease in phagocytic activity due to cytochalasin B is expressed as the inhibition %.

Apoptotic Bodies	No. of Apoptotic Body Engulfing Macrophages	Total No. of Macrophages	Phagocytic Activity %	No. of Apoptotic Body Engulfing Macrophages with Cytochalasin B	Total No. of Macrophages with Cytochalasin B	Phagocytic Activity %	Inhibition % with Cytochalasin B
*Ac*CMV-EGFP Transduction	*21*	*108*	*19.4 ± 3.2*	*10*	*105*	*9.5 ± 3.8*	*51.0*
*Ac*CMV-EGFP-NS1Transduction	*24*	*98*	*24.5 ± 4.5*	*26*	*113*	*23.0 ± 2.7*	*6.0*
Staurosporine Treatment	*21*	*100*	*21.0 ± 2.8*	*4*	*80*	*5.0 ± 5.1*	*76.2*

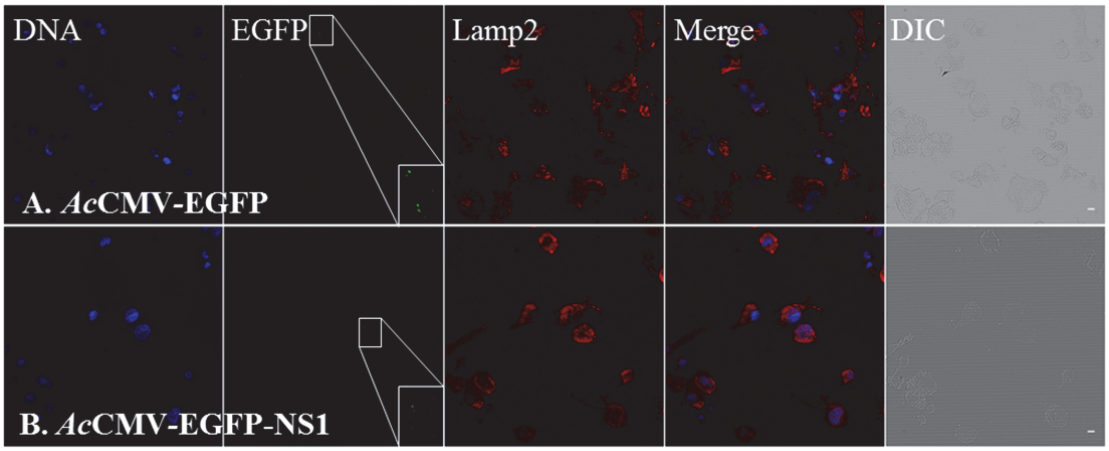

Figure 9. Cytochalasin B treatment in dTHP-1 cells stimulated with apoptotic bodies from A, *Ac*CMV-EGFP and B, *Ac*CMV-EGFP-NS1 transduced HepG2 cells. Although sample A presents more signal originating from EGFP, seen especially in the 2.5x magnifications, this sample type did not engulf apoptotic bodies to extent. DNA/nucleus was visualized through DAPI channel, using excitation wavelength 405 nm, EGFP through Alexa Fluor® 488 (488 nm) and lysosomes, by immunolabeling Lamp2, through Alexa Fluor® 633 (633 nm). DIC microscopy was utilized to visualize the dTHP-1 cell morphology. Scale bar 10 µm.

4.5. Cytokine Production by Differentiated THP-1 Cells

After confirming that dTHP-1 cells are internalizing the apoptotic bodies of interest, the examination of possible immunological effects was carried on to preliminary cytokine study. Using 24 h time point, excreted cytokines were analyzed from the cell culture supernatant with the above mentioned kit. dTHP-1 cells were fed with *Ac*CMV-EGFP and *Ac*CMV-EGFP-NS1 transduced apoptotic bodies as well as with apoptotic bodies from the staurosporine treatment. Culture medium from nonfed dTHP-1 cells was used as a control. The experiment was repeated twice and the results from the both sets can be seen in the A to D western blots of figures 10 and 11 as well as in the included relative intensity graphs. In the graphs, the pixel density of each cytokine was first normalized using the positive control of the respective blot which gave the relative intensity values of the y-axis. The relative intensities were additionally compared between the two experiments by calculating mean values and standard deviations for each cytokine (Figures 10 and 11). Based on the control blots and relative intensity graph from figure 10, cytokines MIF, RANTES and IL-1ra seem to be present in the samples by default. These cytokines can also be found from the staurosporine treated apoptotic body samples, in addition to sICAM-1, IL-8 and Serpin E1. The cytokine that distinguishes the *Ac*CMV-EGFP and *Ac*CMV-EGFP-NS1 transduced apoptotic body feeding conditions from the rest of the samples is IP-10. IP-10 is present in these samples in addition to the cytokines also found in the staurosporine treated apoptotic body samples (Figure 11).

In contrast to all other tested conditions, protein fragment released from complement component C5 (C5a) is not present in the samples produced using *Ac*CMV-EGFP-NS1 transduced apoptotic bodies as can be seen from the blots (Figure 11C and 11D) and from the *Ac*CMV-EGFP-NS1 graph (Figure 11). Although the statistical significance was not tested due to the preliminary nature of the experiment, it seems like MIF on the other hand is expressed slightly more in *Ac*CMV-EGFP-NS1 (Figure 11) than in the rest of the samples (Figures 10 and 11). Given that MIF has been found to be more abundant in synovial fluid and in synovial lining CD14+ macrophages of RA patients compared to

controls (Leech et al., 1999), B19V NS1 induced apoptosis in nonpermissive cells might contribute to loosing tolerance to self. As with MIF, similar results have been gained with IP-10 (Patel et al., 2001) as well as with IL-8 (for review on IL-8, see (Baggiolini and Clark-Lewis, 1992)) and sICAM-1 has been connected to SLE (Elwy et al., 2010) which does encourage to take a closer look into the cytokines expressed by APCs due to B19V NS1.

Staurosporine

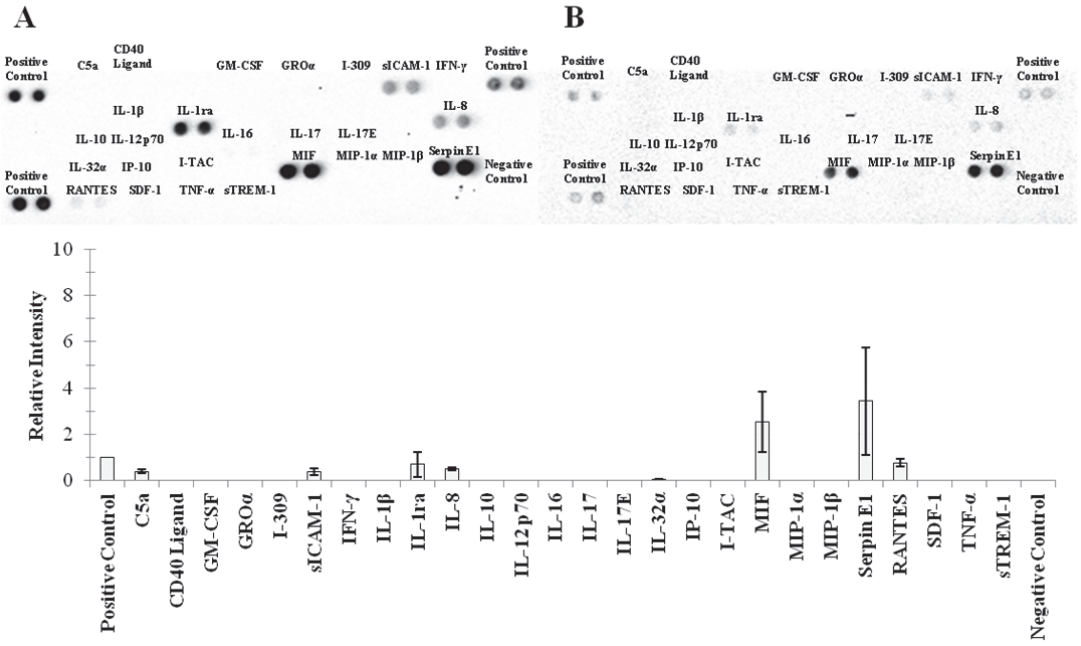

Control

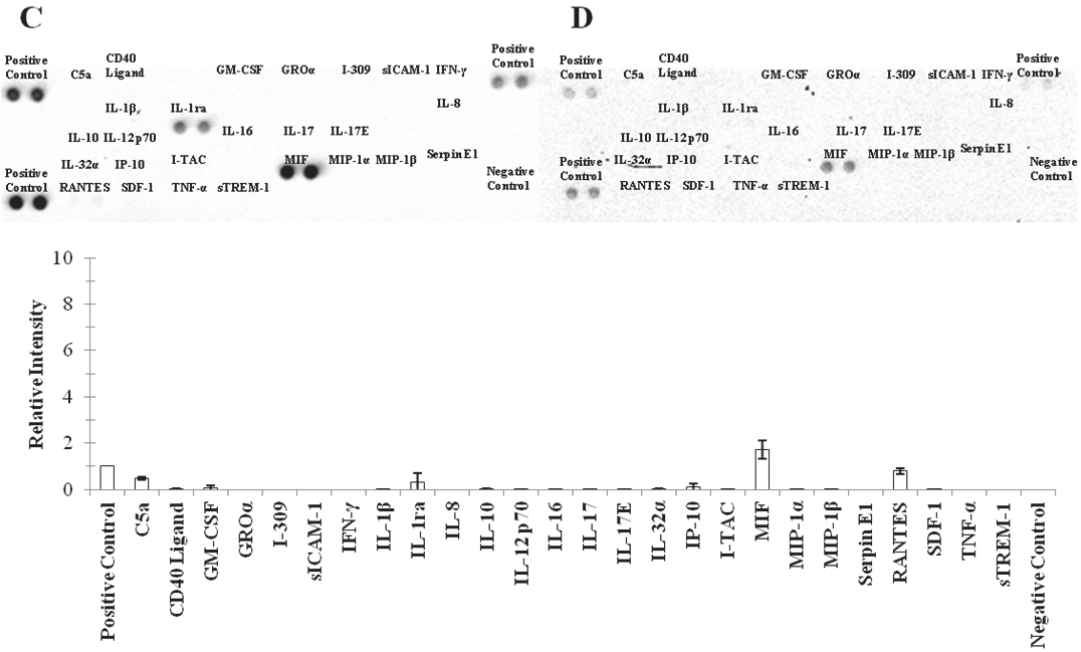

Figure 10. Cytokine production of dTHP-1 cells. Cytokine production of dTHP-1 cells was analyzed in two separate experiments, A and B for staurosporine and C and D for control, respectively. Upper panels represent dTHP-1 cells stimulated with apoptotic bodies from staurosporine treatment and lower panels the control samples without feeding. The samples seem to have same cytokines present, except for sICAM-1, IL-8 and Serpin E1, which are only found in the samples originating from apoptotic body stimulation from staurosporine treatment. The relative intensities presented in the graphs were measured from the presented western blot membranes after 5 min exposure, capturing the chemiluminescence signal with CCD camera and by normalizing the resulting pixel densities using positive control values as standards. Consequently, two separate experiments for both conditions were compared as visualized in the graphs using mean relative intensities on the y-axis for each cytokine and standard deviation to address the differences between the experiments.

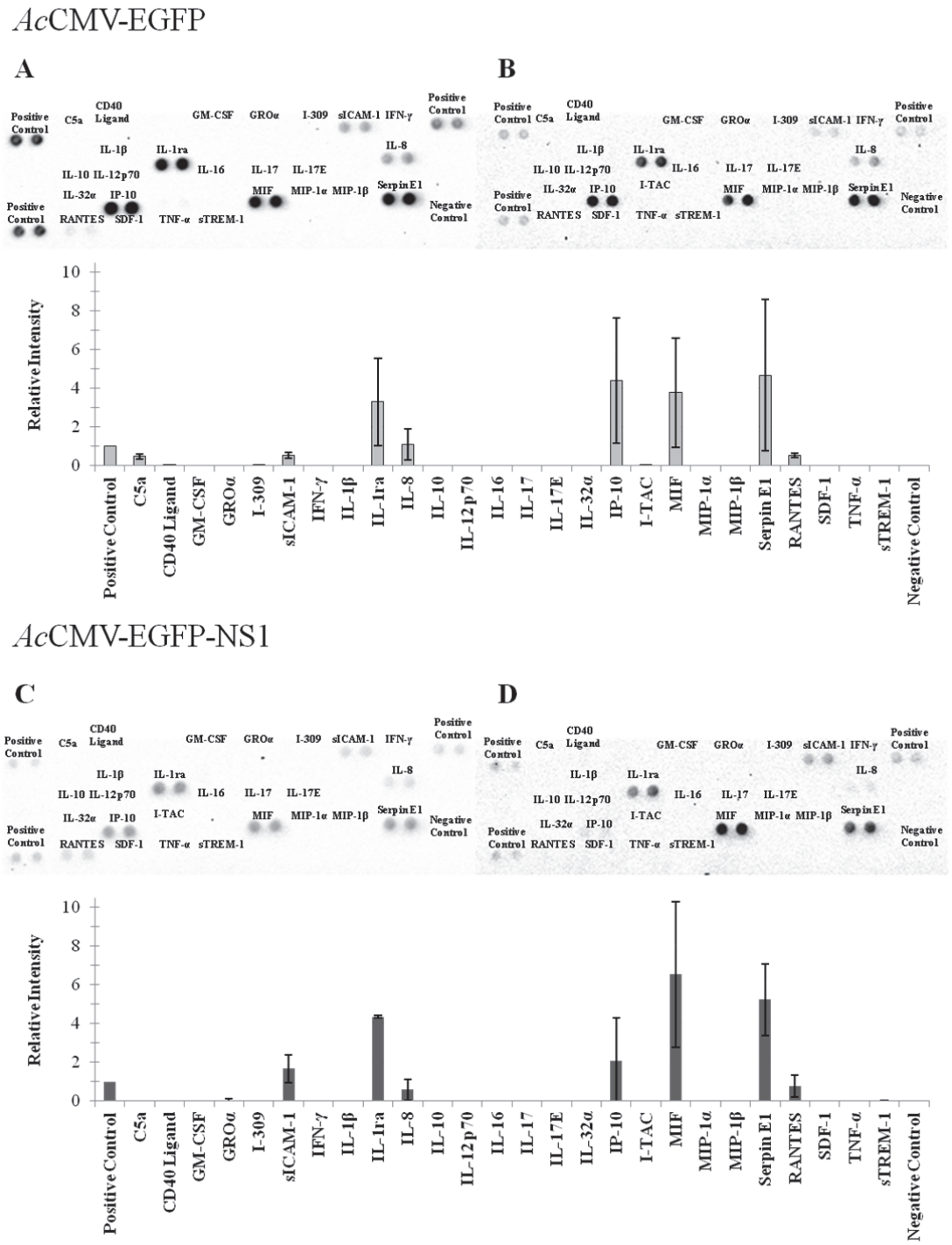

Figure 11. Cytokine production of dTHP-1 cells when fed with apoptotic bodies purified from *Ac*CMV-EGFP and *Ac*CMV-EGFP-NS1 transduced HepG2 cells. The cytokine production was analyzed in two separate experiments, A and B for *Ac*CMV-EGFP and C and D for *Ac*CMV-EGFP-NS1, respectively. In addition to the cytokines found in staurosporine samples in figure 10, IP-10 is present in the conditions above. The pixel densities presented in the graphs were measured from the presented western blot membranes after 5 min exposure, capturing the chemiluminescence signal with CCD camera. Two experiments were compared as in figure 10.

5. Discussion

5.1. Self-Antigens Are Present in B19V NS1 Induced Apoptotic Bodies

For a long time now, viral infections have been linked to apoptosis and the simultaneous occurrence of autoantibodies is not unheard of. However, the underlying mechanism causing such breakage in tolerance to self remains unclear. Rosen et al. (1995) were the first to report the clustering of self-antigens together with viral antigens into small surface blebs due to apoptosis induced by Sindbis virus infection. More specifically, the virus capsid antigens were observed to collocate with ribonucleoprotein Ro autoantigens which are also targeted in SLE (Rosen et al., 1995). Since then, the autoantigens present in apoptotic bodies have been studied extensively, especially in the context of SLE. It has been shown that a variant of a murine autoantibody having specificity to DNA, chromatin and anionic phospholipids binds apoptotic blebs in a caspase dependent manner. This has led to a hypothesis where antibodies could aid the recognition of apoptotic cells and influence the interactions between B cells and apoptotic cells (Cocca et al., 2002). The production of autoantibodies against nucleus has been further investigated by looking into the way how the nucleosomal particles from a fragmented nucleus end up to cell surface during apoptosis. The mechanism has specific, caspase dependent steps where nucleosomes attach to nuclear fragments, migrate to cell surface and break out from the dying cell, making nucleosomes available to the immune system (Radic et al., 2004). Ten years after the discoveries by Rosen et al. (1995), Frisoni et al. (2005) studied the pathway by witch SLE autoantigen H2B is made available to the immune system. By opsonizing apoptotic cell with H2B specific autoantibodies, the uptake of apoptotic material by dendritic cells was increased. The uptake occurred through pro-inflammatory pathway which is required for SLE autoreactivity. In addition, the uptake enhanced the antigen presentation by dendritic cells which led to augmented proliferation of specific T cells (Frisoni et al., 2005). Furthermore, the tolerance to SLE nuclear autoantigens seems to be dependent on caspase activated DNase which is responsible for fragmenting chromatin. This endonuclease is usually in complex with its inhibitor but an activation of caspase 3

will cleave the inhibitor and activate caspase activated DNase. In the absence of caspase activated DNase however, chromatin is abnormally exposed during apoptosis which may lead into increased autoantibody binding and make an autoimmune response feasible (Jog et al., 2012).

Here, both nucleosomal and cytosolic autoantigens are detected in apoptotic bodies together with B19V NS1 (Figures 3 to 5). In this case, the underlying mechanism for B19V induced apoptosis in liver cells is dependent on caspase 3 and 9 activity (Poole et al., 2004) and the main reason for the apoptosis occurring this way in HepG2 cells is B19V NS1 (Poole et al., 2006). Staurosporine was selected as a control because it stimulates apoptosis in similar caspase dependent manner as B19V NS1 does (Stepczynska et al., 2001). Thus, as shown in figures 3 to 5, the tested nucleosomal and cytosolic autoantigens except for H2B were found in all test conditions. However, the *Ac*CMV-EGFP is not capable of inducing apoptosis the way *Ac*CMV-EGFP-NS1 is. Although green fluorescent protein has been demonstrated to be toxic to living cells (Liu et al., 1999), the rate of apoptosis it causes is rather moderate in contrast to the EGFP-NS1 expressed here. In this model system, apoptosis occurs at significantly lower rate in *Ac*CMV-EGFP transduced HepG2 cells than in *Ac*CMV-EGFP-NS1 transduced cells (Kivovich et al., 2012). Same effect is visualized in figure 2. Closer analysis was performed in appendix 1 where the greater occurrence of apoptosis and higher quantity of signal originating from EGFP in *Ac*CMV-EGFP-NS1 transduced samples was addressed by flow cytometer (Appendix 1, Figure 2 and Table S1). The signal originating from *Ac*CMV-EGFP-NS1 is significantly higher ($P < 0.05$) than from *Ac*CMV-EGFP. Moreover, the rate of apoptosis was found to be similar and significantly higher both in *Ac*CMV-EGFP-NS1 transduced and staurosporine treated test conditions than in *Ac*CMV-EGFP transduced samples (Appendix 1, (Thammasri et al., 2013)).

The proportional amounts of markers present in apoptotic bodies were not part of the scope of this thesis. Nevertheless, the matter was addressed in appendix 1 as the amount of antigen signal per the whole area of apoptotic body. Thirty apoptotic bodies ($N = 30$) were

analyzed from all nine tested conditions. Only the amount of signal originating from EGFP (Appendix 1, Figures 3 to 5) and in one case also from DNA (Appendix 1, Figure 4) was found significantly different ($P < 0.05$) in *Ac*CMV-EGFP-NS1 transduced apoptotic bodies in contrast to the *Ac*CMV-EGFP transduced and staurosporine treated samples (Appendix 1, (Thammasri et al., 2013)). Although the amount of the nucleosomal and cytosolic autoantigens does not vary significantly between the samples, certain implications can still be seen here. One thing should also be noted here, this method of approach in determining the proportional amounts of the selected markers is not capable of telling the full story. As already noted above, the *Ac*CMV-EGFP-NS1 transduced and staurosporine treated cells produce significantly more apoptotic bodies than the *Ac*CMV-EGFP transduced cells (Appendix 1, Figure 2 and Table S1). Thus, the apoptosis resulting from the expression of B19V NS1 is likely more capable of making the nucleosomal and cytosolic autoantigens available to the immune system than the expression of EGFP. Similar implications can be seen when comparing the signals from EGFP and from the NS1-EGFP fusion protein. Significantly more signal originates from the EGFP-NS1 fusion protein than from EGFP alone (Appendix 1, Figures 3 to 5) indicating more NS1-EGFP than just EGFP in the apoptotic bodies. Therefore, this method of approach might falsely emphasize the apoptotic bodies resulting from *Ac*CMV-EGFP transduced cells and diminish the notion that certain nucleosomal and cytosolic autoantigens are found in apoptotic bodies together with NS1-EGFP fusion protein. If the purpose is to accurately determine the variation in the amounts of the studied self-antigens in apoptotic bodies, it should be done using a method which takes in to account the fact that the apoptosis occurs in varying rates to begin with. That being said, combining the results seen here with the results gained from previous experiments, it seems like the caspase 3 and 9 dependent apoptosis due to B19V NS1 expression is capable of making self-antigens available to the immune system.

The studied nucleosomal and cytosolic autoantigens were selected because they have been connected to autoimmune conditions. Out of the seven included autoantigens, antibodies against double stranded DNA, ApoH and Smith are part of the new classification criteria for SLE determined by the Systemic Lupus International Collaborating Clinics (SLICC). Antinuclear antibody is also included to the criteria and could thus additionally include

antibodies against H4, H2B and possibly Ku80. According to the new classification, the patient must fulfill as a minimum of four criteria out of which one has to be immunological or the patient must have lupus nephritis proven by biopsy in the presence of antinuclear or anti double stranded DNA antibodies (Petri et al., 2012). The 2010 RA classification criteria only include RF and anti-citrullinated protein antibody as possible serological symptoms in early diagnosis of RA (Aletaha et al., 2010). Antibodies against phospholipids, including ApoH specific antibodies, however, have been connected to juvenile arthritis in patients previously infected with B19V (Von Landenberg et al., 2003; Lehmann et al., 2008). Immunization using ApoH has additionally been connected to faster onset of autoimmunity resembling antiphospholipid syndrome in autoimmune strain of mice (Aron et al., 1995). ApoH has been indicated as a requirement for interactions between antibodies and phospholipids as well. ApoH is particularly required for the recognition of cardiolipin by anticardiolipin antibodies (McNeil et al., 1990). It has also been shown that opsonization by antiphospholipid antibodies is a requirement for pro-inflammatory clearance of apoptotic cells by scavenger macrophages with immense TNFα secretion (Manfredi et al., 1998a) and that ApoH is the mediator for the said opsonization (Manfredi et al., 1998b). Furthermore, B19V infection has been linked to anticardiolipin syndrome (Reitblat et al., 2000). The only tested cytosolic autoantigen, Lamp2 has been linked to autoimmunity as well. Antibodies against Lamp2 are present in vast majority of patients suffering from pauci-immune focal necrotizing glomerulonephritis, an acute inflammatory disease resulting in rapid kidney failure associated with autoantibodies to neutrophil cytoplasmic antigens. Autoantibodies to Lamp2 are also capable of inducing pauci-immune focal necrotizing glomerulonephritis in rodents (Kain et al., 2008). Conversely, Ku80 was originally discovered due to Ku80 specific autoantibodies present in patients of polymyositis-scleroderma overlap syndrome (Mimori et al., 1981).

The autoantigens observed here in apoptotic bodies are comparable to results seen elsewhere. For example Schiller et al. (2008) report the presence of autoantigens, including DNA and histones in apoptotic bodies. In contrast to what is seen during this study, they also detected H2B in their bodies (Schiller et al., 2008). Although it is hardly unusual to observe autoantigens in apoptotic material since the purpose of cell death by apoptosis is to

be a controlled method of releasing cellular content, it is possible that B19V NS1 is more likely to make certain autoantigens available to the immune system. In addition, the presence of B19V in nonpermissive cells in such tissues as liver (Wong et al., 2003) might increase the apoptotic burden imposed to the immune system. Since impaired clearance of apoptotic material has been shown to lead into activation of autoreactive B cells (Qian et al., 2004), apoptosis induced by B19V NS1 is potentially capable of breaking tolerance to self in susceptible individuals.

5.2 Apoptotic Bodies Are Engulfed by Differentiated Macrophages

In order for one to develop an autoimmune reaction, self-antigens must become available to APCs. Macrophages are known for their phagocytic capabilities in innate immune responses but they are also able to process antigens as a part of adaptive immune system. For this reason differentiated macrophages were desired to be utilized to study the immune response to apoptotic bodies. Promonocytic THP-1 strain of cells has been carefully characterized by Daigneault et al. (2010). They have shown that THP-1 cells, stimulated using PMA the way described above, the best resemble monocyte derived macrophages which are a recognized model of differentiated tissue macrophages (Daigneault et al., 2010). Because monocyte derived macrophages are enriched from human peripheral blood mononuclear cells, a stable laboratory strain of cells was more suitable for this study.

At first, it was confirmed the dTHP-1 cells resemble the results gained by Daigneault et al. (2010). Increased cytoplasmic volume and granularity (Figure 6A and 6B) together with autofluorescence (Figure 6C) were considered to be strong enough indicators for successful differentiation. The cytoplasmic volume and granularity repeated the previously seen results but autofluorescence was lower in all experiment than presented by Daigneault et al. (2010). Although the dTHP-1 cells were protected from light prior to the experiments, it is possible that the conditions were not quite the same as used in the article (Daigneault

et al., 2010). Regardless, the results confirmed the differentiation and the dTHP-1 cells were next exposed to apoptotic bodies.

Phagocytosis of apoptotic bodies was confirmed with confocal microscopy as seen in figures 7 and 8. The autofluorescence present in dTHP-1 cells proved problematic in estimating the rate of phagocytosis in the selected test conditions however. Because the autofluorescence and EGFP are visualized using the same 488 nm excitation wavelength, it is challenging to differentiate between the signal originating from internalized apoptotic bodies in contrast to the signal occurring in the dTHP-1 cells themselves. In general, the signal from EGFP is brighter which makes analyzing individual cells feasible. From distance (Figure 9 and Table 2) on the other hand, eliminating the background signal becomes difficult especially since the images are single layer representations of the situation. The issue with background signal is particularly highlighted in the case of staurosporine treated samples (Table 2). Because these samples do not contain EGFP, there should be less visible signal using the 488 nm excitation wavelength. At present, this is not the case but the signal is comparable to the samples containing EGFP. Alternatively, signal originating from labels used for DNA could have been utilized in the analysis of staurosporine samples and for confirming the results seen in the other samples as well. Because of the high amount of signal originating from each nucleus however, this type signal was not observed at all. Moreover, it is not possible to truly distinguish between apoptotic bodies being in the cell or just on the cell surface. Some apoptotic bodies might also not be visible at all due to the selected layer to be imaged. Thus, this type of analysis is at best only the first attempt to distinguish between cells that have engulfed apoptotic bodies and those that have not. In the future, there should also be separate label for internal and external particles in order to distinguish the two. Because of the challenges arising from the selected analysis method, cytochalasin B does not seem to give consistent inhibition results either (Table 2). Internalization of apoptotic bodies is therefore confirmed using stack images of single phagocytosing cells (Figure 7). Since THP-1 cells without PMA-stimulation are also able to phagocytose external material, this is demonstrated in figure 8. Closer analysis of the phagocytosis is presented in Appendix 1, table 1. More dTHP-1 cells were used for the study and consequently the phagocytosis of apoptotic

bodies was confirmed as the phagocytic activity decreased due to cytochalasin B (Appendix 1, (Thammasri et al., 2013)). As a method, confocal microscopy is not ideal for analyzing phagocytosis of apoptotic bodies. More reliable results could be reached using flow cytometry as described by Jersmann et al. (2003). Issues like losing phagocytes due to washing steps or errors arising because of the observer could be avoided with flow cytometry. For instance, the effect of cytochalasin B observed here and especially in Appendix 1 could likely be stronger. Although the 2 h incubation period, as also used in this thesis, is reported to yield maximal phagocytosis, the selected time period for feeding can certainly affect the results. If the feeding duration is too short, the apoptotic bodies are not fully internalized but if it is too long, the apoptotic bodies might end up being processed which would also be seen in the signal. Since confocal microscopy is very laborious method for this type of analysis, examining various time points is not always possible (Jersmann et al., 2003). Even though the engulfment of apoptotic bodies by dTHP-1 cells is confirmed here, closer and more thorough analysis could be performed with flow cytometry. As the faith of the apoptotic bodies after internalization becomes of interest in the future, distinguishing accurately between the cells that have and have not internalized apoptotic bodies could prove to be useful. For that confocal microscopy is not enough, especially if the cells should be separated for additional studies.

Engulfment of apoptotic bodies by APCs can be of immunological importance. For example, uptake of apoptotic bodies has been indicated as a mechanism by which genetic changes can accumulate in tumor cells. This has been implied to occur via horizontal transfer of oncogenes propagated by apoptotic bodies (Bergsmedh et al., 2001). Before immersing into the topic of antigen processing for presentation purposes, the biological processes preceding the possible antigen presentation should be understood better. Therefore the topic was approached by tentatively examining the extracellular signaling molecules produced by dTHP-1 cells fed with apoptotic bodies.

5.3 Cytokine Profiles of Stimulated dTHP-1 Cells

The immunological consequences of stimulating dTHP-1 cells with apoptotic bodies were approached by applying a commercial kit suitable for detecting secreted cytokines and chemokines in cell culture. The manufacturer did not specify the sensitivity of the kit but as the kit is western blot based, the sensitivity should not be a limiting factor. Other factors like the extent of phagocytosis or how many dTHP-1 cells out of total have internalized apoptotic bodies and the duration of incubation on the other hand definitely play a part. Since those factors were not taken into account in the experiment design, the results are only approximate and thus considered to be preliminary. The incubation period of 24 h was probably a reasonable starting point because comparable time scales are often seen in this context (Fadok et al., 1998; Fujita et al., 2007; Sule et al., 2011). With a shorter incubation period certain secreted molecules might not be detected at all but it is also possible that some molecules inhibit other molecules making them undetectable if the incubation period is too long.

Given that phagocytosis has been shown to actively inhibit the production of pro-inflammatory cytokines IL-1β, IL-8, GM-CSF and TNF-α, but also IL-10 (Fadok et al., 1998), this could also explain the absence or low levels of these secreted molecules in the analyzed samples. In THP-1 cells exposed to B19V capsid, TGF-β independent decrease in TNF-α mRNA has been observed as well. TGF-β would thus normally inhibit TNF-α (Fujita et al., 2007) but since TGF-β was not part of this analysis, it is impossible to tell if the absence of TNF-α is due to TGF-β or not. The absence of TNF-α therefore very likely indicates regular reaction to apoptotic material because abnormal increase in TNF-α production has been observed in SLE monocytes (Sule et al., 2011). SerpinE1 production is stimulated by TNF-α and IL-1 in endothelial cells. However, these molecules are not found in any of the samples and thus cannot explain the presence of serpinE1 in the samples stimulated with apoptotic bodies. Increased serpinE1 levels have been linked to such disease states as insulin resistance, hemostatic disorders and obesity and it has additionally been observed in atherosclerotic plaques. As a marker on inflammatory

process, it is also possible that serpinE1 is a contaminant from the apoptotic cells utilized in the feeding (Binder et al., 2002). As the kit used for the analysis was designed only for four parallel test conditions, it was not possible to separately test the cytokine profile originating solely from the apoptotic cells within the scope of this study.

On the other hand, sICAM-1 has been connected to SLE. SLE patients seem to have elevated levels of sICAM-1 in sera, even more so during SLE flares (Elwy et al., 2010). Although the sICAM-1 levels were not particularly high in the tested samples, sICAM-1 might serve as an interesting starting point for further studies. Then again, the presence of IL-8 only in the samples fed with apoptotic material could be explained by the fact that macrophages tend to generate IL-8 when stimulated with phagocytosis. Accumulation of IL-8 has also been observed in synovial fluid of arthritic joints (for review on IL-8, see (Baggiolini and Clark-Lewis, 1992)). IP-10 was the only studied molecule which seemed to be specific to a degree for the samples examined from dTHP-1 cells stimulated with *Ac*CMV-EGFP and *Ac*CMV-EGFP-NS1 transduced apoptotic bodies (Figure 11). Synovial fluid levels of IP-10 are significantly higher in RA and elevated levels of IP-10 have also been observed in synovial tissue of RA patients (Patel et al., 2001). IP-10 is a chemoattractant for activated T cells which could have a role in T cell proliferation and T cell mediated immune responses in vivo (Dufour et al., 2002).

The presence of C5a in all other tested conditions except for *Ac*CMV-EGFP-NS1 (Figures 10 and 11) could be explained by the fact that C5, the precursor of C5a is readily present in HepG2 cells (Morris et al., 1982). Since the levels of C5a, known for its pro-inflammatory properties, are relatively low, the presence of C5a might be contamination originating from the apoptotic body production. On the other hand, macrophages are capable of generating C5a as well (for review on C5a, see (Manthey et al., 2009)). As the extent of apoptotic body production is the highest due to induction by *Ac*CMV-EGFP-NS1 (Figure 2), it likely affects the cytokine profiles first in HepG2 cells and later in dTHP-1 cells, especially since the amount of apoptotic bodies used for stimulation was not controlled. The effect of higher amount of apoptotic bodies might be also seen in the case on MIF. Slightly more

MIF seems to be present in *Ac*CMV-EGFP-NS1 than in the rest of the tested conditions (Figures 10 and 11). Since MIF has been found to be in synovial fluid and in synovial lining CD14+ macrophages of RA patients in higher amounts than in healthy controls (Leech et al., 1999) and macrophages are an important source of MIF (Calandra et al., 1994), MIF deserves further attention in determining the immunological effects of B19V NS1.

Some of the reactions seen here might be of interest in the context of autoimmune diseases. However, single experiment is by no means enough to give a full picture of the likely complex processes occurring as a result of the stimulation of APCs with apoptotic bodies. Furthermore, this study could not fully distinguish between the apoptotic bodies produced by the selected treatments and thus thorough analysis is required in order to shed more light on the immunological consequences of feeding dTHP-1 cells with apoptotic bodies.

5.4 Conclusions

As a result of B19V NS1 expression in nonpermissive HepG2 cells, nucleosomal and cytosolic autoantigens are deposited into apoptotic bodies. Those apoptotic bodies can then be engulfed by APCs which further process the autoantigens. Out of the examined molecules secreted by dTHP-1 cells after feeding on apoptotic bodies, sICAM-1, IL-8, IP-10 and MIF have been linked to autoimmune conditions. Therefore, B19V NS1 induced cell death in nonpermissive cells might potentially be a noteworthy contributing factor for losing tolerance to self, especially in susceptive individuals. In order to shed light on how exactly B19V NS1 might break the tolerance to self and whether it is enough to cause autoimmune diseases, further investigation is definitely required.

References

Agbandje, M., S. Kajigaya, R. McKenna, N.S. Young, and M.G. Rossmann. 1994. The structure of human parvovirus B19 at 8 A resolution. *Virology.* 203:106-115.

Aletaha, D., T. Neogi, A.J. Silman, J. Funovits, D.T. Felson, C.O. Bingham 3rd, N.S. Birnbaum, G.R. Burmester, V.P. Bykerk, M.D. Cohen, B. Combe, K.H. Costenbader, M. Dougados, P. Emery, G. Ferraccioli, J.M. Hazes, K. Hobbs, T.W. Huizinga, A. Kavanaugh, J. Kay, T.K. Kvien, T. Laing, P. Mease, H.A. Menard, L.W. Moreland, R.L. Naden, T. Pincus, J.S. Smolen, E. Stanislawska-Biernat, D. Symmons, P.P. Tak, K.S. Upchurch, J. Vencovsky, F. Wolfe, and G. Hawker. 2010. 2010 Rheumatoid arthritis classification criteria: an American College of Rheumatology/European League Against Rheumatism collaborative initiative. *Arthritis Rheum.* 62:2569-2581.

Anderson, M.J., P.G. Higgins, L.R. Davis, J.S. Willman, S.E. Jones, I.M. Kidd, J.R. Pattison, and D.A. Tyrrell. 1985. Experimental parvoviral infection in humans. *J.Infect.Dis.* 152:257-265.

Aron, A.L., M.L. Cuellar, R.L. Brey, S. Mckeown, L.R. Espinoza, Y. Shoenfeld, and A.E. Gharavi. 1995. Early onset of autoimmunity in MRL/++ mice following immunization with beta 2 glycoprotein I. *Clin.Exp.Immunol.* 101:78-81.

Axline, S.G., and E.P. Reaven. 1974. Inhibition of phagocytosis and plasma membrane mobility of the cultivated macrophage by cytochalasin B. Role of subplasmalemmal microfilaments. *J.Cell Biol.* 62:647-659.

Baggiolini, M., and I. Clark-Lewis. 1992. Interleukin-8, a chemotactic and inflammatory cytokine. *FEBS Lett.* 307:97-101.

Barton, L.L., D. Lax, Z.M. Shehab, and J.C. Keith. 1997. Congenital cardiomyopathy associated with human parvovirus B19 infection. *Am.Heart J.* 133:131-133.

Bergsmedh, A., A. Szeles, M. Henriksson, A. Bratt, M.J. Folkman, A.L. Spetz, and L. Holmgren. 2001. Horizontal transfer of oncogenes by uptake of apoptotic bodies. *Proc.Natl.Acad.Sci.U.S.A.* 98:6407-6411.

Binder, B.R., G. Christ, F. Gruber, N. Grubic, P. Hufnagl, M. Krebs, J. Mihaly, and G.W. Prager. 2002. Plasminogen activator inhibitor 1: physiological and pathophysiological roles. *News Physiol.Sci.* 17:56-61.

Calandra, T., J. Bernhagen, R.A. Mitchell, and R. Bucala. 1994. The macrophage is an important and previously unrecognized source of macrophage migration inhibitory factor. *J.Exp.Med.* 179:1895-1902.

Casciola-Rosen, L.A., G. Anhalt, and A. Rosen. 1994. Autoantigens targeted in systemic lupus erythematosus are clustered in two populations of surface structures on apoptotic keratinocytes. *J.Exp.Med.* 179:1317-1330.

Chen, A.Y., E.Y. Zhang, W. Guan, F. Cheng, S. Kleiboeker, T.M. Yankee, and J. Qiu. 2010. The small 11 kDa nonstructural protein of human parvovirus B19 plays a key role in inducing apoptosis during B19 virus infection of primary erythroid progenitor cells. *Blood.* 115:1070-1080.

Chou, T.N., T.C. Hsu, R.M. Chen, L.I. Lin, and G.J. Tsay. 2000. Parvovirus B19 infection associated with the production of anti-neutrophil cytoplasmic antibody (ANCA) and anticardiolipin antibody (aCL). *Lupus.* 9:551-554.

Clewley, J.P. 1984. Biochemical characterization of a human parvovirus. *J.Gen.Virol.* 65 (Pt 1):241-245.

Clewley, J.P., B.J. Cohen, and A.M. Field. 1987. Detection of parvovirus B19 DNA, antigen, and particles in the human fetus. *J.Med.Virol.* 23:367-376.

Cocca, B.A., A.M. Cline, and M.Z. Radic. 2002. Blebs and apoptotic bodies are B cell autoantigens. *J.Immunol.* 169:159-166.

Cope, A.P., A. Jones, M. Brozovic, M.S. Shafi, and R.N. Maini. 1992. Possible induction of systemic lupus erythematosus by human parvovirus. *Ann.Rheum.Dis.* 51:803-804.

Corcoran, A., and S. Doyle. 2004. Advances in the biology, diagnosis and host-pathogen interactions of parvovirus B19. *J.Med.Microbiol.* 53:459-475.

Cossart, Y.E., A.M. Field, B. Cant, and D. Widdows. 1975. Parvovirus-like particles in human sera. *Lancet.* 1:72-73.

Daigneault, M., J.A. Preston, H.M. Marriott, M.K. Whyte, and D.H. Dockrell. 2010. The identification of markers of macrophage differentiation in PMA-stimulated THP-1 cells and monocyte-derived macrophages. *PLoS One.* 5:e8668.

Doerig, C., B. Hirt, J.P. Antonietti, and P. Beard. 1990. Nonstructural protein of parvoviruses B19 and minute virus of mice controls transcription. *J.Virol.* 64:387-396.

Dong, X., K.J. Hamilton, M. Satoh, J. Wang, and W.H. Reeves. 1994. Initiation of autoimmunity to the p53 tumor suppressor protein by complexes of p53 and SV40 large T antigen. *J.Exp.Med.* 179:1243-1252.

Dufour, J.H., M. Dziejman, M.T. Liu, J.H. Leung, T.E. Lane, and A.D. Luster. 2002. IFN-gamma-inducible protein 10 (IP-10; CXCL10)-deficient mice reveal a role for IP-10 in effector T cell generation and trafficking. *J.Immunol.* 168:3195-3204.

Elwy, M.A., Z.A. Galal, and H.E. Hasan. 2010. Immunoinflammatory markers and disease activity in systemic lupus erythematosus: something old, something new. *East.Mediterr.Health J.* 16:893-900.

Fadok, V.A., D.L. Bratton, A. Konowal, P.W. Freed, J.Y. Westcott, and P.M. Henson. 1998. Macrophages that have ingested apoptotic cells in vitro inhibit proinflammatory cytokine production through autocrine/paracrine mechanisms involving TGF-beta, PGE2, and PAF. *J.Clin.Invest.* 101:890-898.

Fadok, V.A., and G. Chimini. 2001. The phagocytosis of apoptotic cells. *Semin.Immunol.* 13:365-372.

Frisoni, L., L. McPhie, L. Colonna, U. Sriram, M. Monestier, S. Gallucci, and R. Caricchio. 2005. Nuclear autoantigen translocation and autoantibody opsonization lead to increased dendritic cell phagocytosis and presentation of nuclear antigens: a novel pathogenic pathway for autoimmunity? *J.Immunol.* 175:2692-2701.

Fujita, T., H. Ikejima, N. Yamagata, Y. Kudo, and K. Hoshi. 2007. In vitro response of immunoregulatory cytokine expression in human monocytic cells to human parvovirus B19 capsid. *Biol.Pharm.Bull.* 30:2027-2030.

Hemauer, A., K. Beckenlehner, H. Wolf, B. Lang, and S. Modrow. 1999. Acute parvovirus B19 infection in connection with a flare of systemic lupus erythematodes in a female patient. *J.Clin.Virol.* 14:73-77.

Hsu, T.C., and G.J. Tsay. 2001. Human parvovirus B19 infection in patients with systemic lupus erythematosus. *Rheumatology (Oxford).* 40:152-157.

Hsu, T.C., W.J. Wu, M.C. Chen, and G.J. Tsay. 2004. Human parvovirus B19 non-structural protein (NS1) induces apoptosis through mitochondria cell death pathway in COS-7 cells. *Scand.J.Infect.Dis.* 36:570-577.

Isa, A., A. Lundqvist, A. Lindblom, T. Tolfvenstam, and K. Broliden. 2007. Cytokine responses in acute and persistent human parvovirus B19 infection. *Clin.Exp.Immunol.* 147:419-425.

Jersmann, H.P., K.A. Ross, S. Vivers, S.B. Brown, C. Haslett, and I. Dransfield. 2003. Phagocytosis of apoptotic cells by human macrophages: analysis by multiparameter flow cytometry. *Cytometry A.* 51:7-15.

Jog, N.R., L. Frisoni, Q. Shi, M. Monestier, S. Hernandez, J. Craft, E.T. Prak, and R. Caricchio. 2012. Caspase-activated DNase is required for maintenance of tolerance to lupus nuclear autoantigens. *Arthritis Rheum.* 64:1247-1256.

Kain, R., M. Exner, R. Brandes, R. Ziebermayr, D. Cunningham, C.A. Alderson, A. Davidovits, I. Raab, R. Jahn, O. Ashour, S. Spitzauer, G. Sunder-Plassmann, M. Fukuda, P. Klemm, A.J. Rees, and D. Kerjaschki. 2008. Molecular mimicry in pauci-immune focal necrotizing glomerulonephritis. *Nat.Med.* 14:1088-1096.

Kerr, J.R., and N. Boyd. 1996. Autoantibodies following parvovirus B19 infection. *J.Infect.* 32:41-47.

Kerr, S., G. O'Keeffe, C. Kilty, and S. Doyle. 1999. Undenatured parvovirus B19 antigens are essential for the accurate detection of parvovirus B19 IgG. *J.Med.Virol.* 57:179-185.

King, A.M.Q., M.J. Adams, E.B. Carstens, and E.J. Lefkowitz. 2012.
Virus Taxonomy: Classification and Nomenclature of Viruses: Ninth Report of the International Committee on Taxonomy of Viruses. Elsevier Academic Press, San Diego. 1344 pp.

Kivovich, V., L. Gilbert, M. Vuento, and S.J. Naides. 2012. The putative metal coordination motif in the endonuclease domain of human Parvovirus B19 NS1 is critical for NS1 induced S phase arrest and DNA damage. *Int.J.Biol.Sci.* 8:79-92.

Kivovich, V., L. Gilbert, M. Vuento, and S.J. Naides. 2010. Parvovirus B19 genotype specific amino acid substitution in NS1 reduces the protein's cytotoxicity in culture. *Int.J.Med.Sci.* 7:110-119.

Krysko, D.V., G. Denecker, N. Festjens, S. Gabriels, E. Parthoens, K. D'Herde, and P. Vandenabeele. 2006. Macrophages use different internalization mechanisms to clear apoptotic and necrotic cells. *Cell Death Differ.* 13:2011-2022.

Kuronita, T., E.L. Eskelinen, H. Fujita, P. Saftig, M. Himeno, and Y. Tanaka. 2002. A role for the lysosomal membrane protein LGP85 in the biogenesis and maintenance of endosomal and lysosomal morphology. *J.Cell.Sci.* 115:4117-4131.

Lech, M., C. Kantner, O.P. Kulkarni, M. Ryu, E. Vlasova, J. Heesemann, D. Anz, S. Endres, K.S. Kobayashi, R.A. Flavell, J. Martin, and H.J. Anders. 2011. Interleukin-1 receptor-associated kinase-M suppresses systemic lupus erythematosus. *Ann.Rheum.Dis.* 70:2207-2217.

Leech, M., C. Metz, P. Hall, P. Hutchinson, K. Gianis, M. Smith, H. Weedon, S.R. Holdsworth, R. Bucala, and E.F. Morand. 1999. Macrophage migration inhibitory factor in rheumatoid arthritis: evidence of proinflammatory function and regulation by glucocorticoids. *Arthritis Rheum.* 42:1601-1608.

Lehmann, H.W., A. Plentz, P. von Landenberg, R.M. Kuster, and S. Modrow. 2008. Different patterns of disease manifestations of parvovirus B19-associated reactive juvenile arthritis and the induction of antiphospholipid-antibodies. *Clin.Rheumatol.* 27:333-338.

Liu, H.S., M.S. Jan, C.K. Chou, P.H. Chen, and N.J. Ke. 1999. Is green fluorescent protein toxic to the living cells? *Biochem.Biophys.Res.Commun.* 260:712-717.

Manfredi, A.A., P. Rovere, G. Galati, S. Heltai, E. Bozzolo, L. Soldini, J. Davoust, G. Balestrieri, A. Tincani, and M.G. Sabbadini. 1998a. Apoptotic cell clearance in systemic lupus erythematosus. I. Opsonization by antiphospholipid antibodies. *Arthritis Rheum.* 41:205-214.

Manfredi, A.A., P. Rovere, S. Heltai, G. Galati, G. Nebbia, A. Tincani, G. Balestrieri, and M.G. Sabbadini. 1998b. Apoptotic cell clearance in systemic lupus erythematosus. II. Role of beta2-glycoprotein I. *Arthritis Rheum.* 41:215-223.

Manthey, H.D., T.M. Woodruff, S.M. Taylor, and P.N. Monk. 2009. Complement component 5a (C5a). *Int.J.Biochem.Cell Biol.* 41:2114-2117.

McNeil, H.P., R.J. Simpson, C.N. Chesterman, and S.A. Krilis. 1990. Anti-phospholipid antibodies are directed against a complex antigen that includes a lipid-binding inhibitor of coagulation: beta 2-glycoprotein I (apolipoprotein H). *Proc.Natl.Acad.Sci.U.S.A.* 87:4120-4124.

Mevorach, D., J.L. Zhou, X. Song, and K.B. Elkon. 1998. Systemic exposure to irradiated apoptotic cells induces autoantibody production. *J.Exp.Med.* 188:387-392.

Meyer, O. 2003. Parvovirus B19 and autoimmune diseases. *Joint Bone Spine.* 70:6-11.

Michel, N., K. Ganter, S. Venzke, J. Bitzegeio, O.T. Fackler, and O.T. Keppler. 2006. The Nef protein of human immunodeficiency virus is a broad-spectrum modulator of chemokine receptor cell surface levels that acts independently of classical motifs for receptor endocytosis and Galphai signaling. *Mol.Biol.Cell.* 17:3578-3590.

Mimori, T., M. Akizuki, H. Yamagata, S. Inada, S. Yoshida, and M. Homma. 1981. Characterization of a high molecular weight acidic nuclear protein recognized by autoantibodies in sera from patients with polymyositis-scleroderma overlap. *J.Clin.Invest.* 68:611-620.

Moffatt, S., N. Tanaka, K. Tada, M. Nose, M. Nakamura, O. Muraoka, T. Hirano, and K. Sugamura. 1996. A cytotoxic nonstructural protein, NS1, of human parvovirus B19 induces activation of interleukin-6 gene expression. *J.Virol.* 70:8485-8491.

Moffatt, S., N. Yaegashi, K. Tada, N. Tanaka, and K. Sugamura. 1998. Human parvovirus B19 nonstructural (NS1) protein induces apoptosis in erythroid lineage cells. *J.Virol.* 72:3018-3028.

Momoeda, M., S. Wong, M. Kawase, N.S. Young, and S. Kajigaya. 1994. A putative nucleoside triphosphate-binding domain in the nonstructural protein of B19 parvovirus is required for cytotoxicity. *J.Virol.* 68:8443-8446.

Morris, K.M., D.P. Aden, B.B. Knowles, and H.R. Colten. 1982. Complement biosynthesis by the human hepatoma-derived cell line HepG2. *J.Clin.Invest.* 70:906-913.

Mosser, D.M., and J.P. Edwards. 2008. Exploring the full spectrum of macrophage activation. *Nat.Rev.Immunol.* 8:958-969.

Neeli, I., S.N. Khan, and M. Radic. 2008. Histone deimination as a response to inflammatory stimuli in neutrophils. *J.Immunol.* 180:1895-1902.

Niessen, H.W., W.K. Lagrand, H.J. Rensink, C.J. Meijer, L. Aarden, C.E. Hack, and C. Visser. 2000. Apolipoprotein H, a new mediator in the inflammatory changes ensuring in jeopardised human myocardium. *J.Clin.Pathol.* 53:863-867.

Nykky, J., J.E. Tuusa, S. Kirjavainen, M. Vuento, and L. Gilbert. 2010. Mechanisms of cell death in canine parvovirus-infected cells provide intuitive insights to developing nanotools for medicine. *Int.J.Nanomedicine.* 5:417-428.

Oberti, D., M.A. Kirschmann, and R.H. Hahnloser. 2010. Correlative microscopy of densely labeled projection neurons using neural tracers. *Front.Neuroanat.* 4:24.

Opferman, J.T., and S.J. Korsmeyer. 2003. Apoptosis in the development and maintenance of the immune system. *Nat.Immunol.* 4:410-415.

Ozawa, K., J. Ayub, Y.S. Hao, G. Kurtzman, T. Shimada, and N. Young. 1987. Novel transcription map for the B19 (human) pathogenic parvovirus. *J.Virol.* 61:2395-2406.

Ozawa, K., J. Ayub, S. Kajigaya, T. Shimada, and N. Young. 1988. The gene encoding the nonstructural protein of B19 (human) parvovirus may be lethal in transfected cells. *J.Virol.* 62:2884-2889.

Patel, D.D., J.P. Zachariah, and L.P. Whichard. 2001. CXCR3 and CCR5 ligands in rheumatoid arthritis synovium. *Clin.Immunol.* 98:39-45.

Pavlovic, M., A. Kats, M. Cavallo, and Y. Shoenfeld. 2010. Clinical and molecular evidence for association of SLE with parvovirus B19. *Lupus.* 19:783-792.

Petri, M., A.M. Orbai, G.S. Alarcon, C. Gordon, J.T. Merrill, P.R. Fortin, I.N. Bruce, D. Isenberg, D.J. Wallace, O. Nived, G. Sturfelt, R. Ramsey-Goldman, S.C. Bae, J.G. Hanly, J. Sanchez-Guerrero, A. Clarke, C. Aranow, S. Manzi, M. Urowitz, D. Gladman, K. Kalunian, M. Costner, V.P. Werth, A. Zoma, S. Bernatsky, G. Ruiz-Irastorza, M.A. Khamashta, S. Jacobsen, J.P. Buyon, P. Maddison, M.A. Dooley, R.F. van Vollenhoven, E. Ginzler, T. Stoll, C. Peschken, J.L. Jorizzo, J.P. Callen, S.S. Lim, B.J. Fessler, M. Inanc, D.L. Kamen, A. Rahman, K. Steinsson, A.G. Franks Jr, L. Sigler, S. Hameed, H. Fang, N. Pham, R. Brey, M.H. Weisman, G. McGwin Jr, and L.S. Magder. 2012. Derivation and validation of the Systemic Lupus International Collaborating Clinics classification criteria for systemic lupus erythematosus. *Arthritis Rheum.* 64:2677-2686.

Poole, B.D., Y.V. Karetnyi, and S.J. Naides. 2004. Parvovirus B19-induced apoptosis of hepatocytes. *J.Virol.* 78:7775-7783.

Poole, B.D., V. Kivovich, L. Gilbert, and S.J. Naides. 2011. Parvovirus B19 nonstructural protein-induced damage of cellular DNA and resultant apoptosis. *Int.J.Med.Sci.* 8:88-96.

Poole, B.D., J. Zhou, A. Grote, A. Schiffenbauer, and S.J. Naides. 2006. Apoptosis of liver-derived cells induced by parvovirus B19 nonstructural protein. *J.Virol.* 80:4114-4121.

Qian, Y., H. Wang, and S.H. Clarke. 2004. Impaired clearance of apoptotic cells induces the activation of autoreactive anti-Sm marginal zone and B-1 B cells. *J.Immunol.* 172:625-635.

Raab, U., K. Beckenlehner, T. Lowin, H.H. Niller, S. Doyle, and S. Modrow. 2002. NS1 protein of parvovirus B19 interacts directly with DNA sequences of the p6 promoter and with the cellular transcription factors Sp1/Sp3. *Virology.* 293:86-93.

Radic, M., T. Marion, and M. Monestier. 2004. Nucleosomes are exposed at the cell surface in apoptosis. *J.Immunol.* 172:6692-6700.

Reitblat, T., T. Drogenikov, I. Sigalov, S. Oren, and D. London. 2000. Transient anticardiolipin antibody syndrome in a patient with parvovirus B19 infection. *Am.J.Med.* 109:512-513.

Rosen, A., L. Casciola-Rosen, and J. Ahearn. 1995. Novel packages of viral and self-antigens are generated during apoptosis. *J.Exp.Med.* 181:1557-1561.

Savill, J., and V. Fadok. 2000. Corpse clearance defines the meaning of cell death. *Nature.* 407:784-788.

Schiller, M., I. Bekeredjian-Ding, P. Heyder, N. Blank, A.D. Ho, and H.M. Lorenz. 2008. Autoantigens are translocated into small apoptotic bodies during early stages of apoptosis. *Cell Death Differ.* 15:183-191.

Schneider, C.A., W.S. Rasband, and K.W. Eliceiri. 2012. NIH Image to ImageJ: 25 years of image analysis. *Nat.Methods.* 9:671-675.

Schulz, M., H. Dotzlaw, S. Mikkat, M. Eggert, and G. Neeck. 2007. Proteomic analysis of peripheral blood mononuclear cells: selective protein processing observed in patients with rheumatoid arthritis. *J.Proteome Res.* 6:3752-3759.

Sekerkova, G., L. Zheng, P.A. Loomis, B. Changyaleket, D.S. Whitlon, E. Mugnaini, and J.R. Bartles. 2004. Espins are multifunctional actin cytoskeletal regulatory proteins in the microvilli of chemosensory and mechanosensory cells. *J.Neurosci.* 24:5445-5456.

Shade, R.O., M.C. Blundell, S.F. Cotmore, P. Tattersall, and C.R. Astell. 1986. Nucleotide sequence and genome organization of human parvovirus B19 isolated from the serum of a child during aplastic crisis. *J.Virol.* 58:921-936.

Stepczynska, A., K. Lauber, I.H. Engels, O. Janssen, D. Kabelitz, S. Wesselborg, and K. Schulze-Osthoff. 2001. Staurosporine and conventional anticancer drugs induce overlapping, yet distinct pathways of apoptosis and caspase activation. *Oncogene.* 20:1193-1202.

Sule, S., A. Rosen, M. Petri, E. Akhter, and F. Andrade. 2011. Abnormal production of pro- and anti-inflammatory cytokines by lupus monocytes in response to apoptotic cells. *PLoS One.* 6:e17495.

Szekanecz, Z., and A.E. Koch. 2007. Macrophages and their products in rheumatoid arthritis. *Curr.Opin.Rheumatol.* 19:289-295.

Takahashi, Y., C. Murai, S. Shibata, Y. Munakata, T. Ishii, K. Ishii, T. Saitoh, T. Sawai, K. Sugamura, and T. Sasaki. 1998. Human parvovirus B19 as a causative agent for rheumatoid arthritis. *Proc.Natl.Acad.Sci.U.S.A.* 95:8227-8232.

Thammasri, K., S. Rauhamäki, L. Wang, A. Filippou, V. Kivovich, V. Marjomäki, S.J. Naides, and L. Gilbert. 2013. Human Parvovirus B19 Induced Apoptotic Bodies Contain Altered Self-Antigens that are Phagocytosed by Antigen Presenting Cells. *PLoS ONE.* 8 (6):e67179.

Thompson, C.B. 1995. Apoptosis in the pathogenesis and treatment of disease. *Science.* 267:1456-1462.

Tokano, Y., S. Morimoto, H. Kaneko, H. Amano, K. Nozawa, Y. Takasaki, and H. Hashimoto. 1999. Levels of IL-12 in the sera of patients with systemic lupus erythematosus (SLE)--relation to Th1- and Th2-derived cytokines. *Clin.Exp.Immunol.* 116:169-173.

Voll, R.E., M. Herrmann, E.A. Roth, C. Stach, J.R. Kalden, and I. Girkontaite. 1997. Immunosuppressive effects of apoptotic cells. *Nature.* 390:350-351.

Von Landenberg, P., H.W. Lehmann, A. Knoll, S. Dorsch, and S. Modrow. 2003. Antiphospholipid antibodies in pediatric and adult patients with rheumatic disease are associated with parvovirus B19 infection. *Arthritis Rheum.* 48:1939-1947.

White, D.G., A.D. Woolf, P.P. Mortimer, B.J. Cohen, D.R. Blake, and P.A. Bacon. 1985. Human parvovirus arthropathy. *Lancet.* 1:419-421.

Williams, M.D., B.J. Cohen, A.C. Beddall, K.J. Pasi, P.P. Mortimer, and F.G. Hill. 1990. Transmission of human parvovirus B19 by coagulation factor concentrates. *Vox Sang.* 58:177-181.

Wong, S., N.S. Young, and K.E. Brown. 2003. Prevalence of parvovirus B19 in liver tissue: no association with fulminant hepatitis or hepatitis-associated aplastic anemia. *J.Infect.Dis.* 187:1581-1586.

Woolf, A.D., G.V. Campion, A. Chishick, S. Wise, B.J. Cohen, P.T. Klouda, O. Caul, and P.A. Dieppe. 1989. Clinical manifestations of human parvovirus B19 in adults. *Arch.Intern.Med.* 149:1153-1156.

Woolf, A.D., N.D. Hall, N.J. Goulding, B. Kantharia, J. Maymo, G. Evison, and P.J. Maddison. 1991. Predictors of the long-term outcome of early synovitis: a 5-year follow-up study. *Br.J.Rheumatol.* 30:251-254.

Yaegashi, N., T. Niinuma, H. Chisaka, S. Uehara, K. Okamura, O. Shinkawa, A. Tsunoda, S. Moffatt, K. Sugamura, and A. Yajima. 1999. Serologic study of human parvovirus B19 infection in pregnancy in Japan. *J.Infect.* 38:30-35.

Young, N.S., and K.E. Brown. 2004. Parvovirus B19. *N.Engl.J.Med.* 350:586-597.

Appendix

Human Parvovirus B19 Induced Apoptotic Bodies Contain Altered Self-Antigens that are Phagocytosed by Antigen Presenting Cells

Thammasri K, Rauhamäki S, Wang L, Filippou A, Kivovich V, et al. (2013) Human Parvovirus B19 Induced Apoptotic Bodies Contain Altered Self-Antigens that are Phagocytosed by Antigen Presenting Cells. PLoS ONE 8(6): e67179. doi:10.1371/journal.pone.0067179

OPEN ACCESS Freely available online

PLOS ONE

Human Parvovirus B19 Induced Apoptotic Bodies Contain Altered Self-Antigens that are Phagocytosed by Antigen Presenting Cells

Kanoktip Thammasri[1], Sanna Rauhamäki[1], Liping Wang[1], Artemis Filippou[1], Violetta Kivovich[2], Varpu Marjomäki[1], Stanley J. Naides[3], Leona Gilbert[1]*

1 Department of Biological and Environmental Sciences and Nanoscience Center, University of Jyväskylä, Jyväskylä, Finland, **2** Pennsylvania State College of Medicine/Milton S. Hershey Medical Center, Hershey, Pennsylvania, United States of America, **3** Quest Diagnostics Nichols Institute, San Juan Capistrano, California, United States of America

Abstract

Human parvovirus B19 (B19V) from the *erythrovirus* genus is known to be a pathogenic virus in humans. Prevalence of B19V infection has been reported worldwide in all seasons, with a high incidence in the spring. B19V is responsible for erythema infectiosum (fifth disease) commonly seen in children. Its other clinical presentations include arthralgia, arthritis, transient aplastic crisis, chronic anemia, congenital anemia, and hydrops fetalis. In addition, B19V infection has been reported to trigger autoimmune diseases such as systemic lupus erythematosus and rheumatoid arthritis. However, the mechanisms of B19V participation in autoimmunity are not fully understood. B19V induced chronic disease and persistent infection suggests B19V can serve as a model for viral host interactions and the role of viruses in the pathogenesis of autoimmune diseases. Here we investigate the involvement of B19V in the breakdown of immune tolerance. Previously, we demonstrated that the non-structural protein 1 (NS 1) of B19V induces apoptosis in non-permissive cells lines and that this protein can cleave host DNA as well as form NS1-DNA adducts. Here we provide evidence that through programmed cell death, apoptotic bodies (ApoBods) are generated by B19V NS1 expression in a non-permissive cell line. Characterization of purified ApoBods identified potential self-antigens within them. In particular, signature self-antigens such as Smith, ApoH, DNA, histone H4 and phosphatidylserine associated with autoimmunity were present in these ApoBods. In addition, when purified ApoBods were introduced to differentiated macrophages, recognition, engulfment and uptake occurred. This suggests that B19V can produce a source of self-antigens for immune cell processing. The results support our hypothesis that B19V NS1-DNA adducts, and nucleosomal and lysosomal antigens present in ApoBods created in non-permissive cell lines, are a source of self-antigens.

Citation: Thammasri K, Rauhamäki S, Wang L, Filippou A, Kivovich V, et al. (2013) Human Parvovirus B19 Induced Apoptotic Bodies Contain Altered Self-Antigens that are Phagocytosed by Antigen Presenting Cells. PLoS ONE 8(6): e67179. doi:10.1371/journal.pone.0067179

Editor: Pierre Bobé, INSERM-Université Paris-Sud, France

Received March 22, 2013; **Accepted** May 15, 2013; **Published** June 12, 2013

Funding: This study was supported by the Academy of Finland Contract Number 122061. The funders had no role in study design, data collection and analysis, decision to publish, or preparation of the manuscript.

Competing interests: I have read the journal's policy and have the following interest: Dr. Stanley J. Naides is affiliated with Quest Diagnostics Nichols Institute. This affiliation does not alter our adherence to all PLOS ONE policies on sharing data and materials. All other authors have declared that no competing interests exists.

* E-mail: leona.k.gilbert@jyu.fi

Introduction

Human parvovirus B19 (B19V) is a member of the genus *Erythrovirus* of the family *Parvoviridae*. It is a small (20-25 nm in diameter) [1–3] non-enveloped single-stranded linear DNA virus that was discovered in 1975 by Yvonne Cossart [2]. This virus has an icosahedral symmetrical capsid consisting of two structural proteins, viral protein 1 and 2 (VP1 and VP2). The minor capsid protein, VP1, has phospholipase activity that is necessary for viral attachment and cell entry [4,5]. The major capsid protein (95% of the total), VP2, can self-assemble into empty capsids, known as virus-like particles (VLPs). In addition to the capsid proteins, there are three non-structural (NS) proteins, two without known functions, but one known as the

cytotoxic NS1 protein. NS1 protein, a member of superfamily 3 of viral helicases, is a pleiotropic nuclear phosphoprotein and absolutely required for viral replication. It is a multi-functional protein that has a role in control of cellular transcription, virus replication, induction of cell death, and transactivation of cellular promoters [6–8].

Erythroid precursors have been shown to be the demonstrated cell type to best support an B19V productive infection [9,10], but other bone marrow hematopoietic lineages support B19V productive infection, although less efficiently [11,12]. B19V NS1 expression plasmids were also used in permissive cells lines to investigate NS1 protein induced cellular apoptosis, cell life cycle, activation of caspase, and DNA fragmentation [13,14]. Other studies have confirmed that B19 virus does infect primary hepatocytes as well as HepG2 cell lines, and that NS1 protein is expressed while promoting apoptosis [15]. Again, B19V NS1 expression plasmids were constructed to determine the involvement of NS1 protein and apoptosis as well as caspase activation [16] in this non-permissive cell line. A transfection efficiency of less then 10% was obtained from this method. In order to increase the expression level of NS1 protein in HepG2 cells, the recombinant baculovirus expression vector system (BEVS) was created to house the NS1 construct [17,18]. Transduction efficiencies of greater than 60% can be obtained with the BEVS system and in this system NS1 expression induced apoptosis and host DNA damage. HepG2 cells were used in the current study because they allow virus binding and internalization, but they are non-permissive for human parvovirus replication [19].

Clinical diagnosis of B19V infection is very common and has been reported worldwide in all seasons [20,21]. The rate of B19V seropositivity rises with age because of continuous exposure to the virus [22]. Clinical features of B19V infection depend on the host's condition, but common symptoms and signs consist of mild illness with pyrexia, malaise, myalgia, rash, or arthralgia [2324.–25]. The common diseases caused by B19V infection include erythema infectiosum (fifth disease or slapped cheek syndrome), arthralgia, arthritis, transient aplastic crisis, chronic anemia, congenital anemia, and hydrops fetalis [4,26,27]. These general manifestations of B19V infection are very similar to features of several autoimmune diseases such as acute, chronic and autoimmune hepatitis, as well as acute fulminant liver failure [28–40], systemic Lupus erythematosus (SLE) and rheumatoid arthritis (RA) [26,27,41]. Moreover, this infection has been reported to trigger SLE [41] and RA [42], but the mechanisms are still not fully understood.

It has been shown that B19 viral infection may induce anti-phospholipid antibodies through phospholipase-A2-like activity [43–46] and molecular mimicry mechanism leading to immunological cross reaction [45,47]. Others have suggested that the NS1 protein promotes chronic inflammation by transactivation of cellular promoters for the expression of TNF-α and IL-6 genes [8,48]. It also has been implied that the NS1 protein may be a super-antigenic stimulator for T and/or B lymphocytes [47]. Our previous studies have shown that host cell DNA damage occurs with NS1 expression [16–18,49] and that host DNA is covalently attached to the NS1 protein to form bulky adducts [18,49].

We have proposed that B19V induction of autoimmunity may occur when T cells specific for NS1 protein are stimulated during a reoccurrence of B19V infection or re-stimulation of NS1 expression. NS1 protein specific T lymphocyte helper cells would then provide second signal to anergized autoantigen specific B lymphocytes. We hypothesized that B19V-induced ApoBods contain NS1-modified host cell DNA as well as nucleosomal self-proteins and that NS1 protein in ApoBods would be processed by professional antigen presenting cells such as dendritic cells or macrophages. Simultaneously, anergic anti-dsDNA specific B lymphocyte would take up NS1 protein modified self-DNA through its DNA surface IgM receptor; processing NS1 protein to the B lymphocyte surface would allow NS1 specific T helper cell second signaling. Similarly, anergized B lymphocytes specific for DNA binding proteins or NS1 interacting proteins would take up NS1 as part of DNA-protein complexes. The object of this study was to identify cell constituents associated with B19V-induced ApoBods that could be candidate autoantigens in SLE. Understanding the mechanism by which B19V breaks immune tolerance would argue for detection of initial viral insults and may provide insights leading to better patient treatment strategies.

Materials and Methods

Cell Culture

Spodoptera frugiperda-derived cells (*Sf*9 cells, ATCC-CRL-1711, Manassas, VA), were cultured in spinner flasks using Insect-XPress cell medium (BioWhittaker®, Walkersville, MD, USA) at 27 °C. Human hepatocellular liver carcinoma cell line HepG2 cells (ATCC-HB-8065), a B19V non-permissive cell line, was cultured in 440 mL of Hepatocyte Minimum Essential Medium (Gibco®, Invitrogen, Carlsbad, CA, USA) supplemented with 50 mL fetal bovine serum (FBS) (Gibco®), 5 mL L-glutamine (Gibco®) and 5 mL Penicillin-Streptomycin (Pen/Strep) (Gibco®). Acute monocytic leukemia derived human monocytes, THP-1 cells (ATCC-TIB-202), were cultured in 440 mL of RPMI-1640 Medium Hybri-Max™ (Gibco®; modified with L-glutamine, 4500 mg/L glucose and 15 mM HEPES; Sigma, Sigma-Aldrich Inc., St. Louise, MO, USA), and supplemented with 50 mL FBS, 5 mL Pen/Strep and 0.05 mM β-mercaptoethanol. Both HepG2 and THP-1 cells were cultured at 37 ˚C, 5% CO_2, in tissue culture

flasks. For engulfment studies, THP-1 cells were differentiated as previously described by Daigneault and colleagues [50]. In brief, 5 x 10^5 THP-1 cells were seeded in RPMI medium as described above with addition of 200 nM phorbol-12-myristate-13-acetate (PMA) (Sigma) and incubated for 3 days. Replacing the PMA medium with fresh RPMI-1640 medium supplemented with Pen/Strep and β-mercaptoethanol and incubating the cells for an additional 5 days further enhanced differentiation. Experiments were performed on days 8 to 9 post initiation of differentiation.

Baculovirus Transduction of HepG2 Cells

Recombinant baculoviruses expressing enhanced green fluorescent protein (*Ac*EGFP) and *Ac*EGFP-NS1 fusion proteins under the CMV immediate-early promoter were prepared using the Bac-to-Bac® Baculovirus Expression system (Invitrogen, CA, USA) as previously reported [17]. The transduction efficiencies (TE) of these viruses were determined by growth of HepG2 0.5 x 10^6 cells overnight and transduction with recombinant *Ac*EGFP or *Ac*EGFP-NS1. BD FACSCALIBUR flow cytometer (Becton-Dickinson, NJ, USA) was used to verify if the viruses had 70% TE for use in the apoptotic bleb/bodies induction experiments as described by Kivovich and colleagues [17,18]. In the present study, HepG2 cells were transduced with recombinant viruses and kept in the dark rocking at room temperature (RT) for 4 h to promote viral binding to the cellular membrane.

Induction of Apoptotic Blebs

Induction of apoptotic blebs was performed by seeding 0.5 x 10^6 HepG2 cells in 6-well culture plates with 4 sterile cover slips per well and incubated overnight at 37 °C in 5% CO_2. Cells were then transduced at a TE of 70% with recombinant baculoviruses *Ac*EGFP or *Ac*EGFP-NS1. The culture plates were incubated at RT and kept in the dark on a rocking platform for 4 h. Transduced samples were washed once with sterile phosphate buffered saline (PBS), and pre-warmed supplemented medium was added to the culture wells before being incubated at 37 °C in 5% CO_2.

At 48 h post transduction, supernatant from each well was removed then 2 cover slips were taken to another 6-well plate and fixed with 4% paraformaldehyde (PFA)/PBS for 20 min with rocking at RT. The apoptotic blebs were characterized using a scanning electron microscope (SEM) as described in section 2.4. The remaining 2 cover slips in each well with adherent cell were stained with Annexin V-PE as described in section 2.5.

Scanning Electron Microscopy (SEM) Imaging

Cover slips with HepG2 cells were finely coated with a conductive gold film layer. The coating was plated with a fine coat sputter machine at a voltage of 0.9-1 kV and a corresponding current of 5-6 mA. The coating time was 4-6 min, leaving a gold layer of approximately 4 nm thick. After coating with gold the samples were examined by SEM.

A scanning electron microscope (SEM; JEOL JSM 820, Tokyo, Japan) equipped with a digital image acquisition card was used to examine samples fixed by screws on a copper specimen holder and transported into the SEM chamber by a sample transfer rod. The SEM accelerating voltage was 3 to 10 kV, and filament current 260 µA. Fields of interest were located at lower magnification, ~ 250 to 350x, and then the height of the stage and focus were adjusted to specify the working distance of 18 mm; image quality was optimized by adjusting X and Y stigmators, brightness and contrast to obtain the best resolution. The image was captured by the SEM Afore program.

Annexin V-PE Staining

HepG2 cells on cover slips from the previous experiment were submerged in 500 µL Annexin V-PE binding buffer (BioVision, Inc., Milpitas, CA, USA). Each cover slip was incubated with 5 µL Annexin V-PE (BioVision) for 15 min in the dark with rocking at RT. Cells were washed in HBSS (Hank's Balanced Salt Solution) (Mediatech, Inc, Herndon, VA, USA), supplemented with 3 mM $CaCl_2$, and fixed for 15 min in ice-cold 4-6% PFA/HBSS. Stained cover slips were mounted on glass slides with 3-5 µL Prolong Gold Antifade Reagent with DAPI (Invitrogen). The slides were stored at 4 °C before being analyzed by confocal microscope (Olympus).

Purification of ApoBods

An amount of 10 x 10^6 HepG2 cells were seeded in 175 cm^3 cell culture flasks and left to grow at 37 °C in 5% CO_2 for 24 h. Cells were then transduced with *Ac*EGFP and *Ac*EGFP-NS1 viruses with a TE of 70%. An inducer of cellular apoptosis, staurosporine (a protein kinase inhibitor; S4400 staurosporine from *Streptomyces sp.*, Sigma), was used as a positive control in this study. HepG2 cells seeded simultaneously, using the same seeding density as with the transduced cells, were treated with 1 µM concentration of staurosporine in growth medium in parallel with viral treated samples. At 72 h post transduction, supernatant from each was centrifuged 1,700 x g (Heraeus Labofuge 400, Thermo Fisher Scientific Inc., UK) for 3 min and filtered with gravity through a 5.0 µm filter (Millipore, Billerica, MA, USA).

A volume of 2 mL from the filtered supernatant was taken for verifying the quantity of ApoBods and fluorescence EGFP-NS1 signal by flow cytometry (FC). The supernatant was centrifuged at 16,100 x g for 20 min and the pellet was resuspended in 400 µL Annexin V-PE binding buffer (BioVision). Half of the ApoBods (200 µl) were analyzed directly by FC as described in section 2.7. The other half of the ApoBods were mixed

with 10 µL Annexin V-PE (BioVision) and incubated for 5 min in the dark on ice. Samples were centrifuged at 16,100 x g for 20 min and pellets were fixed with 50 µL 4% PFA/PBS at RT for 10 min. Again the samples were centrifuged at 16,100 x g for 10 min and ApoBods pellets mounted with Prolong Gold Antifade Reagent with DAPI (Invitrogen) on a glass slide and covered with a cover slip. Samples were stored at 4 °C and analyzed by wide-field microscopy imaging (Leica DM5500B, GmbH, Germany) (section 2.8).

The remaining filtered supernatant was ultracentrifuged at 285,000 x g (Beckman Coulter Optima L-90K Ultracentrifuge) for 1 h at 4 °C. ApoBod pellets were resuspended in 100 µL PBS overnight at 4 °C. These purified ApoBods were stored at 4 °C for the immunolabeling and engulfment studies (sections 2.9 and 2.10, respectively)

Flow Cytometry (FC)

FC analysis was performed to determine the amount of apoptotic body induction (section 2.6). Initially the samples were examined for the amount of events within one minute time period with low speed. Then a total of 10,000 events from the filtered ApoBods were examined for the EGFP fluorescent signal with high speed. FC results were measured by the BD FACSCALIBUR flow cytometer (Becton-Dickinson). Data were collected and interpreted by using Cell-Quest pro software version 5.2.1 (Becton-Dickinson). The statistical analysis was performed with FlowJo Flow Cytometry Analysis Software version 8.4.5 (Tree Star Inc., Ashland, OR, USA).

Wide-field Imaging

ApoBods stained with Annexin V-PE (from section 2.6) were analyzed by Leica fluorescent microscopy (Leica DM5500B) to determine expression of phosphatidylserine (PS) as a consequence of apoptosis. The fluorescence images were taken with a 100x/1.3 oil immersion objective and with excitation filters of 365, 470 and 530 nm. Components of ApoBods were identified by the green fluorescence signal from EGFP or EGFP-NS1, blue signal demonstrating DNA stained with DAPI, and red signal representing PS stained with Annexin V-PE. The appropriate exposure, gain and intensity were adjusted prior to recording the images. ImageJA 1.45B program (National Institutes of Health (NIH), Bethesda, MD, USA) was used to analyze the Leica images.

Immunolabeling of ApoBods

The purified ApoBods from section 2.6 were immunolabeled for further characterization. A volume of 50 µl ApoBods were pelleted at 16,100 x g for 20 min and fixed with 4% PFA/PBS for 20 min before being washed twice with PBS. The remaining immunolabeling procedure had centrifugation steps (16,100 x g for 20 min) between them in order to remove the supernatant and pellet the ApoBods. Free aldehyde in ApoBods were blocked for 10 min with 0.15% glycine in PBS and permeabilized for 20 min with Triton solution (0.1% Triton X-100 (Fisher, Hampton, NH, USA), 0.01% NaN_3 and 1% bovine serum albumin (BSA) in PBS). Primary antibodies at a concentration of 1 mg/mL were diluted 1/50 in Triton solution and incubated with the purified ApoBods for 1 h RT while rocking. The specific primary antibodies used were rabbit polyclonal anti-histone H4 (BioVision), mouse monoclonal anti-Ku80 (111, Abcam, Cambridge, UK), sheep polyclonal anti-apolipoprotein-H (ApoH) (Invitrogen, Camarillo, CA), rabbit polyclonal anti-Lamp2 (Abgent, CA, USA), rabbit monoclonal anti-phospho-histone H2B (ser14) (Upstate, NY, USA) or mouse monoclonal anti-Smith (GeneTex, Inc., GmbH, Germany) antibodies. After the incubation, the Apobods were washed in Triton solution for 15 min. The corresponding secondary antibodies (Molecular Probes, CA, USA) used for detection were goat anti-rabbit Alexa Fluor 594 for H4 and H2B, goat anti-mouse Alexa Fluor 633 for Ku80 and Smith, donkey anti-sheep Alexa Fluor 568 for apolipoprotein-H, and goat anti-rabbit Alexa Fluor 633 for Lamp2. The secondary antibodies were diluted at 1/200 in Triton solution and incubated with the ApoBods for 1 h RT while rocking. The ApoBods were washed with Triton solution and then the DNA was stain in 1/1,000 dilution of Hoechst (Sigma) in water for 10 min. Finally, the immunolabeled ApoBods mounted with 10 µL Mowiol® mounting medium (supplemented with 2.5% w/v of Dabco) and covered with a cover slip. Slides were stored at 4 ˚C until analyzed by confocal microscopy (Olympus).

Feeding and Labeling THP-1 Cells

For THP-1 immunolabeling, ApoBods collected from 10 x 10^6 Hep2G cells as described in section 2.6 were suspended into 500 µl of HBSS supplemented with 3 mM $CaCl_2$ of which half was used to feed 1 x 10^5 dTHP-1. The ratio between fed cells and feeder cells used to produce ApoBods were thus 1:100. The ApoBods were added to fresh RPMI-1640 medium, supplemented as described above, and added to cover the dTHP-1. The cells were then incubated for 2 h at 37 ˚C, 5% CO_2. After the feeding, the cells were fixed with 4% PFA for 10 min and immunolabeled with rabbit polyclonal anti-Lamp2 (1 mg/mL, Abgent) at a dilution of 1/50 in Triton solution; anti-Lamp2 labeling was detected with 1/200 dilution of goat anti-rabbit Alexa Fluor 594 secondary antibody (Molecular Probes) in Triton solution. As a negative control, phagocytosis was inhibited in THP-1 and dTHP-1 cells by treatment with 1 x 10^{-5} M cytochalasin B (CB) from *Helminthosporium dematioideum* (Sigma) for 30 min before feeding and maintained throughout the feeding. These immunolabeled samples were stained with Hoescht (Sigma) and mounted as above. Slides were stored at 4 ˚C until analyzed with laser scanning confocal microscopy (Olympus). Phagocytic activities (PA) of

THP-1 (monocytes) and dTHP-1 (macrophages) were analyzed by counting green fluorescence signal inside the cells. Inhibitory effect of CB was also calculated by comparing PA of CB treated and non-treated cells. Percentage PA was analyzed by counting the green signal contained in 1,200 macrophages.

Confocal Imaging

An Olympus IX-81 with a Fluoview-1000 confocal microscope (Olympus Corporation, Tokyo, Japan) set-up was used for imaging of fixed cells and immunolabeled samples. The images of these samples were taken with 40x and 60x oil immersion objectives at 405, 488 and 543 nm excitation wavelengths; excitation at 633 nm was also used for acquiring images of ApoBods. Induced ApoBods and differentiated macrophages fixed on glass cover slips were identified and examined by using emission filters as follows: 425-455 nm for blue-fluorescence (DAPI), 500-530 nm for green-fluorescence (for Alexa Flour 488), 555-625 nm for red-fluorescence (for Alexa Flour 594), and 625-800 nm purple-fluorescence (for Alexa Flour 633). The appropriate exposure, gain and intensity were corrected before recording the images. These images were analyzed using the ImageJA 1.45B program (NIH).

For ApoBods images, quantification of fluorescence intensity was performed by 3 independent assays of each condition (N = 30) and determined with a free, open source software package, BioImageXD [51]. Levels for the laser power, detector amplification and optical sections were optimized for each channel in confocal microscope before starting the quantification. The volume of the labeled structures from confocal images was evaluated by intensity threshold segmentation. The sum of volumes over the threshold was normalized to average area of the ApoBods. The total area of ApoBods base on the DNA image was quantified using a threshold that distinguished them from the background. Regions for cell area calculation were defined by first smoothing images with Gaussian kernel and thresholding.

Statistical Analysis

The statistical analyses of the amount of ApoBods, antigen signal in ApoBods, PA and CB inhibition percentages were performed using PASW Statistics software (SPSS Inc., Hong Kong). The calculated means were compared according to the following groups: ApoBods induced by transductions of *Ac*EGFP with *Ac*EGFP-NS1, *Ac*EGFP transduction with staurosporine, and *Ac*EGFP-NS1 transduction with staurosporine. These data were further evaluated by one-way ANOVA post hoc test analysis and expressed as mean ± standard error of the mean (SEM). Values of $P < 0.05$ were considered statistically significant.

Results

NS1 protein expression induces production of apoptotic blebs and ApoBods in non-permissive cells

To examine the role of B19V NS1 protein in providing a source of self-antigens characteristic apoptosis events were induced. Apoptotic blebs and hence bodies were created when a non-permissive cell line, HepG2, was transduced with recombinant baculoviruses *Ac*EGFP and *Ac*EGFP-NS1 (Figure 1). Figure 1A illustrates scanning electron micrographs of HepG2 in normal conditions, and then transduced with *Ac*EGFP and *Ac*EGFP-NS1 for 48 h. As displayed in Figure 1A, apoptotic blebbing seen on the cell's surface (arrows) characteristic of apoptotic events was enhanced with the expression of B19V NS1 protein compared to non-transduced cells or cells transduced with a baculovirus vector expressing EGFP, a protein that does not induce significant apoptosis. Blebbing increased as a consequence of NS1 expression, which was greater than that in *Ac*EGFP transduced or non-transduced cells. When non-transduced (Figure 1B), *Ac*EGFP (Figure 1C) and *Ac*EGFP-NS1 (Figure 1D) tranduced, and staurosporine treated cells (Figure 1E) were viewed directly for EGFP fluorescence (green), DAPI staining (blue) and Annexin V-PE staining (red), cells expressing *Ac*EGFP (Figure 1C) and *Ac*EGFP-NS1 (Figure 1D) displayed Annexin V-PE staining with intensity greater in *Ac*EGFP-NS1 expressing cells compared to *Ac*EGFP. Staurosporine treated cells demonstrated Annexin V-PE staining. DAPI staining demonstrated nuclear fragmentation and apparent blebbing in *Ac*EGFP and *Ac*EGFP-NS1 transduced cells and staurosporine treated cells with destruction more extensive in *Ac*EGFP-NS1 expression cells.

In order to evaluate whether B19V NS1 can generate a large-scale source of ApoBods, transductions of HepG2 cells were performed on a larger scale and ApoBods were consequently purified. After purification, the number of ApoBods was counted by FC (Figure 2A–C). The forward and side scatters from FC studies provided an overview of the apoptotic body population. As shown in Figure 2, dot plot analysis of data was recorded only for 1 min in order to compare the amounts of ApoBods created for each condition; buffer control, *Ac*EGFP transduction, *Ac*EGFP-NS1 transduction and staurosporine treatment as a positive control (Figure 2A–C, respectively). The event counts recorded for each condition showed more ApoBods produced from the transduction of *Ac*EGFP-NS1 (910 ± 70.00) compared to *Ac*EGFP transduction (430 ± 50.74). The number of ApoBods generated by *Ac*EGFP-NS1 transduction was comparable to staurosporine, the positive control of apoptosis, (995 ± 70.00) (Table S1, data not shown). The results demonstrated the ability of NS1 to induce apoptosis in the non-permissive cells,

Figure 1

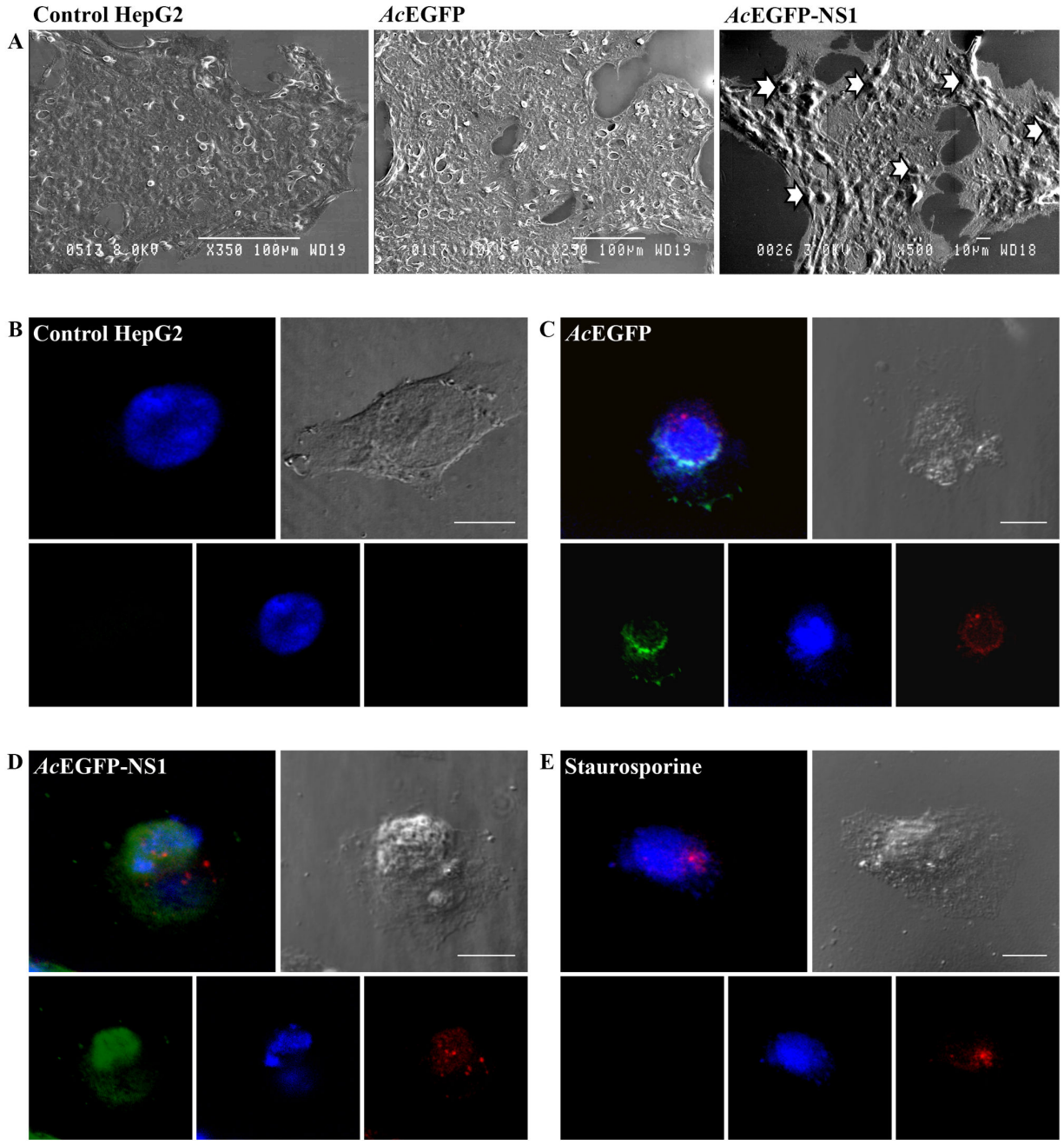

Figure 1. Human Parvovirus B19 NS1 protein induces apoptotic blebs and bodies in non-permissive cell line. (**A**) Scanning electron microscopic images of non-infected cells, cells transduced with *Ac*EGFP and *Ac*EGFP-NS1, respectively. ApoBods with potential self-antigens are detected at 48 h post-transduction as indicated with arrows. Bars 100 µm or 10 µm. (**B**–**E**) Apoptotic blebs created from NS1 expression show positively for Annexin V-PE. Laser scanning confocal microscopy images of (**B**) non-transduced HepG2 cells, (**C**) cells transduced with *Ac*EGFP, (**D**) cells transduced with *Ac*EGFP-NS1, and (**E**) staurosporine treated cells. Cells were visualized (lower panels) directly for EGFP (green), stained for DNA with DAPI (blue), and labeled for phosphatidylserine (PS) with Annexin V-PE (red). Upper panels represent the merged image of the bottom panels and the DIC micrograph to see the morphology of the surface of the cell. Bars 20 µm.

doi: 10.1371/journal.pone.0067179.g001

and that ApoBods can be produced in an amount sufficient for further characterization.

Initial characterization of the ApoBods was conducted with the use of FC. 10,000 events counted from the purified ApoBods were displayed in dot plots for *Ac*EGFP and *Ac*EGFP-NS1 transductions, as well as staurosporine treatment (Figure 2B, respectively). The percentage of green signal of ApoBods from *Ac*EGFP (18.06 ± 2.44) or *Ac*EGFP-NS1 (31.77 ± 4.74) transductions calculated from 10,000 events and compared to ApoBods from staurosporine (8.44 ± 1.32) treatment is shown as a histogram in Figure 2C. The approximately time to collect 10,000 events from *Ac*EGFP ApoBods (6.47 ± 0.29 min) were double compared to the time to collect the events from *Ac*EGFP-NS1 (2.57 ± 0.23 min) and staurosporine ApoBods (2.50 ± 0.29 min) (Table S1, data not shown). The analyzed results showed that the percentage of green signal in the ApoBods from *Ac*EGFP-NS1 induction is higher than *Ac*EGFP induction. In addition, these results indicate that during NS1 expression, a high amount of ApoBods can be created from a non-permissive cell line and NS1 remains inside these bodies as seen in Table S1. Figure 2A–C displays a representative experiment from 3 independent assays.

Nucleosomal and cytosolic self-antigens are in ApoBods induced with B19V NS1

The presence of EGFP-NS1 in the ApoBods suggests that other associated proteins may also be present, such as DNA damage or associated repair proteins. To further characterize the ApoBods, the bodies were stained with DAPI and Annexin V-PE to see if DNA and PS antigens were present. Representative fluorescent microscopy images of purified ApoBods created from *Ac*EGFP and *Ac*EGFP-NS1 transductions, as well as staurosporine treated cells (Figure 2D–F) indicated the presence of green signal from EGFP and EGFP-NS1 and red signal from Annexin V-PE binding to external membrane PS as seen in Figure 2D and 2E, respectively. Staurosporine induced ApoBods stained for DNA (blue) and PS (red) (Figure 2F). The morphology of the ApoBods were as expected and are shown in the DIC images.

Additional examinations were conducted with purified ApoBods to identify other self-antigens. Apoptosis was induced in HepG2 cells for 72 h with *Ac*EGFP or *Ac*EGFP-NS1 recombinant baculoviruses, or staurosporine. The purified ApoBods were immunolabeled for nuclear self-antigens histone H4 (seen as red) and Ku80 (viewed as violet) (Figure 3). ApoBods were stained for DNA with Hoechst (blue) and the morphology is seen in the DIC images. Laser scanning confocal microscopy was then used to image the contents of immunolabeled ApoBods and evaluate the volume of antigen signal compared to total area of the DNA signal. Representative confocal images indicated that ApoBods from *Ac*EGFP, *Ac*EGFP-NS1 and staurosporine, Figure 3A–C, respectively, all contain DNA as previously seen. The ApoBods also contained H4 and Ku80, but to a lesser extent in EGFP induced ApoBods. The ApoBods generated by transduction contained nucleosomal antigens as well as NS1. Percentages of antigens in ApoBods are displayed in Figure 3D; *Ac*EGFP-NS1 ApoBods showed highest in all protein signals, including nucleosomal antigens. The EGFP signal was significantly greater than in *Ac*EGFP induced ApoBods ($P = 0.002$) and, as expected, the control staurosporine ($P = 0.000$). Similar labeling experiments were conducted (Figure 4) for apolipoprotein H/beta-2-glycoprotein I (ApoH; red) and lysosomes (Lamp2; violet). These cytosolic constituents were present in the purified ApoBods. Antigens within ApoBods from *Ac*EGFP-NS1 transductions had significantly increased EGFP and DNA signals when compared with *Ac*EGFP ApoBods ($P = 0.001$ for EGFP and $P = 0.028$ for DNA) and staurosporine ApoBods ($P = 0.000$ for EGFP and $P = 0.033$ for DNA), Figure 4D. Purified ApoBods were also labeled for histones (H2B; red) and another nuclear antigen (Smith; violet) (Figure 5). ApoBods from *Ac*EGFP and *Ac*EGFP-NS1 recombinant baculoviruses transduction, and from staurosporine treated cells, did not show the presence of H2B within ApoBods, but Smith was present. In Figure 5D, EGFP signal of *Ac*EGFP-NS1 ApoBods was higher than those from cells transduced with *Ac*EGFP alone ($P = 0.141$) or treated by staurosporine ($P = 0.014$). Moreover, *Ac*EGFP-NS1 ApoBods also presented Smith signal (an SLE marker) even though not at a significantly higher level than *Ac*EGFP. In addition, consistent DNA presence is seen (blue) with these samples, and the characteristic morphology is displayed as viewed in the DIC images. Taken together, specific nucleosomal antigens and specific cytosolic antigens are indeed present in purified ApoBods from NS1 induction.

Immune cell recognition of purified ApoBods by differentiated macrophages.

In order to investigate whether these purified ApoBods would have immunological consequence, differentiated macrophages or differentiated THP-1 cells (dTHP-1) were exposed to the ApoBods from *Ac*EGFP and *Ac*EGFP-NS1 transductions and staurosporine treatment. After 2 h exposure to the ApoBods, the macrophages were washed, fixed and immunolabeled for lysosomes (red) and stained for DNA (blue). Figure 6 represents images from macrophages exposed to no ApoBods (Figure 6A), ApoBods from *Ac*EGFP transductions (Figure 6B), ApoBods produced from transductions of *Ac*EGFP-NS1 (Figure 6C), and ApoBods produced from staurosporine (Figure 6D). The representative confocal images reveal the green fluorescence signal of EGFP (Figure 6B) or EGFP-NS1 (Figure 6C) inside the macrophages. Staurosporine induced ApoBods, as expected (Figure

Figure 2

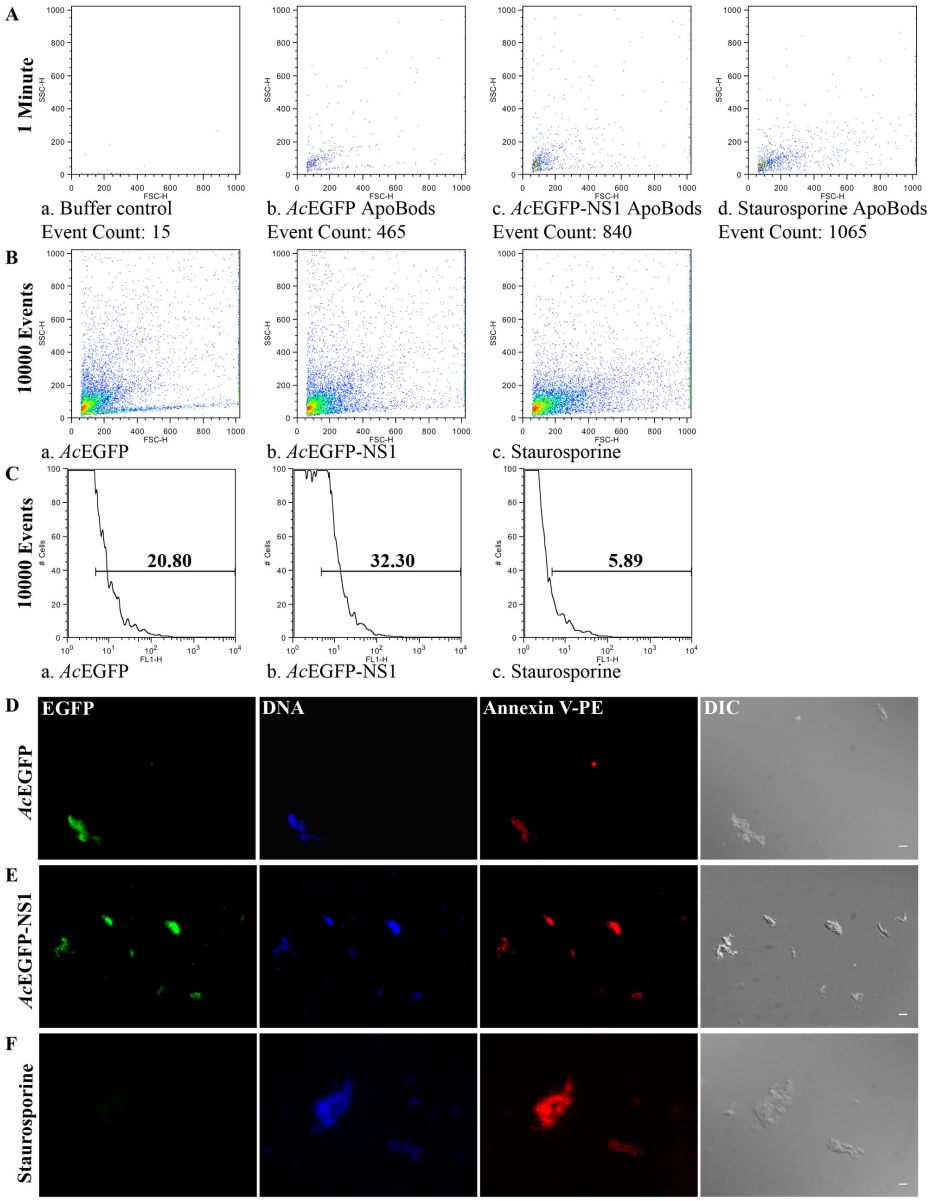

Figure 2. Self-antigens are present in ApoBods created by NS1 expression and those ApoBods can be purified and quantified. Flow cytometry analysis was conducted on purified ApoBods from *Ac*EGFP and *Ac*EGFP-NS1 transduced cells, and staurosporine positive samples. Representative dot plots and histograms are provided. Experiments were conducted independently three times. (**A**) Counts were recorded for 1 min to compare the amount of ApoBods produced in each condition, buffer control, ApoBods produced from transductions of *Ac*EGFP, ApoBods from *Ac*EGFP-NS1 transduction, and ApoBods from staurosporine treated cells. (**B**) Event counts were recorded in order to reach 10,000 events to compare the percentage of green signal from each ApoBods production situation. ApoBods produced from transductions of *Ac*EGFP, ApoBods from *Ac*EGFP-NS1 transduction, and ApoBods from staurosporine treated cells were verified. Buffer control was not added here due to absence of events. (**C**) Histograms of the green fluorescent signal from the previous event counts for each ApoBods production condition. Gated bar indicated the percentage of green signal. Fluorescent microscopy images of purified ApoBods created from (**D**) *Ac*EGFP and (**E**) *Ac*EGFP-NS1 transductions and, (**F**) Staurosporine treated cells. Purified ApoBods were visualized directly for EGFP (green), stained for DNA with DAPI (blue), labeled for PS with Annexin V-PE (red), and visualized with DIC microscopy to see the morphology. Bars 5 µm.

doi: 10.1371/journal.pone.0067179.g002

Figure 3

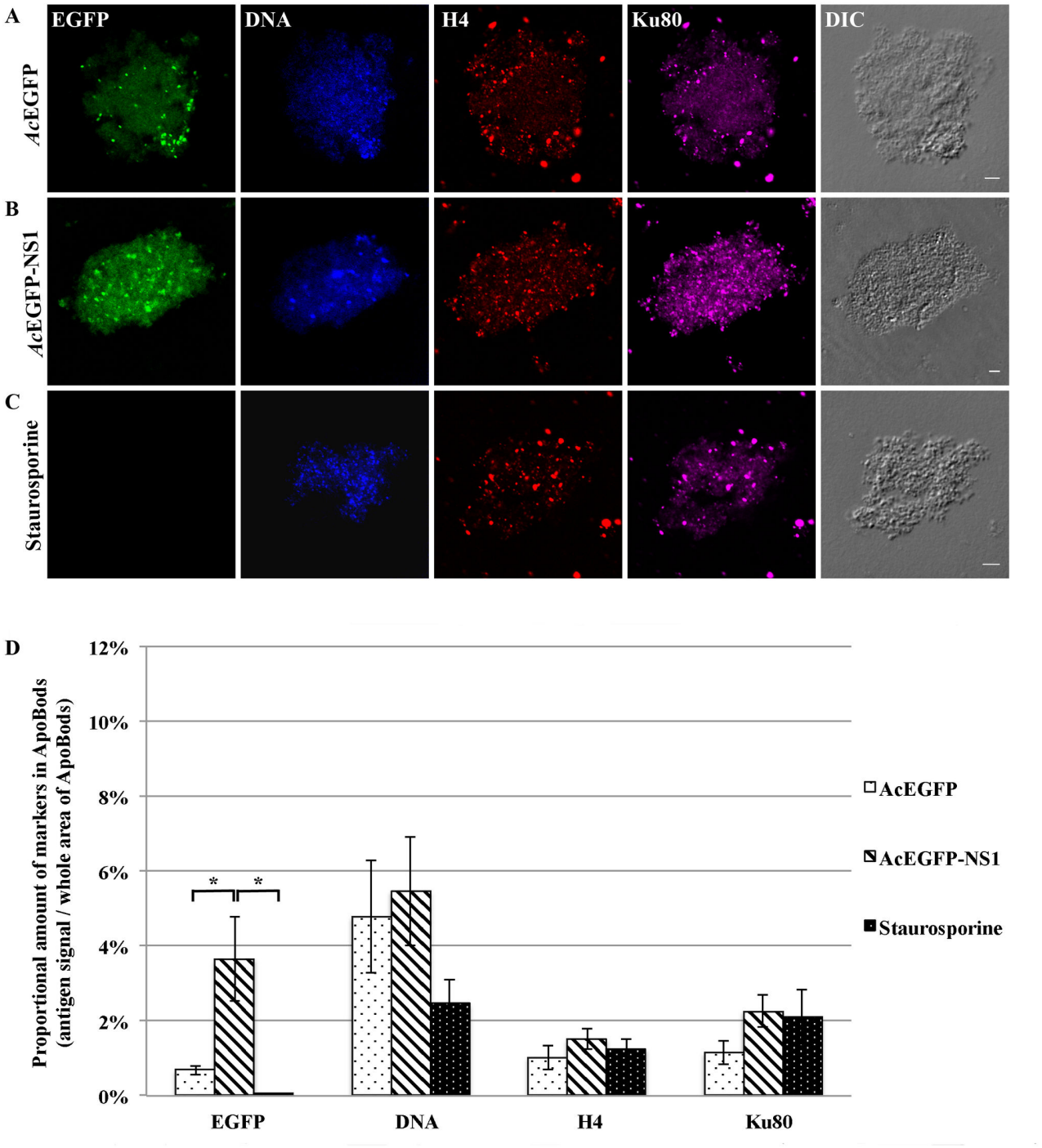

Figure 3. Nuclear antigens histone H4, Ku80, and DNA, are present in NS1 induced ApoBods. Laser scanning confocal images of purified ApoBods produced from with (**A**) *Ac*EGFP, and (**B**) *Ac*EGFP-NS1 transduced cells and (**C**) staurosporine treated HepG2 cells. Purified ApoBods were visualized directly for EGFP (green), stained for DNA with DAPI (blue), immune-labeled for H4 (histone-4; red), and for Ku80 (Ku protein; violet) antigens. DIC microscopy was used to visualize the morphology of the ApoBods. Bars 5 µm. (**D**) amount of antigen markers in ApoBods under different conditions presented as mean ± SEM, N = 30. *$P < 0.05$.

doi: 10.1371/journal.pone.0067179.g003

Figure 4

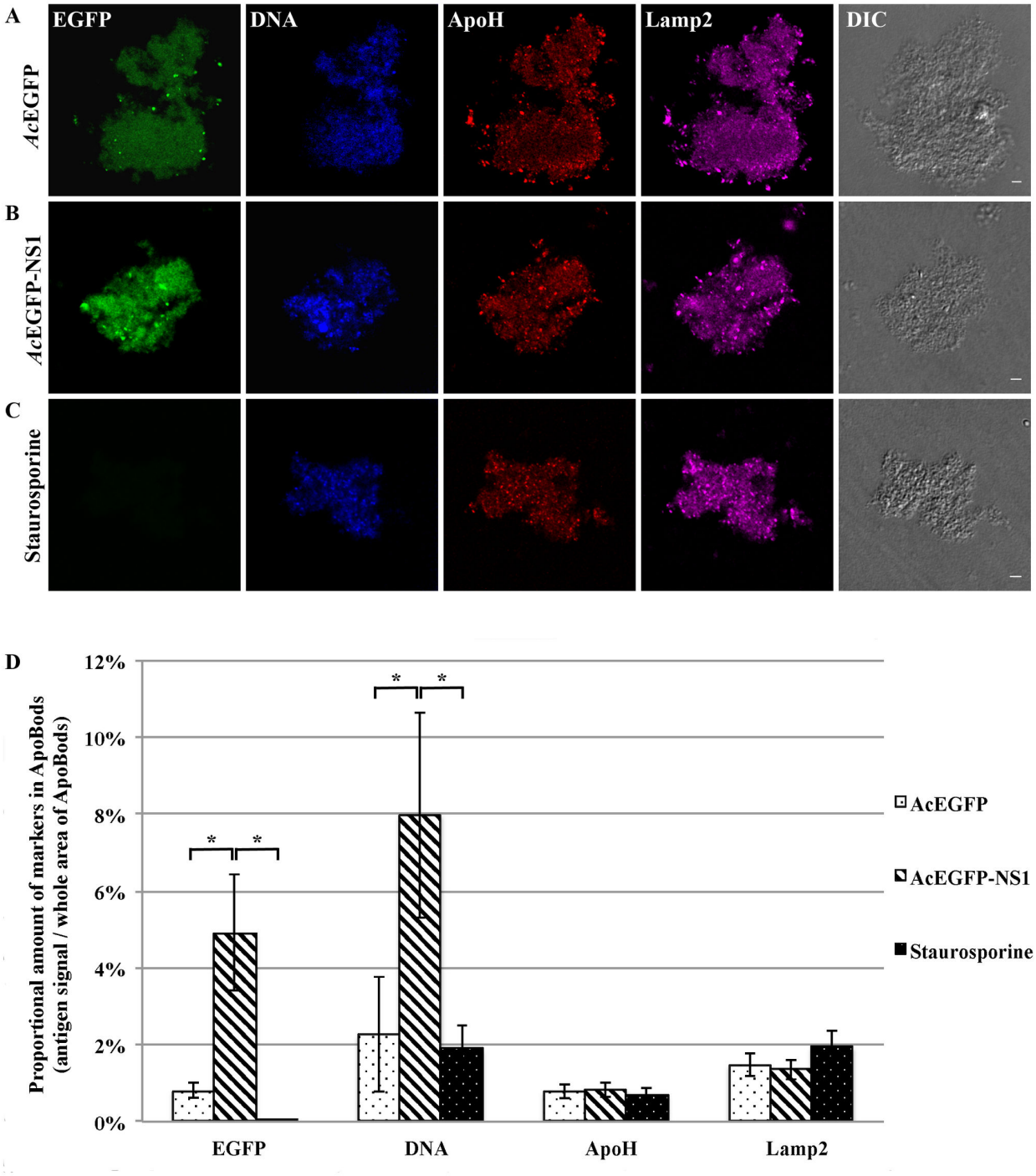

Figure 4. Cytosolic antigens apolipoprotein-H and lysosomal, exist in NS1 induced ApoBods. Confocal microscopy of purified ApoBods produced from with (**A**) *Ac*EGFP, and (**B**) *Ac*EGFP-NS1 transduced cells and (**C**) Staurosporine treated HepG2 cells. Presence of EGFP, DNA, ApoH (apolipoprotein-H), and Lamp2 (lysosomal) antigens are highlighted as green, blue, red and violet, respectively. DIC is displayed to indicate morphology of the ApoBods. Bars 5 µm. The proportion of amount of antigen markers in ApoBods (volume of antigens / total area of ApoBods) was presented as mean ± SEM (N = 30), (**D**). *$P < 0.05$.

doi: 10.1371/journal.pone.0067179.g004

Figure 5

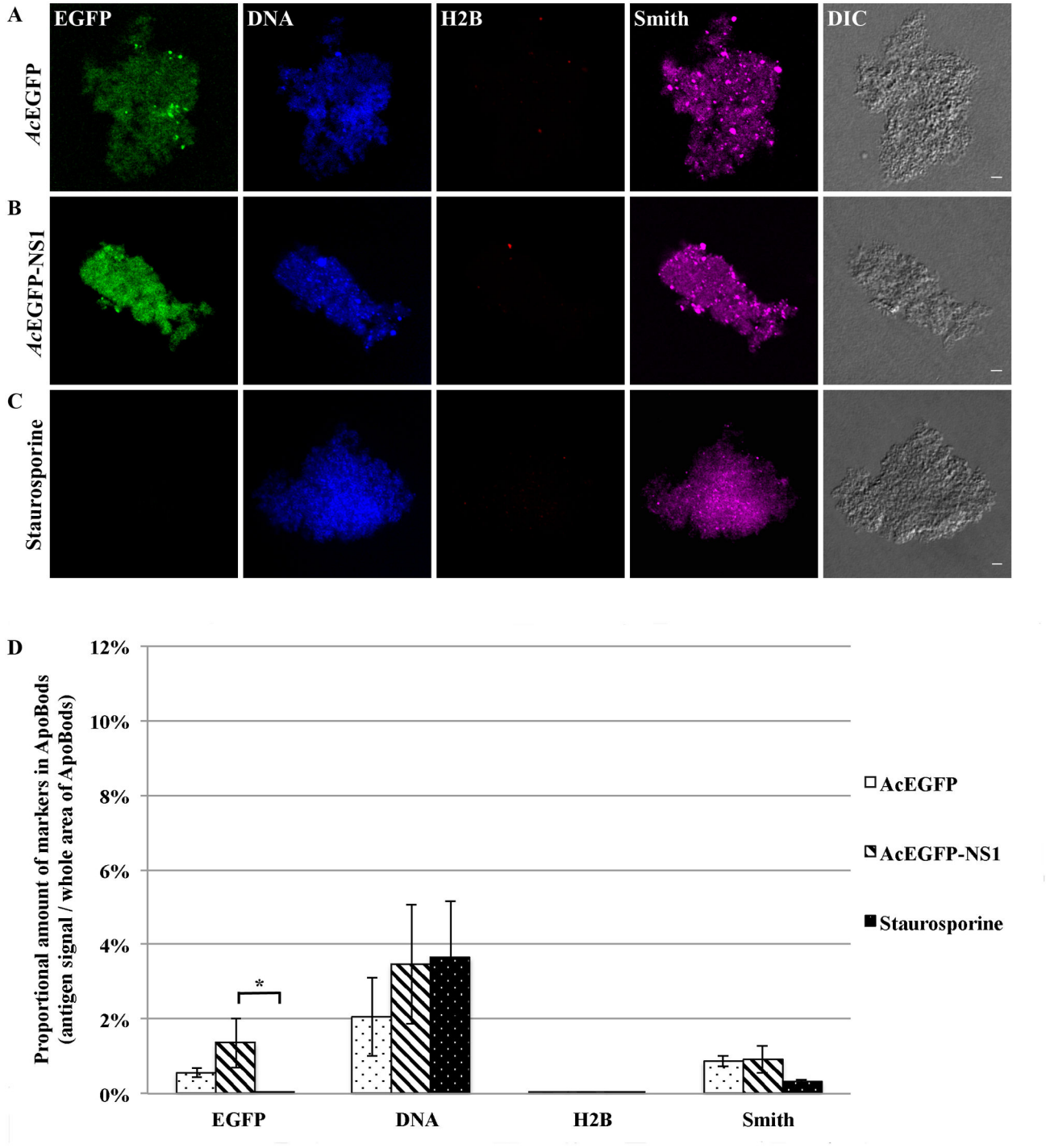

Figure 5. Lupus specific antigens DNA and Smith are seen in purified ApoBods. Confocal microscopy images of purified ApoBods produced from with (**A**) *Ac*EGFP, and (**B**) *Ac*EGFP-NS1 transduced cells and (**C**) Staurosporine treated HepG2 cells. The visualized for EGFP, DNA, H2B and Smith antigens are presented as green, blue, red and violet. Morphology of the ApoBods are seen in the DIC image. Bars 5 µm. Antigen markers of ApoBods from each group was seen in (**D**) by showing as mean ± SEM, N = 30. *$P < 0.05$.

doi: 10.1371/journal.pone.0067179.g005

6D), did not show signal in the green channel. The DIC images depict the morphology of the cell. The larger frame is the merged format of the represented cell. ApoBods from *Ac*EGFP and *Ac*EGFP-NS1 transductions were engulfed, these results were verified by the green signal of ApoBods contained in the macrophages. Thus, engulfment of staurosporine induced ApoBods could not be viewed in this study and hence acted as the negative control for this experiment. In order to further confirm that the ApoBods were internalized, macrophage engulfment inhibitor studies were conducted with the use of cytochalasin B (CB, Figure S1A-B). Confocal images indicated that CB treated dTHP-1 cells engulfed fewer ApoBods from *Ac*EGFP (Figure S1A) and *Ac*EGFP-NS1 (Figure S1B) transductions, as viewed by a lack of green signal inside the cells. When undifferentiated monocytes, THP-1 cells, were exposed to ApoBods from *Ac*EGFP (Figure S1C) and *Ac*EGFP-NS1 (Figure S1D) transductions, or staurosporine treatment (Figure S1E), the cells did not engulf ApoBods as seen by a lack of green signal from the ApoBods in the composition images. The number of cells that engulfed the ApoBods and the phagocytic activities (PA) of differentiated macrophages exposed to the ApoBods were calculated and presented in Table 1. From 1200 cells, 28.6% of the macrophages recognized and engulfed the ApoBods from *Ac*EGFP transductions; this was similar to *Ac*EGFP-NS1 transductions at 26.3% ($P = 0.219$). Uptake was inhibited approximately 56.0% when cytochalasin B was present. Similarly, the macrophages engulfed ApoBods from *Ac*EGFP-NS1 inductions was inhibited by 59.0% in the presence of CB. As expected ApoBods from the staurosporine treatment provided the null values in this experiment.

Discussion

NS1 protein stimulate ApoBods production

The mechanisms by which viruses break immune tolerance require further investigation. Apoptosis is an intracellular death pathway to remove cells without provoking a response to cell debris [52,53]. Morphological evidence of apoptosis consists of cell shrinkage, chromatin condensation, membrane blebbing, and the formation of ApoBods [53,54] as seen also here (Figure 1). The important roles of apoptosis include the regulation of hematopoetic progenitor cells, the elimination of cells that have sustained genetic damage or that undergo uncontrolled cellular proliferation, and the prevention of viral replication [55]. Characteristically, the loss of phosphatidylserine (PS) from the intercellular surface to the outer layer of the plasma lipid bilayer membrane occurs in the early stages of apoptosis [56,57]. During advanced stages of apoptosis, intracellular fragments independently move to the cell surface creating two discrete structures, namely surface blebs then ApoBods that actually separate from the remainder cell [57]. Our results demonstrated that B19V NS1 protein in a non-permissive cell line induces high quantities of apoptotic blebs (Figure 1) and bodies that contain NS1 protein and exposed PS (Figure 2). These NS1 protein induced apoptotic events have been reported earlier [15].

Detection of self-antigens and viral proteins

Apoptotic bleb/bodies usually contain only self-antigens; these self-antigens typically do not cause inflammatory or immune responses [52,53,56]. Impaired clearance of apoptotic cells has been proposed to cause autoimmunity by increasing the quantity of ApoBods and expanding the diversity of self-antigens presented to the immune system [58]. In systemic immune diseases such like SLE, antibodies to self-antigens may be used for diagnosis including circulating antibodies to DNA, nuclear fragments and histones [58,59]. B19V NS1 has been reported to provoke cellular DNA damage [13,18,49,60]. Other studies have detected autoantibodies to self-antigens post B19V infection [46,61]. Several studies have hypothesized that the mechanism of B19V induced autoimmunity is due to molecular mimicry [6263.–64]. Here, we confirm that the purified ApoBods have self-antigens from the cytoplasm and nucleus (Figures 2-5). In addition, some specific autoimmune disease biomarker autoantibody targets such as DNA, H4, Ku80, ApoH and Smith are present (Figures 3-5). While it has previously been shown that high amounts of EGFP alone expressed in recombinant systems can adversely affect cell physiology [65], which can lead to apoptosis [66], and components of ApoBods from *Ac*EGFP and *Ac*EGFP-NS1 transductions were qualitatively quit similar, quantitatively there were 2-fold fewer ApoBods produced from *Ac*EGFP transduction.

Established clinical viral infections, as in the case with herpes simplex virus 1 (HSV-1) [67], hepatitis C virus (HCV) [68], Epstein–Barr virus (EBV) [69], and cytomegalovirus (CMV) [70], have been reported to induce or exacerbate autoimmune diseases. At least three mechanisms have been proposed to explain this exacerbation: (1) the immune response to pathogens provides a specific or nonspecific stimulus that promotes activation and expansion of auto-reactive T cells, (2) the viral pathogen itself may provide a potential role of antigenic stimulus to provoke auto-reactive T cells, and (3) molecular mimicry of a viral epitope may allow self-antigen expression that can be taken up, processed and cross-presented by APCs [67,71,72].

Engulfment of ApoBods

Generally, apoptotic cells are cleared rapidly and efficiently as intact cells or ApoBods by professional antigen presenting cells (APCs) or neighboring cells [52–54,56]. This engulfment typically does not elicit an

Figure 6

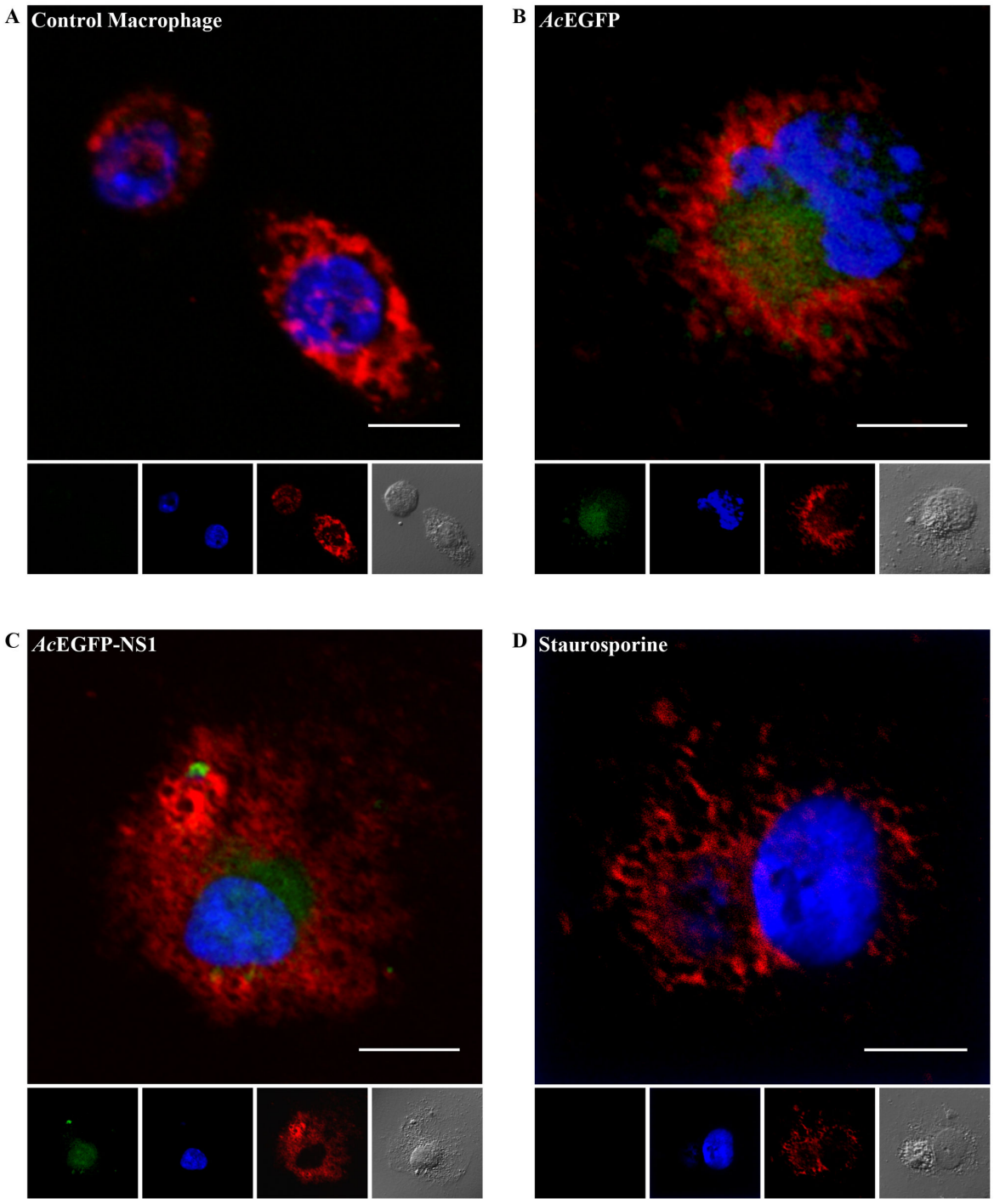

Figure 6. Purified ApoBods induced by NS1 can be engulfed by antigen presenting cells. Laser scanning confocal microscopy images of differentiated macrophages exposed to (**A**) no ApoBods, (**B**) ApoBods from *Ac*EGFP transductions, (**C**) ApoBods from *Ac*EGFP-NS1 transductions, and (**D**) ApoBods produced from staurosporine. Direct viewing from EGFP is seen in green panels, DAPI stained DNA shown as blue, and lysosomes are immunolabeled with Lamp2 antibody with Alexa594 secondary antibody seen as red. DIC frames represent the cell of interest. Merged images represent the compositions of labels seen for the particular treated macrophage. Bars 20 µm.

doi: 10.1371/journal.pone.0067179.g006

Table 1. Phagocytoic activities of differentiated monocytes exposed to ApoBods.

Apoptotic bodies(ApoBods)	No. of macrophages that engulfed ApoBods(200 cells x 6)	PA (%)	No. of macrophages that engulfed ApoBods with cytochalasin B(200 cells x 6)	PA (%)	Inhibited % with cytochalasin B
Without	0	0	Not Applicable	-	-
***Ac*EGFP transduction**	57.2 ± 3.7	28.6	25.2 ± 2.3	12.6	56
***Ac*EGFP-NS1 transduction**	52.5 ± 2.4	26.3	21.8 ± 1.9	10.9	59
Staurosporine	0	0	0	0	0

Macrophages exposed to ApoBods from different treatments, without ApoBods, from *Ac*EGFP transductions, transductions of *Ac*EGFP-NS1, and produced from staurosporine, were evaluated regarding the number of cells that engulfed the ApoBods. The phagocytic activity was calculated according to the following formula: PA% = (number of macrophages containing engulfed ApoBods/total number of counted macrophages) × 100. Phagocytotic cells with the preceding ApoBods were treated with CB. The number of cells that engulfed the ApoBods and the number of inhibition percentage are given. Engulfed ApoBods were counted for 200 cells x 6, total N = 1,200 cells.

inflammatory or immune responses [53]. Self-antigen translocation can enhance phagocytosis of apoptotic fragments and presentation of autoantigens [73,74]. We have shown here that the ApoBods are recognized and engulfed by differentiated macrophages (Figure 6 Table 1 Figure S1F), and this suggests that the B19V induced ApoBods have the potential to provide a repertoire of self-antigens to the immune system. It has been previously reported that deficiencies of apoptotic clearance processes may expose the immune system to more advanced stages of apoptotic structures [58,74,75]. In apoptosis, intracellular fragments independently move to the cell surface creating two discrete structures, apoptotic blebs then bodies that actually separate from the remainder cell [57]. These structures serve as autoantigens generating autoantibodies [76]. Nucleosomal NS1 protein modified DNA may contain additional nuclear antigens as DNA binding protein or NS1 interactive proteins. Uptake of this complex by anergic B lymphocytes specific for DNA or self-antigen would allow presentation of NS1 peptides to NS1 specific T helper cells, thereby breaking tolerance. Reaction to self- and nonself-antigens by APCs and lymphocytes would elicit tissue damage that in turn accelerates autoimmune disease [77]. Therefore, immune processing of B19V NS1 protein induced ApoBods warrants further investigation.

Supporting Information

Figure S1. Laser scanning confocal microscopy images of the engulfment study that showed no phagocytosis. Macrophages with the inhibitor cytochalasin B (CB) were exposed to ApoBods from the following productions (**A**) *Ac*EGFP and (**B**) *Ac*EGFP-NS1 transductions. Monocytes exposed to ApoBods from (**C**) *Ac*EGFP transductions, (**D**) *Ac*EGFP-NS1 transductions, and (**E**) staurosporine treatment. (**F**) positive control is macrophages exposed to ApoBods from *Ac*EGFP-NS1 transduction. EGFP signal is viewed directly in the green frame, DNA is stain with DAPI seen in the blue images, and lysosomes depicted as red when labeled with Lamp2 antibody. Compositions of the labels are seen in merged images. DIC represents the morphology of the cells. Bars 20 µm.

Table S1. Purified ApoBods in consequence of NS1 expression presented high quantity and green signal. Quantity of purified ApoBods from transduced cells with *Ac*EGFP and *Ac*EGFP-NS1, and treated with staurosporine control from FC 3 different assays were analyzed. The results from each condition presented as mean ± SEM (N = 3). *P* value < 0.05 is significantly; *compare between *Ac*EGFP and *Ac*EGFP-NS1, **compare between *Ac*EGFP and staurosporine, and ***compare between *Ac*EGFP-NS1 and staurosporine.

Author Contributions

Conceived and designed the experiments: KT SJN LG. Performed the experiments: KT SR LW AF LG. Analyzed the data: KT VK VM SJN LG. Contributed reagents/materials/analysis tools: LG. Wrote the manuscript: KT SR VK VM SJN LG.

References

1. Clewley JP (1984) Biochemical characterization of a human parvovirus. J Gen Virol 65(1): 241-245. doi: 10.1099/0022-1317-65-1-241.
2. Cossart YE, Field AM, Cant B, Widdows D (1975) Parvovirus-like particles in human sera. Lancet 1: 72-73. PubMed: 46024.
3. Shade RO, Blundell MC, Cotmore SF, Tattersall P, Astell CR (1986) Nucleotide sequence and genome organization of human parvovirus B19 isolated from the serum of a child during aplastic crisis. J Virol 58: 921-936. PubMed: 3701931.
4. Young NS, Brown KE (2004) Parvovirus B19. N Engl J Med 350: 586-597. doi:10.1056/NEJMra030840. PubMed: 14762186.
5. Zádori Z, Szelei J, Lacoste MC, Li Y, Gariépy S et al. (2001) A viral phospholipase A2 is required for parvovirus infectivity.

Dev Cell 1: 291-302. doi:10.1016/S1534-5807(01)00031-4. PubMed: 11702787.
6. Raab U, Beckenlehner K, Lowin T, Niller HH, Doyle S et al. (2002) NS1 protein of parvovirus B19 interacts directly with DNA sequences of the p6 promoter and with the cellular transcription factors Sp1/Sp3. Virology 293: 86-93. doi: 10.1006/viro.2001.1285. PubMed: 11853402.
7. Fu Y, Ishii KK, Munakata Y, Saitoh T, Kaku M et al. (2002) Regulation of tumor necrosis factor alpha promoter by human parvovirus B19 NS1 through activation of AP-1 and AP-2. J Virol 76: 5395-5403. doi:10.1128/JVI.76.11.5395-5403.2002. PubMed: 11991968.
8. Mitchell LA (2002) Parvovirus B19 nonstructural (NS1) protein as a transactivator of interleukin-6 synthesis: common pathway in inflammatory sequelae of human parvovirus infections? J Med Virol 67: 267-274. doi:10.1002/jmv.2217. PubMed: 11992589.
9. Young N, Harrison M, Moore J, Mortimer P, Humphries RK (1984) Direct demonstration of the human parvovirus in erythroid progenitor cells infected in vitro. J Clin Invest 74: 2024-2032. doi:10.1172/JCI111625. PubMed: 6392340.
10. Ozawa K, Kurtzman G, Young N (1987) Productive infection by B19 parvovirus of human erythroid bone marrow cells in vitro. Blood 70: 384-391. PubMed: 3038211.
11. Srivastava A, Bruno E, Briddell R, Cooper R, Srivastava C et al. (1990) Parvovirus B19-induced perturbation of human megakaryocytopoiesis in vitro. Blood 76: 1997-2004. PubMed: 2146978.
12. Munshi NC, Zhou S, Woody MJ, Morgan DA, Srivastava A (1993) Successful replication of parvovirus B19 in the human megakaryocytic leukemia cell line MB-02. J Virol 67: 562-566. PubMed: 8416383.
13. Moffatt S, Yaegashi N, Tada K, Tanaka N, Sugamura K (1998) Human parvovirus B19 nonstructural (NS1) protein induces apoptosis in erythroid lineage cells. J Virol 72: 3018-3028. PubMed: 9525624.
14. Sol N, Le Junter J, Vassias I, Freyssinier JM, Thomas A et al. (1999) Possible interactions between the NS-1 protein and tumor necrosis factor alpha pathways in erythroid cell apoptosis induced by human parvovirus B19. J Virol 73: 8762-8770. PubMed: 10482630.
15. Poole BD, Karetnyi YV, Naides SJ (2004) Parvovirus B19-induced apoptosis of hepatocytes. J Virol 78: 7775-7783. doi: 10.1128/JVI.78.14.7775-7783.2004. PubMed: 15220451.
16. Poole BD, Zhou J, Grote A, Schiffenbauer A, Naides SJ (2006) Apoptosis of liver-derived cells induced by parvovirus B19 nonstructural protein. J Virol 80: 4114-4121. doi:10.1128/JVI.80.8.4114-4121.2006. PubMed: 16571827.
17. Kivovich V, Gilbert L, Vuento M, Naides SJ (2010) Parvovirus B19 genotype specific amino acid substitution in NS1 reduces the protein's cytotoxicity in culture. Int J Med Sci 7: 110-119. PubMed: 20567611.
18. Kivovich V, Gilbert L, Vuento M, Naides SJ (2012) The putative metal coordination motif in the endonuclease domain of human Parvovirus B19 NS1 is critical for NS1 induced S phase arrest and DNA damage. Int J Biol Sci 8: 79-92. doi:10.3923/ijb.2012.79.81. PubMed: 22211107.
19. Bonvicini F, Filippone C, Manaresi E, Zerbini M, Musiani M et al. (2008) HepG2 hepatocellular carcinoma cells are a non-permissive system for B19 virus infection. J Gen Virol 89: 3034-3038. doi:10.1099/vir.0.2008/004341-0. PubMed: 19008390.
20. Kerr JR (1996) Parvovirus B19 infection. Eur J Clin Microbiol Infect Dis 15: 10-29. doi:10.1007/BF01586181. PubMed: 8641299.
21. Kerr S, O'Keeffe G, Kilty C, Doyle S (1999) Undenatured parvovirus B19 antigens are essential for the accurate detection of parvovirus B19 IgG. J Med Virol 57: 179-185. doi: 10.1002/(SICI)1096-9071(199902)57:2. PubMed: 9892405.
22. Anderson MJ, Cohen BJ (1987) Human Parvovirus B19 Infections in United-Kingdom 1984-86. Lancet 1: 738-739.
23. Heegaard ED, Brown KE (2002) Human parvovirus B19. Clin Microbiol Rev 15: 485-505. doi:10.1128/CMR.15.3.485-505.2002. PubMed: 12097253.
24. Anderson MJ, Higgins PG, Davis LR, Willman JS, Jones SE et al. (1985) Experimental Parvoviral Infection in Humans. J Infect Dis 152: 257-265. doi:10.1093/infdis/152.2.257. PubMed: 2993431.
25. Potter CG, Potter AC, Hatton CS, Chapel HM, Anderson MJ et al. (1987) Variation of erythroid and myeloid precursors in the marrow and peripheral blood of volunteer subjects infected with human parvovirus (B19). J Clin Invest 79: 1486-1492. doi: 10.1172/JCI112978. PubMed: 3033026.
26. Lehmann HW, von Landenberg P, Modrow S (2003) Parvovirus B19 infection and autoimmune disease. Autoimmun Rev 2: 218-223. doi:10.1016/S1568-9972(03)00014-4. PubMed: 12848949.
27. Corcoran A, Doyle S (2004) Advances in the biology, diagnosis and host-pathogen interactions of parvovirus B19. J Med Microbiol 53: 459-475. doi:10.1099/jmm.0.05485-0. PubMed: 15150324.
28. Drago F, Semino M, Rampini P, Rebora A (1999) Parvovirus B19 infection associated with acute hepatitis and a purpuric exanthem. Br J Dermatol 141: 160-161. doi:10.1046/j.1365-2133.1999.02943.x. PubMed: 10417538.
29. Yang SH, Lin LW, Fang YJ, Cheng AL, Kuo SH (2012) Parvovirus B19 infection-related acute hepatitis after rituximab-containing regimen for treatment of diffuse large B-cell lymphoma. Ann Hematol 91: 291-294. doi:10.1007/s00277-011-1238-8. PubMed: 21538062.
30. Pinho JR, Alves VA, Vieira AF, Moralez MO, Fonseca LE et al. (2001) Detection of human parvovirus B19 in a patient with hepatitis. Braz J Med Biol Res 34: 1131-1138. PubMed: 11514836.
31. Arista S, De Grazia S, Di Marco V, Di Stefano R, Craxì A (2003) Parvovirus B19 and "cryptogenic" chronic hepatitis. J Hepatol 38: 375-376. doi:10.1016/S0270-9139(03)80488-3. PubMed: 12586308.
32. Mogensen TH, Jensen JM, Hamilton-Dutoit S, Larsen CS (2010) Chronic hepatitis caused by persistent parvovirus B19 infection. BMC Infect Dis 10: 246. doi: 10.1186/1471-2334-10-246. PubMed: 20727151.
33. Nobili V, Vento S, Comparcola D, Sartorelli MR, Luciani M et al. (2004) Autoimmune hemolytic anemia and autoimmune hepatitis associated with parvovirus B19 infection. Pediatr Infect Dis J 23: 184-185. doi:10.1097/01.inf.0000110270.38240.51. PubMed: 14872194.
34. Kordes U, Schneppenheim R, Briem-Richter A, Scherpe S, Schäfer HJ (2011) Parvovirus B19 infection and autoimmune hepatitis in a child with sickle cell anemia. Pediatr Blood Cancer 56: 323-324. doi:10.1002/pbc.22820. PubMed: 21157899.
35. Díaz F, Collazos J (2000) Hepatic dysfunction due to parvovirus B19 infection. J Infect Chemother 6: 63-64. doi:10.1007/s101560050052. PubMed: 11810534.
36. Dame C, Hasan C, Bode U, Eis-Hübinger AM (2002) Acute liver disease and aplastic anemia associated with the persistence of B19 DNA in liver and bone marrow. Pediatr Pathol Mol Med 21: 25-29. doi:10.1080/pdp.21.1.25.29. PubMed: 11842976.
37. Krygier DS, Steinbrecher UP, Petric M, Erb SR, Chung SW et al. (2009) Parvovirus B19 induced hepatic failure in an adult requiring liver transplantation. World J Gastroenterol 15: 4067-4069. doi:10.3748/wjg.15.4067. PubMed: 19705505.
38. Karetnyi YV, Beck PR, Markin RS, Langnas AN, Naides SJ (1999) Human parvovirus B19 infection in acute fulminant liver failure. Arch Virol 144: 1713-1724. doi:10.1007/s007050050699. PubMed: 10542021.
39. Abe K, Kiuchi T, Tanaka K, Edamoto Y, Aiba N et al. (2007) Characterization of erythrovirus B19 genomes isolated in liver tissues from patients with fulminant hepatitis and biliary atresia who underwent liver transplantation. Int J Med Sci 4: 105-109. PubMed: 17479159.
40. Sun L, Zhang JC (2012) Acute fulminant hepatitis with bone marrow failure in an adult due to parvovirus B19 infection. Hepatology 55: 329-330. doi:10.1002/hep.24720. PubMed: 21969057.
41. Hemauer A, Beckenlehner K, Wolf H, Lang B, Modrow S (1999) Acute parvovirus B19 infection in connection with a flare of systemic lupus erythematodes in a female patient. J Clin Virol 14: 73-77. doi:10.1016/S1386-6532(99)00038-4. PubMed: 10548133.
42. Takahashi Y, Murai C, Shibata S, Munakata Y, Ishii T et al. (1998) Human parvovirus B19 as a causative agent for rheumatoid arthritis. Proc Natl Acad Sci U S A 95: 8227-8232. doi:10.1073/pnas.95.14.8227. PubMed: 9653169.
43. Dorsch S, Liebisch G, Kaufmann B, von Landenberg P, Hoffmann JH et al. (2002) The VP1 unique region of parvovirus

B19 and its constituent phospholipase A2-like activity. J Virol 76: 2014-2018. doi:10.1128/JVI.76.4.2014-2018.2002. PubMed: 11799199.
44. von Landenberg P, Lehmann HW, Knöll A, Dorsch S, Modrow S (2003) Antiphospholipid antibodies in pediatric and adult patients with rheumatic disease are associated with parvovirus B19 infection. Arthritis Rheum 48: 1939-1947. doi: 10.1002/art.11038. PubMed: 12847688.
45. von Landenberg P, Lehmann HW, Modrow S (2007) Human parvovirus B19 infection and antiphospholipid antibodies. Autoimmun Rev 6: 278-285. doi:10.1016/j.autrev.2006.09.006. PubMed: 17412298.
46. Lunardi C, Tinazzi E, Bason C, Dolcino M, Corrocher R et al. (2008) Human parvovirus B19 infection and autoimmunity. Autoimmun Rev 8: 116-120. doi:10.1016/j.autrev.2008.07.005. PubMed: 18700174.
47. Lunardi C, Tiso M, Borgato L, Nanni L, Millo R et al. (1998) Chronic parvovirus B19 infection induces the production of anti-virus antibodies with autoantigen binding properties. Eur J Immunol 28: 936-948. doi:10.1002/(SICI)1521-4141(199803)28:03. PubMed: 9541589.
48. Moffatt S, Tanaka N, Tada K, Nose M, Nakamura M et al. (1996) A cytotoxic nonstructural protein, NS1, of human parvovirus B19 induces activation of interleukin-6 gene expression. J Virol 70: 8485-8491. PubMed: 8970971.
49. Poole BD, Kivovich V, Gilbert L, Naides SJ (2011) Parvovirus B19 nonstructural protein-induced damage of cellular DNA and resultant apoptosis. Int J Med Sci 8: 88-96. PubMed: 21278893.
50. Daigneault M, Preston JA, Marriott HM, Whyte MK, Dockrell DH (2010) The identification of markers of macrophage differentiation in PMA-stimulated THP-1 cells and monocyte-derived macrophages. PLOS ONE 5: e8668. doi:10.1371/journal.pone.0008668. PubMed: 20084270.
51. Kankaanpää P, Paavolainen L, Tiitta S, Karjalainen M, Päivärinne J et al. (2012) BioImageXD: An open, general-purpose and high-throughput image-processing platform. Nat Methods 9: 683-689. doi:10.1038/nmeth.2047. PubMed: 22743773.
52. Kerr JF, Wyllie AH, Currie AR (1972) Apoptosis: a basic biological phenomenon with wide-ranging implications in tissue kinetics. Br J Cancer 26: 239-257. doi:10.1038/bjc.1972.33. PubMed: 4561027.
53. Arends MJ, Wyllie AH (1991) Apoptosis: mechanisms and roles in pathology. Int Rev Exp Pathol 32: 223-254. PubMed: 1677933.
54. Krysko DV, Denecker G, Festjens N, Gabriels S, Parthoens E et al. (2006) Macrophages use different internalization mechanisms to clear apoptotic and necrotic cells. Cell Death Differ 13: 2011-2022. doi:10.1038/sj.cdd.4401900. PubMed: 16628234.
55. Barber GN (2001) Host defense, viruses and apoptosis. Cell Death Differ 8: 113-126. doi:10.1038/sj.cdd.4400823. PubMed: 11313713.
56. Radic M, Marion T, Monestier M (2004) Nucleosomes are exposed at the cell surface in apoptosis. J Immunol 172: 6692-6700. PubMed: 15153485.
57. Casciola-Rosen LA, Anhalt G, Rosen A (1994) Autoantigens targeted in systemic lupus erythematosus are clustered in two populations of surface structures on apoptotic keratinocytes. J Exp Med 179: 1317-1330. doi:10.1084/jem.179.4.1317. PubMed: 7511686.
58. Cline AM, Radic MZ (2004) Apoptosis, subcellular particles, and autoimmunity. Clin Immunol 112: 175-182. doi:10.1016/j.clim.2004.02.017. PubMed: 15240161.
59. Fadok VA, Voelker DR, Campbell PA, Cohen JJ, Bratton DL et al. (1992) Exposure of Phosphatidylserine on the Surface of Apoptotic Lymphocytes Triggers Specific Recognition and Removal by Macrophages. J Immunol 148: 2207-2216. PubMed: 1545126.
60. Ozawa K, Ayub J, Kajigaya S, Shimada T, Young N (1988) The Gene Encoding the Nonstructural Protein of B19 (Human) Parvovirus May Be Lethal in Transfected Cells. J Virol 62: 2884-2889. PubMed: 2969055.
61. Meyer O (2003) Parvovirus B19 and autoimmune diseases. Joint Bone Spine 70: 6-11. doi:10.1016/S1297-319X(02)00004-0. PubMed: 12639611.
62. Murphy PM (2001) Viral exploitation and subversion of the immune system through chemokine mimicry. Nat Immunol 2: 116-122. doi:10.1038/84214. PubMed: 11175803.
63. Alcami A (2003) Viral mimicry of cytokines, chemokines and their receptors. Nat Rev Immunol 3: 36-50. doi:10.1038/nri980. PubMed: 12511874.
64. Bruggeman LA (2007) Viral subversion mechanisms in chronic kidney disease pathogenesis. Clin J Am Soc Nephrol 2 Suppl 1: S13-S19. doi:10.2215/CJN.04311206. PubMed: 17699505
65. Baens M, Noels H, Broeckx V, Hagens S, Fevery S et al. (2006) The Dark Side of EGFP: Defective Polyubiquitination. PLOS ONE 1: e54. doi:10.1371/journal.pone.0000054. PubMed: 17183684.
66. Liu HS, Jan MS, Chou CK, Chen PH, Ke NJ (1999) Is green fluorescent protein toxic to the living cells? Biochem Biophys Res Commun 260: 712-717. doi:10.1006/bbrc.1999.0954. PubMed: 10403831.
67. Panoutsakopoulou V, Sanchirico ME, Huster KM, Jansson M, Granucci F et al. (2001) Analysis of the relationship between viral infection and autoimmune disease. Immunity 15: 137-147. doi:10.1016/S1074-7613(01)00172-8. PubMed: 11485745.
68. Wagner B, Vierhapper H, Hofmann H (1996) Prevalence of hepatitis C virus infection in Hashimoto's thyroiditis. BMJ 312: 640-641. doi:10.1136/bmj.312.7031.640b. PubMed: 8595364.
69. Vento S, Guella L, Mirandola F, Cainelli F, Di Perri G et al. (1995) Epstein-Barr virus as a trigger for autoimmune hepatitis in susceptible individuals. Lancet 346: 608-609. doi: 10.1016/S0140-6736(95)91438-2. PubMed: 7651006.
70. Lawson CM, O'Donoghue HL, Reed WD (1992) Mouse cytomegalovirus infection induces antibodies which cross-react with virus and cardiac myosin: A model for the study of molecular mimicry in the pathogenesis of viral myocarditis. Immunology 75: 513-519. PubMed: 1315309.
71. von Herrath MG, Oldstone MB (1996) Virus-induced autoimmune disease. Curr Opin Immunol 8: 878-885. doi: 10.1016/S0952-7915(96)80019-7. PubMed: 8994870.
72. Wraith DC, Goldman M, Lambert PH (2003) Vaccination and autoimmune disease: what is the evidence? Lancet 362: 1659-1666. doi:10.1016/S0140-6736(03)14802-7. PubMed: 14630450.
73. Frisoni L, McPhie L, Colonna L, Sriram U, Monestier M et al. (2005) Nuclear autoantigen translocation and autoantibody opsonization lead to increased dendritic cell phagocytosis and presentation of nuclear antigens: a novel pathogenic pathway for autoimmunity? J Immunol 175: 2692-2701. PubMed: 16081846.
74. Schiller M, Bekeredjian-Ding I, Heyder P, Blank N, Ho AD et al. (2008) Autoantigens are translocated into small apoptotic bodies during early stages of apoptosis. Cell Death Differ 15: 183-191. doi:10.1038/sj.cdd.4402239. PubMed: 17932498.
75. Cline AM, Radic MZ (2004) Murine lupus autoantibodies identify distinct subsets of apoptotic bodies. Autoimmunity 37: 85-93. doi:10.1080/0891693042000196219. PubMed: 15293878.
76. Cocca BA, Cline AM, Radic MZ (2002) Blebs and apoptotic bodies are B cell autoantigens. J Immunol 169: 159-166. PubMed: 12077241.
77. Murphy K, Travers P, Walport M (2008) Janeway's immunobiology. New York Garlan. Science Publishing House.